

Journal of Molecular Structure
Synthesis of oxadiazole derivatives: Anti-bacterial, DNA binding and in silico molecular modelling approaches
--Manuscript Draft--

Manuscript Number:	MOLSTRUC-D-24-01971
Article Type:	Research Paper
Keywords:	Synthesis, Antibacterial activity, Molecular Modelling, DNA Binding
Corresponding Author:	Uddin Rahis, PhD Jamia Millia Islamia New Delhi, INDIA
First Author:	Razia Sultana
Order of Authors:	Razia Sultana Asghar Ali Manish Rana Iqbal Ahmad Mohan Kamthan Haider Thaer Abdulhameed Almuqdati Nouman Nouman Rabiya Mehandi Mohammad Abid Zeinhom M El-Bahy Uddin Rahis, PhD
Abstract:	1,3,4-Oxadiazole derivatives containing pyrazole moiety 5a–5l and amine substituted oxadiazole derivatives 5m-5p were synthesized and also characterized by spectroscopic methods such as FT-IR, 1H, 13C NMR spectroscopy, and mass spectrometry. Compounds 5a–5p were tested for their in vitro antibacterial activity against gram-positive (<i>Bacillus subtilis</i> and <i>Staphylococcus aureus</i>) and gram-negative (<i>Pseudomonas aeruginosa</i> and <i>E. coli</i>) bacterial strains using the agar well disc diffusion method in contrast to the drug ciprofloxacin (CIP). The most active analogs 5e and 5f were thought to be investigated for their ability to interact with CT-DNA by using absorption titration, emission titration, circular dichroism, competitive binding with EtBr, and cyclic voltammetry and the results demonstrated that the compounds bind with CT-DNA through intercalation mode. Schrödinger Release 2022-4 was used to investigate the best hits of pyrazoline derivatives through in silico molecular modelling by DNA gyrase (PDB ID: 2XCT). Additionally, pharmacokinetic properties of all the derivatives were also calculated by using Swiss ADME software.
Suggested Reviewers:	mahendra nath University of Delhi mnath@chemistry.du.ac.in Rakesh ranjan Amity University krranjan@amity.edu abhinav grover Jawaharlal Nehru University agrover@jnu.ac.in

Rui Fausto
Editor in Chief
Journal of Molecular Structure

08/03/2024

Dear Sir,

I am pleased to submit an original research article entitled "**Synthesis of oxadiazole derivatives: Anti-bacterial, DNA binding and in silico molecular modelling approaches**" for consideration for publication in esteemed Journal of Molecular structure. We believe that manuscript is appropriate for publication by the Journal of Molecular structure and the studies conducted in the experiment falls under the aims and scope of the journal.

Thank you for receiving our manuscript and considering it for review. We appreciate your time and look forward to your response.

Sincerely,

Dr. Rahisuddin, PhD
Associate Professor
Department of Chemistry
Jamia Millia Islamia
New Delhi-110025

- Synthesis, experimental spectral characterization of synthesized compounds.
- Evaluation of antibacterial activity, DNA binding, antioxidant and drug likeness studies of **5e** and **5f**.
- The molecular modelling study also carried out of lead compounds.

1
2
3
**Synthesis of oxadiazole derivatives: Anti-bacterial, DNA binding and *in silico*
4 molecular modelling approaches**

5 Razia Sultana^a, Asghar Ali^b, Manish Rana^{c*}, Iqbal Ahmad^d, Mohan Kamthan^b, Haider
6 Thaer Abdulhameed Almuqdati^e, Nouman^a, Rabiya Mehandi^a, Mohammad Abid^e,
7 Zeinhom M. El-Bahy^f, Rahisuddin^{a*}

8
9 ^aMolecular and Biophysical Research Laboratory (MBRL), Department of Chemistry,
10 Jamia Millia Islamia, New Delhi 110025, India
11

12 ^bClinical Biochemistry lab, Department of Biochemistry, School of Chemical and Life
13 Sciences, Jamia Hamdard, New Delhi-110062, India
14

15 ^cDepartment of Chemistry, Ramjas College, University of Delhi, Delhi 110007, India
16

17 ^dDepartment of Agricultural Microbiology, Faculty of Agricultural Sciences, Aligarh
Muslim University, Aligarh (UP), 202002, India.
18

19 ^eDepartment of Biosciences, Jamia Millia Islamia, New Delhi 110025, India
20

21 ^fDepartment of Chemistry, Faculty of Science, Al-Azhar University, Nasr City 11884,
Cairo, Egypt
22
23
24
25

26 * Corresponding author:
27 rahisuddin@jmi.ac.in (Rahisuddin)
28
29
30
31
32
33
34
35
36
37
38
39
40
41
42
43
44
45
46
47
48
49
50
51
52
53
54
55
56
57
58
59
60
61
62
63
64
65

1
2
3
4
5
6
7
8
9
10
11
12
13
14
15
16
17
18
19
20
21
22
23
24
25
26
27
28
29
30
31
32
33
34
35
36
37
38
39
40
41
42
43
44
45
46
47
48
49
50
51
52
53
54
55
56
57
58
59
60
61
62
63
64
65

Abstract

1,3,4-Oxadiazole derivatives containing pyrazole moiety **5a–5l** and amine substituted oxadiazole derivatives **5m–5p** were synthesized and also characterized by spectroscopic methods such as FT-IR, ^1H , ^{13}C NMR spectroscopy, and mass spectrometry. Compounds **5a–5p** were tested for their *in vitro* antibacterial activity against gram-positive (*Bacillus subtilis* and *Staphylococcus aureus*) and gram-negative (*Pseudomonas aeruginosa* and *E. coli*) bacterial strains using the agar well disc diffusion method in contrast to the drug ciprofloxacin (CIP). The most active analogs **5e** and **5f** were thought to be investigated for their ability to interact with CT-DNA by using absorption titration, emission titration, circular dichroism, competitive binding with EtBr, and cyclic voltammetry and the results demonstrated that the compounds bind with CT-DNA through intercalation mode. Schrödinger Release 2022-4 was used to investigate the best hits of pyrazoline derivatives through *in silico* molecular modelling by DNA gyrase (PDB ID: 2XCT). Additionally, pharmacokinetic properties of all the derivatives were also calculated by using Swiss ADME software.

1
2
3
4
5
6
7
8
9
10
11
12
13
14
15
16
17
18
19
20
21
22
23
24
25
26
27
28
29
30
31
32
33
34
35
36
37
38
39
40
41
42
43
44
45
46
47
48
49
50
51
52
53
54
55
56
57
58
59
60
61
62
63
64
65

1. Introduction

Microorganisms harmful impacts are becoming unavoidable due to the fast expansion of human existence. A wide range of bacteria live with humans and other living things in a healthy balance, but an extreme and uncontrolled rapid proliferation of microbes can have disastrous consequences [1]. Bacterial infection is one of the primary causes of death. In 2019, infections were responsible for nearly 13.7 million deaths, with 33 prevalent bacteria accounting for approximately 7.7 million [2]. *Pseudomonas aeruginosa*, *Streptococcus pneumoniae*, *Escherichia coli*, and *Staphylococcus aureus* contribute for 54.9% of these deaths. *S. aureus* infections are the leading cause of death worldwide [3]. Many antimicrobial compounds were used over a number of years to prevent bacteria growth or to control. Due to growing germ resistance brought on by antibiotic misuse, several well-known antimicrobial medicines are currently ineffective against microorganisms [4]. Therefore, the requirement to produce new and better antimicrobial drugs is essential.

It has been found that heterocyclic structures, which make up the bulk of naturally occurring bioactive molecules, are essential for the synthesis of new pharmacologically and physiologically active molecules [5]. Many recently discovered antibacterial agents contain at least one heterocycle ring [6-8]. According to this viewpoint, one area of interest within the field of medicinal and pharmaceutical chemistry is the synthesis of novel heterocyclic compounds made of -N atoms, such as pyrazole moieties, because of their diverse biological properties. Because of the wide spectrum of biological activities of pyrazole and its derivatives, medicinal chemistry has drawn a lot of attention in recent decades., particularly antibacterial [9], anticancer [10], anti-inflammatory [11], antiviral [12], antioxidants [13], anti-diabetic [14]. Researchers are also interested in oxadiazole moieties, which consist of a five-membered heterocyclic

ring with two carbon, two nitrogen, and one oxygen atom [15]. Because of the vast array of medicinal properties. activities of 1,3,4-oxadiazole, including antimicrobial activity, The majority of studies on oxadiazole in the literature focused on the 1,3,4-oxadiazole isomer rather than the other less studied isomers, which are 1,2,3-, 1,2,4-, and 1,2,5-oxadiazole [16]. The 1,3,4-oxadiazoles have a toxophoric linkage -N=C-O- shows effective pharmacologically active components. The alkyl substitutions on the oxadiazole ring, as compared to phenyl substitution at the 5th position on oxadiazole rings with an electron-withdrawing or electron-donating group exhibited higher activity [17]. In drug discovery and medicinal chemistry, 1,3,4-oxadiazole and its derivatives have been used in a wide range of applications. These moieties show significant activities, including anti-bacterial [18], anti-diabetic [19], anti-tubercular [20], antifungal [21], anticonvulsant [22], antioxidant [23], and anti-cancer [24]. Commercially marketed drugs with a 1,3,4-oxadiazole ring, such as Furamizol, have significant antibacterial activity [25], likewise do Raltegravir and Zibotentan, both of which possess a 1,3,4-oxadiazole ring and are frequently used as antiviral and chemotherapy agents [26-27].

In this work we were synthesized new derivatives (**4e** and **4f**) and (**4g-4l**) and them cyclized using iodobenzene diacetate to achieve the target oxadiazole derivatives (**5a-5l**). Also, synthesized amine substituted oxadiazole derivatives **5m-5p**. Additionally, we described the antibacterial activity of all the synthesized compounds against bacterial strains *B. subtilis*, *S. aureus*, *E. coli*, and *P. aeruginosa*. Results observed that the oxadiazole derivatives (**5a-5l**) were more biologically active then (**4e** and **4f**) and (**4g-4l**). The DNA binding study of test compounds were carried out with calf Thymus DNA. Further, molecular docking studies have been carried out to clarify the binding interactions with PDB ID: 1BNA and 2XCT.

1
2 **2. Experimental Section**
3
4
5
6
7
8
9
10
11
12
13
14
15
16
17
18
19
20
21
22
23
24
25
26
27
28
29
30
31
32
33
34
35
36
37
38
39
40
41
42
43
44
45
46
47
48
49
50
51
52
53
54
55
56
57
58
59
60
61
62
63
64
65

2.1. Synthesis of compounds **4e** and **4f**

Compounds **3a-3f** and **4a-4d** were synthesized in previous work [28]. The nicotinic hydrazide (1.5 mmol) was dissolved in ethanol by stirring. The ethanolic solution of nicotinic hydrazide was then added in derivatives **3e** and **3f** with stirring, and refluxed at 60°C in the presence of a few drops of conc. HCl for 3-4 h. The precipitates of final products **4e** and **4f** were filtered, collected, and washed with water and then recrystallized from EtOH.

2.2. Synthesis of compounds (**4g-4l**)

The compounds **3e** and **3f**, **3g-3l** were synthesized using previous reported method [28].

The 0.5 mmol of **3g-3l** was separately dissolved in ethanol with constant stirring. The ethanolic solution of 1.5 mmol of isoniazid was also dissolve in ethanol then added in the solution of **3g-3l** with stirring, and refluxed at 60-80°C in the presence of a few drops of conc. HCl for 2-6 h. The coloured precipitates of final products **4g-4l** were filtered, washed with ethanol, and water and then recrystallized in ethanol.

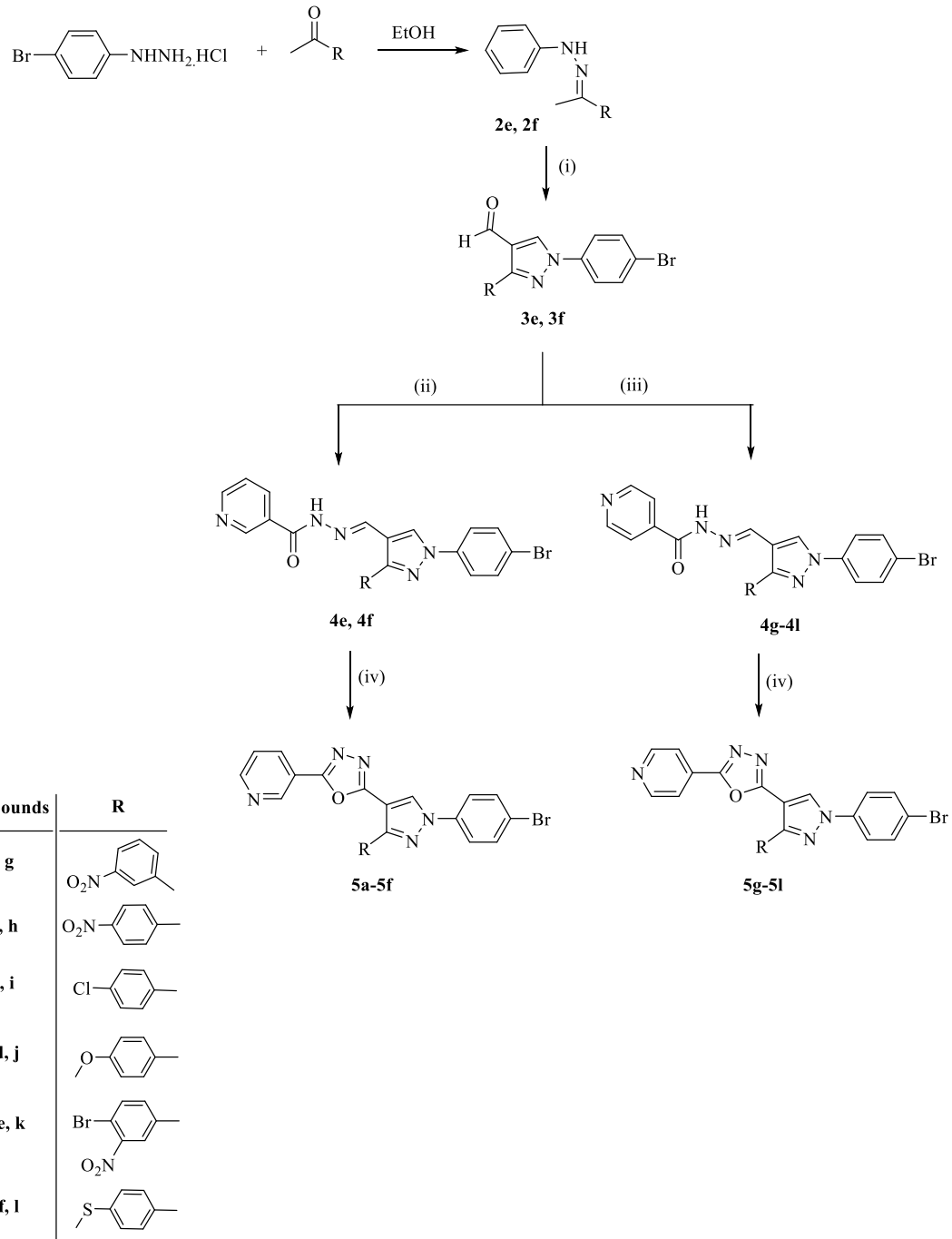
2.3. Synthesis of compounds (**5a-5l**)

The derivatives **4a-4f** (1 mmol) were dissolved in 5 ml dichloromethane (DCM) at r. t. Iodobenzene diacetate (2mmol) was dissolved in 5ml DCM and kept the solution of **4a-4f** in an ice bath. The reaction mixture was kept at room temperature and stirred overnight. After evaporation the solvent, and the resulting precipitates of oxadiazole derivatives (**5a-5f**) were collected, washed with acetonitrile to remove excess iodobenzene diacetate, and recrystallized in DCM. The derivatives of oxadiazole **5g-5l** were also synthesized from the compounds **4g-4l** by the above similar procedure. The synthetic scheme for oxadiazole derivatives **5a-5l** is presented in **Scheme 1**.

1
2
3
4
5
6
7
8
9
10
11
12
13
14
15
16
17
18
19
20
21
22
23
24
25
26
27
28
29
30
31
32
33
34
35
36
37
38
39
40
41
42
43
44
45
46
47
48
49
50
51
52
53
54
55
56
57
58
59
60
61
62
63
64
65

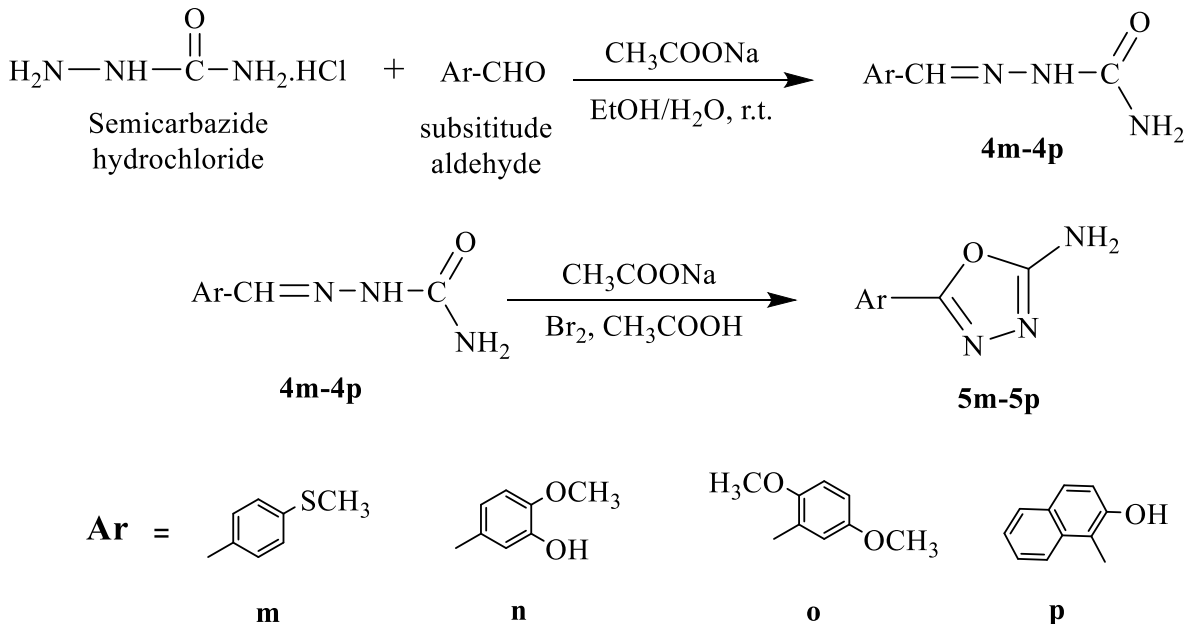
2.4. Synthesis of compounds (**5m-5p**)

To the stirred solution of substituted aldehydes (1 mmol) in ethanol, sodium acetate (1 mmol) and NH₂NHCONH₂.HCl (1 mmol) in water/ethanol were slowly added. Refluxed the resulting reaction mixture at 40°C for 2 h and then precipitates of semicarbazone (**4m-4p**) were obtained. Continuous stirring was used to add the semicarbazone (**4m-4p**) (1 mmol) solution in 2 ml glacial acetic acid to the sodium acetate (2 mmol) in 2 ml glacial acetic acid. A dropping funnel was used to carefully add 0.5 ml of bromine solution from the stock solution (20 ml Br₂ in 50 ml glacial acetic acid) while stirring continuously. Resulting reaction mixture was refluxed at 60–70°C for 4 h while being constantly stirred, and the reaction was then finished by pouring the resulting solution over crushed ice. Vacuum filtration was used to separate the resulting precipitate, dried it, and recrystallized in ethanol. Synthetic procedure of oxadiazole derivatives **5m-5p** is given in **Scheme 2**.



Scheme 1. Synthetic route of Heterocyclic derivatives.

Reaction Conditions: (i) DMF, POCl₃, 0-80 °C (ii) nicotinic hydrochloride, EtOH/HCl, reflux reflux (iii) isoniazid hydrochloride, 60-80 °C EtOH/HCl (iv) Iodobenzene diacetate, DCM, reflux.



Scheme 2. Synthetic route of Heterocyclic derivatives.

(E)-N'-(3-(4-bromo-3-nitrophenyl)-1-(4-bromophenyl)-1H-pyrazol-4-yl)methylene)nicotinohydrazide (4e)

Molecular formula: C₂₂H₁₄Br₂N₆O₃. Yield: 80%. M.P: >300°C. IR (ν_{max} cm⁻¹): 3208 (-NH), 1693 (C=O), 1532 (C=N), 825, 728 (C-Br). ¹H NMR (δ ppm): 12.37 (s, 1H, -NH-C=O), 9.94 (s, 1H, CH=C of pyrazole), 9.62 (s, 1H, -CH=N), 9.44 (s, 1H), 9.25- 9.10 (dd, 1H), 8.88 (s, 1H), 8.63-8.59 (d, 1H), 8.19-8.17 (d, 1H), 8.13-8.11 (d, 1H), 7.98-7.68 (dd, 4H), 7.56-7.53 (d, 1H). ¹³C NMR (δ ppm): 164.53 (C=O), 138.09 (C=N), 153.32, 150.48, 150.07, 135.49, 135.23, 133.85, 133.79, 133.16, 132.99, 130.61, 129.21, 125.52, 123.07, 121.79, 121.43, 121.15, 120.40, 114.39. MS: 571.15 [M+1]⁺.

1
2
3
4
5
6
7
8
9
10
11
12
13
14
15
16
17
18
19
20
21
22
23
24
25
26
27
28
29
30
31
32
33
34
35
36
37
38
39
40
41
42
43
44
45
46
47
48
49
50
51
52
53
54
55
56
57
58
59
60
61
62
63
64
65

(*E*)-*N'*-((1-(4-bromophenyl)-3-(4-(methylthio)phenyl)-1*H*-pyrazol-4-
yl)methylene)nicotinohydrazide (**4f**)

Molecular formula: C₂₃H₁₈BrN₅OS. Yield: 77 %. M.P: >300°C. IR (ν_{\max} cm⁻¹): 3394 (-NH), 1666 (C=O), 1596 (C=N), 1499, 825, 706 (C-Br). ¹H NMR (δ ppm): 12.11 (s, 1H, -NH-C=O), 9.17 (s, 1H, CH=C of pyrazole), 9.06 (s, 1H, -CH=N), 8.84-8.83 (d, 1H), 8.61 (s, 1H), 8.45-8.44 (d, 1H), 8.01- 7.90 (dd, 1H), 7.72-7.57 (dd, 4H, -SCH₃ ring), 7.41-7.23 (dd, 4H), 2.54 (s, 3H, -SCH₃); ¹³C NMR (δ ppm): 161.05 (C=O), 138.68 (C=N), 152.16, 151.08, 147.63, 142.23, 139.69, 137.68, 132.85, 130.23, 129.32, 128.57, 128.13, 126.32, 124.76, 121.25, 119.87, 117.41, 14.98. MS: 492.20 [M]⁺.

(*E*)-*N'*-((1-(4-bromophenyl)-3-(3-nitrophenyl)-1*H*-pyrazol-4-
yl)methylene)isonicotinohydrazide (**4g**)

Molecular formula: C₂₂H₁₅BrN₆O₃. Yield: 89%. M.P: >300°C. IR (ν_{\max} cm⁻¹): 3499 (-NH), 3182-3041 (C-H stretching), 1681 (C=O), 1525 (C=N), 1499, 825, 717 (C-Br). ¹H NMR (δ ppm): 12.59 (s, 1H, -NH-C=O), 9.16 (s, 1H, CH=C of pyrazole), 9.00-8.99 (d, 1H), 8.77 (s, 1H, -CH=N), 8.60 (s, 1H), 8.33-8.31 (d, 2H), 8.28-8.26 (d, 1H), 8.03-7.96 (dd, 4H), 7.83-7.80 (t, 1H), 7.75-7.73 (d, 2H); ¹³C NMR (δ ppm): 160.18 (C=O), 138.45 (C=N), 150.04, 148.45, 146.26, 142.71, 135.46, 133.81, 132.93, 130.73, 129.84, 126.01, 124.34, 123.81, 123.31, 121.41, 120.29, 117.69. MS: 491.15 [M]⁺.

(*E*)-*N'*-((1-(4-bromophenyl)-3-(4-nitrophenyl)-1*H*-pyrazol-4-
yl)methylene)isonicotinohydrazide (**4h**)

Molecular formula: C₂₂H₁₅BrN₆O₃. Yield: 85%. M. P: >300°C. IR (ν_{\max} cm⁻¹): 3406 (-NH), 3193-3037 (C-H stretching), 1689 (C=O), 1547 (C=N), 1499, 825, 721 (C-Br). ¹H NMR (δ ppm): 12.40 (s, 1H, -NH-C=O), 9.11 (s, 1H, CH=C of pyrazole), 8.87-8.85

1 (d, 2H), 8.76 (s, 1H, -CH=N), 8.33-8.31 (d, 2H), 8.15-8.14 (d, 2H), 8.03-7.99 (dd, 4H),
2 7.73-7.72 (d, 2H); ^{13}C NMR (δ ppm): 161.13 (C=O), 138.65 (C=N), 149.92, 149.26,
3 147.65, 142.22, 138.42, 132.91, 130.02, 129.60, 124.18, 122.80, 122.69, 121.39,
4 120.35, 118.15. MS: 491.14 [M] $^+$.
5
6
7
8
9

10 *(E)-N'-(1-(4-bromophenyl)-3-(4-chlorophenyl)-1H-pyrazol-4-yl)methylene)*
11
12 *isonicotinohydrazide (4i)*
13
14
15

16 Molecular formula: C₂₂H₁₅BrClN₅O. Yield: 91%. M. P: >300°C. IR (ν_{\max} cm $^{-1}$): 3402
17 (-NH), 3145-3052 (C-H stretching), 1685 (C=O), 1540 (C=N), 1499, 825, 736 (C-Br).
18 ^1H NMR (δ ppm): 12.40 (s, 1H, -NH-C=O), 9.10 (s, 1H, CH=C of pyrazole), 8.93-8.92
19 (d, 2H), 8.70 (s, 1H, -CH=N), 8.15-8.13 (d, 2H), 8.02-8.00 (d, 2H), 7.83-7.72 (dd, 4H),
20 7.59-7.58 (d, 2H); ^{13}C NMR (δ ppm): 160.61 (C=O), 138.59 (C=N), 151.36, 147.84,
21 143.89, 142.93, 134.04, 132.89, 131.03, 130.71, 129.20, 128.74, 123.50, 121.34,
22 120.07, 117.46. MS: 480.12 [M] $^+$.
23
24
25
26
27
28
29
30
31
32
33

34 *(E)-N'-(1-(4-bromophenyl)-3-(4-methoxyphenyl)-1H-pyrazol-4-yl)methylene)*
35
36 *isonicotinohydrazide (4j)*
37
38
39

40 Molecular formula: C₂₃H₁₈BrN₅O₂. Yield: 92 %. M. P: >300°C. IR (ν_{\max} cm $^{-1}$): 3454 (-
41 NH), 3104-3048 (C-H stretching), 1681 (C=O), 1596 (C=N), 829, 713 (C-Br). ^1H NMR
42 (δ ppm): 12.54 (s, 1H, -NH-C=O), 9.06 (s, 1H, CH=C of pyrazole), 9.03-9.02 (d, 2H),
43 8.73 (s, 1H, -CH=N), 8.32-8.31 (d, 2H), 8.02-8.00 (d, 2H), 7.73-7.54 (dd, 4H), 7.09-
44 7.07 (d, 2H), 3.83 (s, 3H, -OCH₃); ^{13}C NMR (δ ppm): 160.19 (C=O), 138.70 (C=N),
45 159.94, 152.64, 145.89, 143.80, 132.84, 130.27, 130.17, 128.13, 124.49, 121.24,
46 119.80, 117.05, 114.66, 114.26, 55.77. MS: 476.05 [M] $^+$.
47
48
49
50
51
52
53
54
55
56
57
58
59
60
61
62
63
64
65

*(E)-N'-(3-(4-bromo-3-nitrophenyl)-1-(4-bromophenyl)-1*H*-pyrazol-4-yl)methylene)isonicotinohydrazide (**4k**)*

Molecular formula: C₂₂H₁₄Br₂N₆O₃. Yield: 87%. M.P: >300°C. IR (ν_{max} cm⁻¹): 3178 (-NH), 3048 (C-H stretching), 1648 (C=O), 1536 (C=N), 1499, 825, 717 (C-Br). ¹H NMR (δ ppm): 12.43 (s, 1H, -NH-C=O), 9.07 (s, 1H, CH=C of pyrazole), 8.88-8.87 (d, 2H, pyridine ring), 8.65 (s, 1H, -CH=N), 8.56 (s, 1H), 8.11-8.10 (d, 1H), 8.08-8.07 (d, 1H), 7.95-7.92 (dd, 4H), 7.68-7.66 (d, 2H); ¹³C NMR (δ ppm): 160.82 (C=O), 138.38 (C=N), 150.39, 148.79, 148.11, 143.58, 142.21, 135.22, 133.82, 133.20, 132.97, 130.61, 125.49, 123.50, 121.37, 120.39, 117.90, 113.61; MS: 571.14 [M+1]⁺.

*(E)-N'-(1-(4-bromophenyl)-3-(4-(methylthio)phenyl)-1*H*-pyrazol-4-yl)methylene)isonicotinohydrazide (**4l**)*

Molecular formula: C₂₃H₁₈BrN₅OS. Yield: 88%. M.P: >300°C. IR (ν_{max} cm⁻¹): 3417 (-NH), 3145-3052 (C-H stretching), 1678 (C=O), 1592 (C=N), 1499, 829, 739 (C-Br). ¹H NMR (δ ppm): 12.40 (s, 1H, -NH-C=O), 9.02 (s, 1H, CH=C of pyrazole), 8.93, - 8.86 (d, 2H, pyridine ring), 8.67 (s, 1H, -CH=N), 8.16-8.15 (d, 2H), 7.97-7.94 (d, 2H), 7.68- 7.65 (dd, 4H), 7.36-7.34 (d, 2H), 2.49 (s, 3H, -SCH₃). ¹³C NMR (δ ppm): 160.45 (C=O), 138.70 (C=N), 152.30, 147.31, 144.51, 143.40, 139.79, 132.92, 129.39, 128.53, 128.35, 126.35, 123.90, 121.33, 119.98, 117.34, 15.01; MS: 492.15 [M]⁺.

2-(1-(4-bromophenyl)-3-(3-nitrophenyl)-1*H*-pyrazol-4-yl)-5-(pyridin-3-yl)-1,3,4-oxadiazole (5a)

1 Molecular formula: C₂₂H₁₃BrN₆O₃. Yield: 76%. IR (ν_{max} cm⁻¹): 3141, 3082, 1626, 1518.

2 ¹H NMR (δ ppm): 9.95 (s, 1H), 9.59 (s, 1H), 9.42 (s, 1H), 9.15-9.09 (d, 1H), 8.84-8.75
3 (d, 1H), 8.41- 8.31(d, 1H), 8.01-7.99 (d, 1H), 7.95-7.93 (d, 1H), 7.89- 7.53 (m, 1H),
4 7.32-7.06 (dd, 4H). ¹³C NMR (δ ppm): 164.85, 164.19, 151.10, 148.66, 147.07, 145.39,
5 138.23, 133.25, 133.16, 132.47, 131.20, 125.11, 124.26, 123.33, 121.78, 121.55,
6 120.52, 117.87, 106.00. MS: 489.12 [M]⁺

7 *2-(1-(4-bromophenyl)-3-(4-nitrophenyl)-1H-pyrazol-4-yl)-5-(pyridin-3-yl)-1,3,4-*
8 *oxadiazole (5b)*

9 Molecular formula: C₂₂H₁₃BrN₆O₃. Yield: 81%. IR (ν_{max} cm⁻¹): 3149, 3085, 1629,
10 1514. ¹H NMR (δ ppm): 9.54 (s, 1H), 9.06 (s, 1H), 8.91-8.90 (d, 1H), 8.81-8.79 (d, 1H),
11 8.05- 8.02 (m, 1H), 7.99- 7.76 (dd, 4H), 7.48-7.34 (dd, 4H). ¹³C NMR (δ ppm): 164.30,
12 164.13, 152.04, 147.70, 145.28, 139.20, 138.64, 134.56, 131.41, 129.68, 124.46,
13 124.05, 121.06, 119.36, 118.32, 106.11. MS: 489.12 [M]⁺

14 *2-(1-(4-bromophenyl)-3-(4-chlorophenyl)-1H-pyrazol-4-yl)-5-(pyridin-3-yl)-1,3,4-*
15 *oxadiazole (5c)*

16 Molecular formula: C₂₂H₁₃BrClN₅O. Yield: 65%. IR (ν_{max} cm⁻¹): 3141, 3082, 1626,
17 1514. ¹H NMR (δ ppm): 9.53 (s, 1H), 9.17 (s, 1H), 8.79-8.78 (d, 1H), 8.37- 8.34 (d,
18 1H), 8.05-7.97 (dd, 4H), 7.78-7.76 (d, 1H), 7.66- 7.63 (m, 1H), 7.58-7.56 (d, 1H). ¹³C
19 NMR (δ ppm): 162.48, 161.97, 152.42, 147.68, 145.95, 137.53, 134.56, 133.15, 131.10,
20 130.60, 130.31, 128.90, 124.86, 124.26, 121.46, 120.99, 117.90, 106.61. MS: 478.33
21 [M]⁺

1
2
3
4
5
6
7
8
9
10
11
12
13
14
15
16
17
18
19
20
21
22
23
24
25
26
27
28
29
30
31
32
33
34
35
36
37
38
39
40
41
42
43
44
45
46
47
48
49
50
51
52
53
54
55
56
57
58
59
60
61
62
63
64
65

*2-(1-(4-bromophenyl)-3-(4-methoxyphenyl)-1*H*-pyrazol-4-yl)-5-(pyridin-3-yl)-1,3,4-oxadiazole (**5d**)*

Molecular formula: C₂₃H₁₆BrN₅O₂. Yield: 72%. IR (ν_{\max} cm⁻¹): 3059, 1607, 1514. ¹H NMR: (δ ppm): 9.47 (s, 1H), 9.13 (s, 1H), 8.86-8.85 (d, 1H), 8.47-8.44 (dd, 1H), 8.35-8.32 (m, 1H), 8.01-7.96 (dd, 4H), 7.84-7.77 (dd, 4H), 3.34 (s, 3H). ¹³C NMR (δ ppm): 164.24, 164.08, 160.89, 150.33, 148.40, 145.67, 138.09, 135.32, 133.11, 130.62, 124.41, 123.48, 123.00, 121.73, 121.02, 118.47, 114.50, 108.42, 56.46. MS: 475.98 [M+1]⁺.

*2-(3-(4-bromo-3-nitrophenyl)-1-(4-bromophenyl)-1*H*-pyrazol-4-yl)-5-(pyridin-3-yl)-1,3,4-oxadiazole (**5e**)*

Molecular formula: C₂₂H₁₂Br₂N₆O₃. Yield: 64%. IR (ν_{\max} cm⁻¹): 3104, 3063, 1618, 1532. ¹H NMR (δ ppm): 9.60 (s, 1H), 9.19 (s, 1H), 8.83 (s, 1H), 8.43- 8.41 (d, 1H), 8.38-8.36 (d, 1H), 8.04-8.02 (d, 1H), 7.98-7.96 (d, 1H), 7.82-7.73 (dd, 2H), 7.69-7.66 (dd, 2H), 7.60-7.55 (m, 1H); ¹³C NMR (δ ppm): 164.93, 164.45, 153.00, 150.13, 149.45, 147.67, 137.58, 134.46, 133.09, 132.28, 131.14, 129.47, 128.17, 126.98, 124.88, 123.96, 121.44, 120.76, 120.33, 107.02. MS: 569.11 [M+1]⁺.

*2-(1-(4-bromophenyl)-3-(4-(methylthio)phenyl)-1*H*-pyrazol-4-yl)-5-(pyridin-3-yl)-1,3,4-oxadiazole (**5f**)*

Molecular formula: C₂₃H₁₆BrN₅OS. Yield: 87%. IR (ν_{\max} cm⁻¹): 3123, 3015, 1629, 1599. ¹H NMR (δ ppm): 9.56 (s, 1H), 9.18 (s, 1H), 8.83-8.82 (d, 1H), 8.39- 8.36 (m, 1H), 8.32-8.21 (d, 1H), 8.09-8.00 (dd, 2H), 7.84-7.78 (dd, 4H), 7.70-7.66 (dd, 2H), 2.84 (s, 3H). ¹³C NMR (δ ppm): 164.74, 164.38, 152.83, 147.67, 147.55, 138.22, 134.61,

1 133.84, 133.05, 132.35, 130.00, 124.93, 123.99, 121.34, 120.66, 120.37, 118.51,
2 106.72, 21.53. MS: 491.14 [M+1]⁺.
3
4
5
6
7
8
9

10
11
12
13
14
15
16
17
18
19
20
21
22
23
24
25
26
27
28
29
30
31
32
33
2-(1-(4-bromophenyl)-3-(3-nitrophenyl)-1H-pyrazol-4-yl)-5-(pyridin-4-yl)-1,3,4-
(5g)

34 Molecular formula: C₂₂H₁₃BrN₆O₃. Yield: 61%. IR (ν_{\max} cm⁻¹): 3137, 3082, 1626,
35 1518. ¹H NMR (δ ppm): 9.46 (s, 1H), 9.11 (s, 1H), 8.05-7.96 (dd, 2H), 7.82-7.80 (d,
36 1H), 7.75-7.73 (d, 1H), 7.70-7.66 (dd, 2H), 7.63-7.58 (m, 1H), 7.42-7.38 (dd, 2H), 7.21-
37 7.17 (dd, 2H). ¹³C NMR (δ ppm): 164.32, 164.03, 150.35, 148.40, 145.96, 142.87,
38 138.11, 133.15, 133.00, 132.45, 130.66, 123.53, 123.03, 121.71, 121.07, 119.90,
39 115.01, 106.86. MS: 489.15 [M]⁺.
40
41
42
43
44
45
46
47

48
49
50
51
52
53
54
55
2-(1-(4-bromophenyl)-3-(4-nitrophenyl)-1H-pyrazol-4-yl)-5-(pyridin-4-yl)-1,3,4-
(5h)

56 Molecular formula: C₂₂H₁₃BrN₆O₃. Yield: 68%. IR (ν_{\max} cm⁻¹): 3141, 3059, 1629,
57 1514. ¹H NMR (δ ppm): 9.02 (s, 1H), 7.99-7.98 (d, 2H), 7.95-7.92 (d, 2H), 7.75-7.71
58 (dd, 4H), 7.31-7.28 (d, 2H), 6.83-6.80 (d, 2H). ¹³C NMR (δ ppm): 164.95, 164.14,
59 156.96, 147.02, 144.93, 143.57, 139.74, 138.58, 133.06, 132.28, 129.88, 121.11,
60 120.17, 116.65, 114.24, 109.88, 40.66, 40.45, 40.24, 40.03, 39.82, 39.60, 39.39. MS:
61 489.16 [M]⁺.
62
63
64
65

66
67
68
69
70
71
72
73
2-(1-(4-bromophenyl)-3-(4-chlorophenyl)-1H-pyrazol-4-yl)-5-(pyridin-4-yl)-1,3,4-
(5i)

74 Molecular formula: C₂₂H₁₃BrClN₅O. Yield: 77%. IR (ν_{\max} cm⁻¹): 3082, 1626, 1603,
75 1510. ¹H NMR (δ ppm): 9.41 (s, 1H), 8.63-8.62 (d, 2H), 8.19-8.17 (dd, 4H), 8.01- 7.91
76
77
78
79
80
81
82
83
84
85
86
87
88
89
90
91
92
93
94
95
96
97
98
99
100

1 (dd, 4H), 7.75-7.72 (dd, 2H). ^{13}C NMR (δ ppm): 164.73, 164.03, 149.45, 145.52,
2 143.54, 138.08, 137.66, 135.49, 133.79, 133.16, 132.46, 125.52, 123.08, 121.79,
3 118.36, 107.68. MS: 478.18 [M]⁺.

4
5
6
7 **2-(1-(4-bromophenyl)-3-(4-methoxyphenyl)-1*H*-pyrazol-4-yl)-5-(pyridin-4-yl)-1,3,4-**
8 **oxadiazole (5j)**

9
10 Molecular formula: C₂₃H₁₆BrN₅O₂. Yield: 81%. IR (ν_{\max} cm⁻¹): 3074, 3011, 1614,
11 1518. ^1H NMR (δ ppm): 9.26 (s, 1H), 8.95-8.80 (dd, 2H), 8.02-7.92 (dd, 2H), 7.72-7.70
12 (d, 2H), 6.97-6.95 (d, 2H), 6.84-6.78 (dd, 4H), 3.65 (s, 3H); ^{13}C NMR (δ ppm): 164.28,
13 164.03, 160.19, 152.64, 145.89, 143.80, 138.70, 132.84, 128.13, 126.42, 121.24,
14 120.47, 119.80, 117.05, 114.66, 107.21, 55.77. MS: 474.20 [M]⁺.

15
16
17 **2-(3-(4-bromo-3-nitrophenyl)-1-(4-bromophenyl)-1*H*-pyrazol-4-yl)-5-(pyridin-4-yl)-**
18 **1,3,4-oxadiazole (5k)**

19
20 Molecular formula: C₂₂H₁₂Br₂N₆O₃. Yield: 66%. IR (ν_{\max} cm⁻¹): 3145, 3078, 1622,
21 1514. ^1H NMR (δ ppm): 9.14 (s, 1H), 8.70 (s, 1H), 8.51- 8.32 (dd, 1H), 8.09-8.06 (dd,
22 1H), 8.01-7.83 (dd, 4H), 7.70-7.67 (dd, 2H), 7.55-7.50 (dd, 2H). ^{13}C NMR (δ ppm):
23 164.10, 164.02, 150.27, 149.83, 138.69, 138.30, 137.63, 134.88, 134.51, 133.00,
24 131.94, 127.03, 121.02, 120.72, 119.90, 117.16, 115.15, 108.83. MS: 569.09 [M+1]⁺.

25
26 **2-(1-(4-bromophenyl)-3-(4-(methylthio)phenyl)-1*H*-pyrazol-4-yl)-5-(pyridin-4-yl)-**
27 **1,3,4-oxadiazole (5l)**

28
29 Molecular formula: C₂₃H₁₆BrN₅OS. Yield: 75%. IR (ν_{\max} cm⁻¹): 3123, 1670, 1592,
30 1566. ^1H NMR (δ ppm): 9.05 (s, 1H), 8.13-8.09 (dd, 2H), 8.00-7.97 (d, 2H), 7.78-7.75
31 (d, 2H), 7.30-7.25 (dd, 2H), 7.22-7.16 (dd, 4H), 2.09 (s, 3H). ^{13}C NMR (δ ppm):
32 164.82, 164.22, 146.09, 145.55, 143.73, 142.68, 138.51, 132.98, 129.62, 128.76,

126.89, 121.83, 121.05, 120.08, 120.02, 108.39, 40.60, 40.39, 40.18, 39.97, 39.76,
39.56, 39.35, 31.17. MS: 490.97 [M]⁺.

5-(4-(methylthio)phenyl)-1,3,4-oxadiazol-2-amine (**5m**)

Molecular formula: C₉H₉N₃OS Yield: 55%. IR (ν_{max} cm⁻¹): 3465, 3353, 3137, 1596, 1536; ¹H NMR (δ ppm): 7.80 (s, 2H), 7.18-7.09 (dd, 4H), 2.34 (s, 3H); ¹³C NMR (δ ppm): 169.34, 161.23, 137.62, 128.27, 127.25, 122.17, 21.54. MS: 207.04 [M]⁺.

5-(5-amino-1,3,4-oxadiazol-2-yl)-2-methoxyphenol (**5n**)

Molecular formula: C₉H₉N₃O₃. Yield: 65%. IR (ν_{max} cm⁻¹): 3429, 3196, 1609, 1501. ¹H NMR (δ ppm): 7.60 (s, 2H), 7.23 (s, 1H), 7.12-7.11 (d, 1H), 7.04-7.02 (d, 1H), 4.26 (s, 1H), 3.86 (s, 3H); ¹³C NMR (δ ppm): 169.28, 162.03, 148.39, 147.48, 119.85, 115.08, 113.35, 108.60, 55.77. MS: 207.14 [M]⁺.

5-(2,5-dimethoxyphenyl)-1,3,4-oxadiazol-2-amine (**5o**)

Molecular formula: C₁₀H₁₁N₃O₃. Yield: 49%. IR (ν_{max} cm⁻¹): 3110, 3080, 1603. ¹H NMR (δ ppm): 7.74 (s, 2H), 7.42-7.38 (dd, 2H), 7.19-7.17 (d, 1H), 3.75 (s, 6H); ¹³C NMR (δ ppm): 168.13, 165.08, 156.21, 150.47, 120.33, 117.70, 111.26, 109.69, 56.75, 56.41.

1-(5-amino-1,3,4-oxadiazol-2-yl)naphthalen-2-ol (**5p**)

Molecular formula: C₁₂H₉N₃O₂. Yield: 61%. IR (ν_{max} cm⁻¹): 3402, 3253, 3130, 1685, 1596. ¹H NMR (δ ppm): 10.18 (s, OH), 9.15-9.09 (d, 1H), 8.81-8.56 (m, 2H), 7.95 (s, 2H), 7.89-7.87 (d, 1H), 7.76-7.73 (dd, 2H); ¹³C NMR (δ ppm): 168.61, 163.91, 156.27, 154.82, 132.66, 131.82, 130.55, 128.48, 127.73, 125.78, 123.49, 123.36, 119.58. MS: 228.14 [M+1]⁺.

1
2
3
4
5
6
7
8
2.5. DNA binding and antibacterial study

9
The Calf-thymus DNA interactions and antibacterial were studied by previous reported
10 methods [28, 29].
11

12
2.6. MTT Assay of the compound 5f
13
14

15 RAW 264.7 macrophages were cultured in DMEM media supplemented with 10%
16 fetal bovine serum (FBS) and 1% antibiotics. The cells were maintained in a
17 humidified incubator at 37°C with 5% CO₂. Cells were plated in 96-well plates. The
18 compound **5f** was dissolved in dimethyl sulfoxide (DMSO) to prepare stock solutions.
19 Different concentrations (10, 50, 100, 250, 500 µg/mL) of **5f** were added to the wells,
20 and the cells were treated for 24 hours. Cell viability was assessed using the MTT (3-
21 (4,5-dimethylthiazol-2-yl)-2,5-diphenyltetrazolium bromide) assay. After 24 hours,
22 MTT solution was added to each well, and plate was incubated for 3 hours in CO₂
23 incubator. The formazan crystals formed were solubilized in DMSO. Absorbance was
24 measured at 570 nm using a microplate reader.
25
26
27
28
29
30
31
32
33
34
35
36
37

38
2.7. Molecular modelling
39
40

41 Desmond module of Schrödinger Release 2022-4 on the Linux system was employed
42 to evaluate the interactions between compounds **5e** and **5f** using molecular dynamic
43 simulation. To verify the structural integrity of the protein complex, we were used
44 optimized potentials for liquid simulations (OPLS4) force field at pH 7.4. To identify
45 better binding complexes, we performed 100ns simulations, starting by solvating the
46 selecting protein and complex with water molecules, with an orthorhombic box serving
47 as the complex's boundaries. To counterbalance the charges and keep the salt
48 concentration at 0.15M, we added Na⁺ and Cl⁻ charges. The simulation was finished
49
50
51
52
53
54
55
56
57
58
59
60
61
62
63
64
65

1 with a mainlining recorder interval of 5 ps, at 300 K temperature and 1.01325 bar
2 pressure. Using RMSD and RMSF, we were able to ascertain the protein-ligand
3 interactions and assess the stability of the ligand protein complex.
4
5
6
7
8

9 **3. Results and Discussion**

10 **3.1. Chemistry**

11 The synthesized compounds **4a-4d** in previous work and newly synthesized **4e-4l** were
12 used for cyclization in the presence of iodobenzene diacetate yield the final products
13 **5a-5l** and is shown in **Scheme 1**. While the derivatives **5m-5p** were synthesized by
14 reaction between semicarbazide hydrochloride and aromatic aldehydes in presence of
15 NaOAc to get the compounds **4m-4p**. Further, analogs **4m-4p** were cyclized in
16 presence of bromine and sodium acetate yield the oxadiazole **5m-5p** and proposed
17 structure of the derivatives is depicted in **Scheme 2**.
18
19

20 ¹H NMR spectra of analogs **5a-5l** were recorded in DMSO-*d*₆. A peak observed at 9.42-
21 9.02 ppm as singlet (s) due the presence of CH=C proton of pyrazole derivatives **5a-5l**.
22 The absence of the peak of -NH proton which in range of 12.31-10.09 ppm, confirms
23 cyclization of **4a-4l** into oxadiazole target compounds. The -NH₂ proton in oxadiazole
24 derivatives **5m-5p** gives a singlet proton in range of 7.95-7.60 ppm.
25
26

27 ¹³C NMR spectra of analogs **5a-5l** were recorded in DMSO-*d*₆ and characteristic carbon
28 signal on the oxadiazole ring was found in the region of 164.95-162.48 ppm. The carbon
29 signal on the oxadiazole ring of derivatives **5m-5p** shows characteristic peak in the
30 range of 169.34-161.23 ppm. The ¹H and ¹³C NMR spectra of lead compound **5e** and
31 **5f** is presented in **Figure 1** and **2**, respectively. The FT-IR and remaining ¹H and ¹³C
32 NMR spectra were given in **S1** and **S2** respectively. The mass spectra of all compounds
33 were also shown in **S3**.
34
35
36
37
38
39
40
41
42
43
44
45
46
47
48
49
50
51
52
53
54
55
56
57
58
59
60
61
62
63
64
65

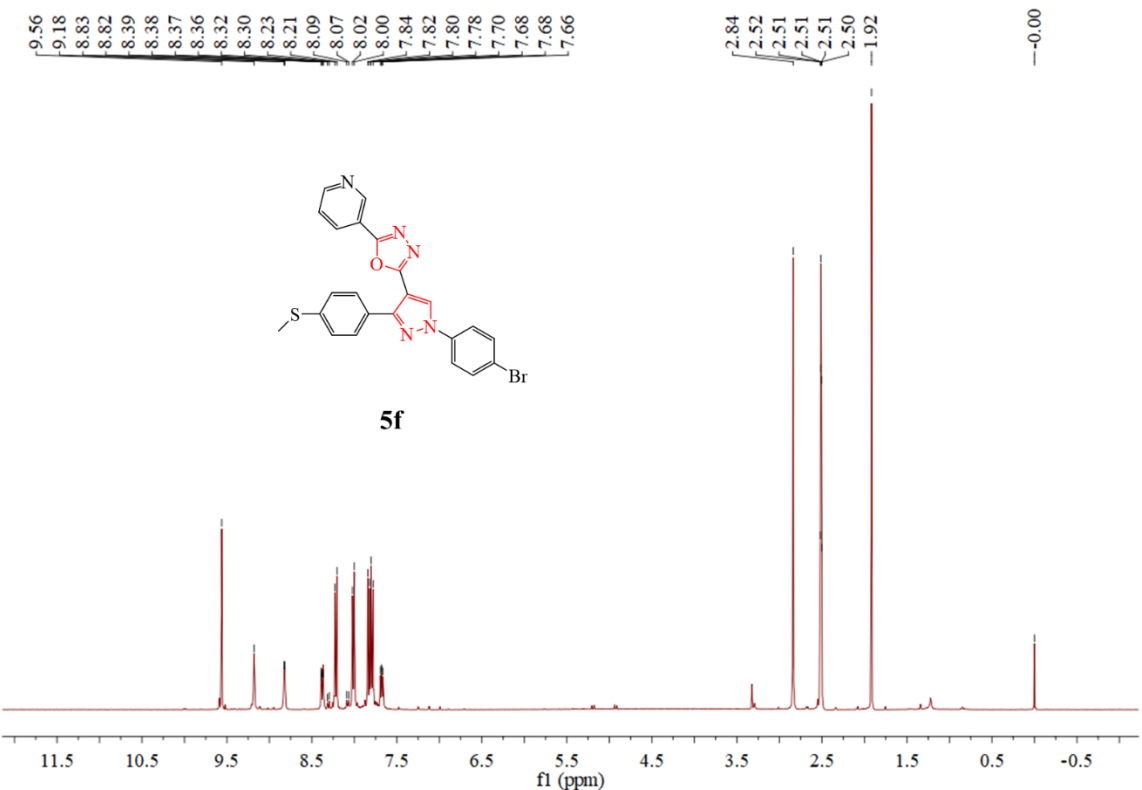
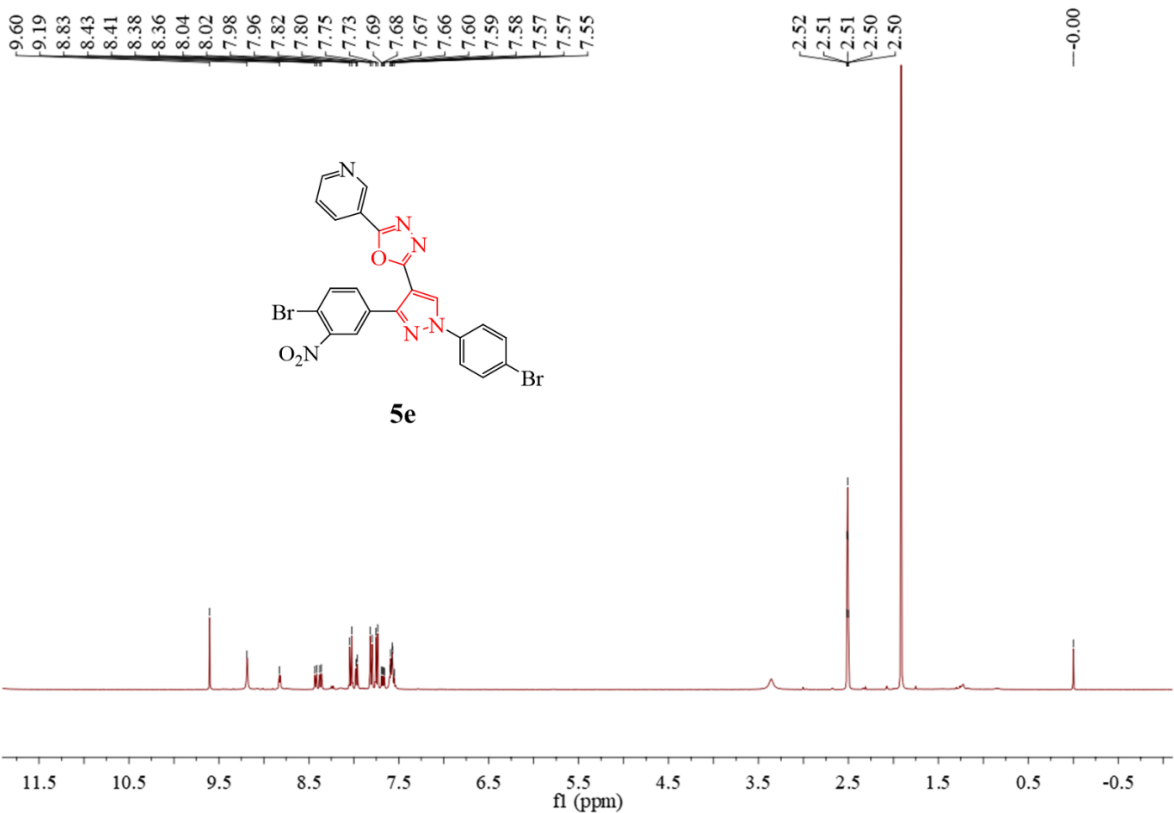


Figure 1. ^1H NMR spectra of analogs **5e** and **5f**.

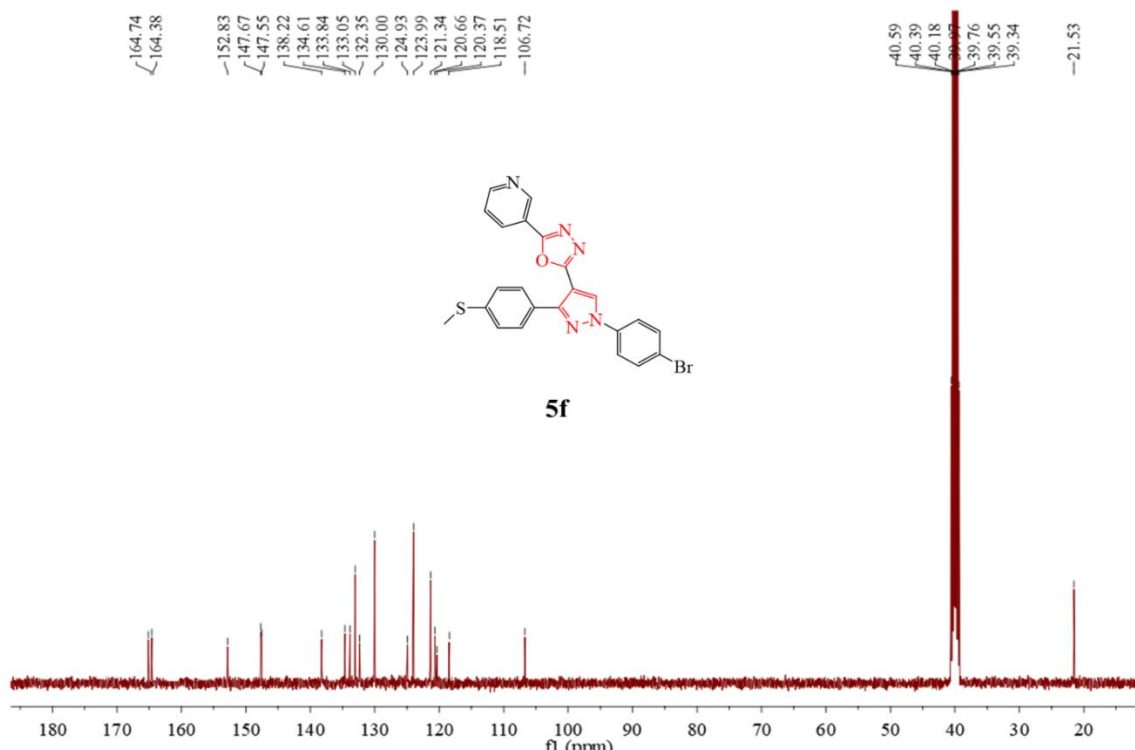
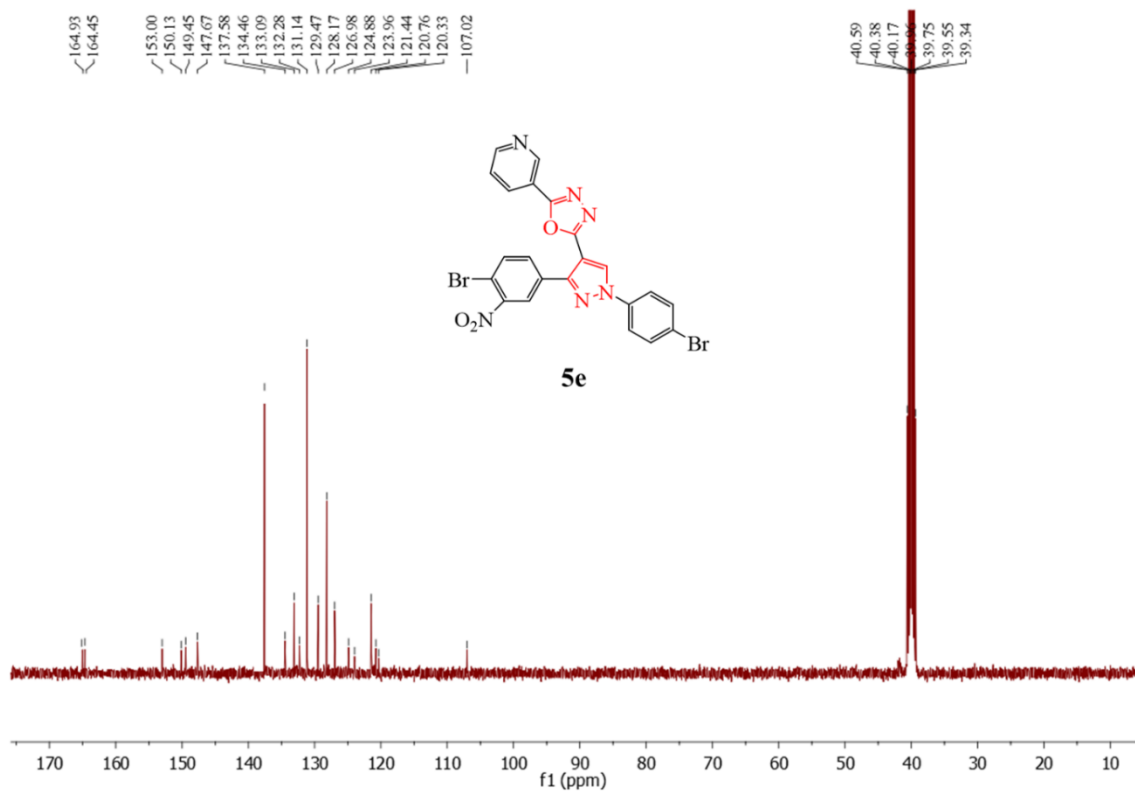


Figure 2. ^{13}C NMR spectra of analog **5e** and **5f**.

1
2 **3.2. In vitro Antibacterial Activity**
3
4
5
6
7

8 **3.2.1. Disc diffusion**
9
10
11
12
13
14
15
16
17
18
19
20
21
22
23
24
25
26
27
28
29
30
31
32
33
34
35
36
37
38
39
40
41
42
43
44
45
46
47
48
49
50
51
52
53
54
55
56
57
58
59
60
61
62
63
64
65

In this paper, the screening of compounds **4e**, **4f**, **4g-4l**, **5a-5l** and **5m-5p** was performed by disc diffusion method. A zone of inhibition for all the compounds against the bacterial strain are given in **Table 1**. In isonicotinichydrazide based derivatives (**4g-4l**) only the compound **4g** showed 13mm ZOI against *B. subtilis* and compound **4j** with 11 and 10mm against *B. subtilis* and *S. aureus* bacteria. The analogs **5b**, **5g**, **5k**, **5m**, **5n**, and **5p** do not show any inhibition against bacterial strains, respectively. The derivatives **5a**, **5c**, **5d**, **5e**, **5f**, **5h**, **5i**, **5j**, **5l**, and **5o** gave a considerable ZOI against all four tested microbial strains. The analog **5a**, **5d**, **5e**, **5f**, **5h** and **5o** displayed 10-30 mm ZOI against these bacterial strains. Compounds **5j** and **5l** exhibited inhibition against *B. subtilis* and *S. aureus*. Compound **5d** displayed antibacterial activity against all strains except *P. aeruginosa* while analog **5i** exhibited inhibition only against *E. coli*. Furthermore, compound **5c** observed a clear zone of inhibition against *E. coli* and *B. subtilis*. Based on preliminary screening, analogs **5a**, **5c**, **5d**, **5e**, **5f**, **5h**, **5i**, **5j**, **5l** and **5o** were selected for further studies of antibacterial properties.

Table 1. Preliminary screening of oxadiazole derivatives **5a-5p** (ZOI in mm).

Compounds	Gram positive bacteria		Gram negative bacteria	
	<i>B. subtilis</i>	<i>S. aureus</i>	<i>P. aeruginosa</i>	<i>E. coli</i>
4e	-	-	-	-
4f	-	-	-	-
4g	13	-	-	-
4h	-	-	-	-

1	4i	-	-	-	-
2	4j	11	10	-	-
3	4k	-	-	-	-
4	4l	-	-	-	-
5	5a	25	15	24	25
6	5b	-	-	-	-
7	5c	24	-	-	21
8	5d	14	13	-	18
9	5e	30	19	11	27
10	5f	30	20	12	25
11	5g	-	-	-	-
12	5h	27	17	18	27
13	5i	-	-	-	08
14	5j	13	14	-	-
15	5k	-	-	-	-
16	5l	14	12	-	-
17	5m	-	-	-	-
18	5n	-	-	-	-
19	5o	18	20	11	10
20	5p	-	-	-	-
21	CIP	16	25	15	17

44 **3.2.2. Percent (%) inhibition method**

45
46 Effective inhibition against *B. subtilis*, *S. aureus*, *P. aeruginosa* and *E. coli* bacteria
47 strains was determined through the % inhibition method. From the Table 2, we
48 summarised that most of the compounds had an inhibitory effect on *B. subtilis* greater
49 than 90% inhibition except compound **5d** (38%) and **5j** (85%), and CIP used as standard
50 drug. Analogs **5e**, **5f**, and **5h** showed 100% inhibition against *B. subtilis*, and *E. coli*,
51 while the analog **5a** and **5o** only against *B. subtilis*. Compounds **5e** and **5f** also
52
53
54
55
56
57
58
59
60
61
62
63
64
65

displayed 100% inhibition against *P. aeruginosa*, however, after treatment with **5c** and **5d**, no substantial suppression of *P. aeruginosa* was detected. Additionally, it was observed that compounds **5c**, **5j**, and **5l** displayed less efficiency against *E. coli* (15%), *P. aeruginosa* (12 %), and *S. aureus* (19%), respectively (**Table 2**). The compounds **5a**, **5e**, **5f**, **5h**, and **5o** have the highest effect on inhibition (100%) against the tested isolates, according to the % inhibition study which were chosen as the lead for further studies.

Table 2. Antibacterial activity of most active analogs against different strains of bacteria at concentration of 250 µg/mL.

Compounds	<i>B. subtilis</i>	<i>S. aureus</i>	<i>E. coli</i>	<i>P. aeruginosa</i>
4g	100	11	18	00
4j	100	85	58	15
5a	100	52	45	85
5c	92	86	00	15
5d	38	42	00	00
5e	100	72	100	100
5f	100	85	100	100
5h	100	66	80	100
5j	85	62	12	52
5l	94	19	92	57
5o	100	94	85	87
AMP	100	100	100	100
CIP	100	100	100	100

3.2.3. MIC and MBC determination

This study was performed according to the standard protocol of NCCLS using the conventional broth dilution method [30-32]. For this study only those compounds were selected which showed 80–100% inhibition at 250 μ g/mL concentration against all four bacterial strains. Compounds **5a**, **5e**, **5f**, **5h**, and **5o** demonstrated excellent percentage inhibition in all assessments of their antibacterial activity. With MIC values ranging from 16 to 128 μ g/mL, compounds **5e** and **5f** showed good activity in these bacterial isolates under investigation, while compound **5h** showed moderate activity between 32 to 128 μ g/mL. In keeping with the outcomes that were attained, the compound **5a** and **5o** were shown to be the least inhibition 256-1024 μ g/mL. Compound **5e** and **5f** demonstrated the highest activity (MIC = 16 μ g/mL) against *B. subtilis* and *E. coli* strain. Also, both compounds **5e** and **5f** showed considerable activity (MIC = 32-128 μ g/mL) against *B. subtilis* and *E. coli*. The MBC values of compounds **5a**, **5e**, **5f**, **5h**, and **5o** were also calculated and the results demonstrate that the compound **5a** and **5o** showed the least activity (\geq 1024 μ g/mL) while the compound **5h** exhibited considerable MBC value (32-256 μ g/mL). The MBC value for both analogs **5e** and **5f** was found to be 32 μ g/mL (*E. coli*) and 16 μ g/mL (*B. subtilis*). Based on the above explanation and obtained value of MIC and MBC as given in **Tables 3** and **4**, the findings show that the compounds **5e** and **5f** selectively inhibit the growth of *B. subtilis* and *E. coli*., leading us to conclude that they have strong antibacterial activity against these strains.

Table 3. MIC values in μ g/mL of most active screened compounds.

Bacterial strains	MIC values in μ g/mL						
	5a	5e	5f	5h	5o	AMP	CIP
<i>B. subtilis</i>	256	32	16	64	256	4	1
<i>S. aureus</i>	512	128	128	128	256	8	0.5

<i>P. aeruginosa</i>	1024	32	32	64	512	16	2
<i>E. coli</i>	256	16	32	32	512	8	4

Table 4. MBC values in $\mu\text{g/mL}$ of the selected compounds.

Bacterial Strains	5a	5e	5f	5h	5o
<i>B. subtilis</i>	>1024	128	16	128	>1024
<i>S. aureus</i>	>1024	128	256	256	>1024
<i>P. aeruginosa</i>	>1024	64	32	32	>1024
<i>E. coli</i>	1024	32	32	32	>1024

3.2.4. Disc diffusion assay

After calculation of MIC and MBC at $250\mu\text{g/mL}$ concentration, we found that the compounds **5e** and **5f** have the highest inhibition activity, next, we assess ZOI at concentrations equivalent to $\frac{1}{2}\text{MIC}$, MIC, and 2MIC . The measured clear ZOI surrounding the disc for each of the four tested bacterial strains was found to be between 08 and 30 mm, as indicated in **Table 5**. Compound **5e** showed maximum ZOI at all the three concentrations was found to be 20, 21, and 30mm against *E. coli*, while compound **5f** with 12, 20, and 22mm against *B. subtilis* respectively. Compound **5e** appearances significant ZOI at all concentrations except *S. aureus* with no zone of inhibition at $\frac{1}{2}\text{MIC}$, MIC. Compound **5f** also displayed a sufficient zone of inhibition in of all concentrations against the rest of the strains (10-19mm).

Table: 5. ZOI (in mm) of the selected compounds.

Compounds	Bacterial strain	ZOI of test Compounds		
		½MIC	MIC	2MIC
5e	<i>B. subtilis</i>	08	09	12
	<i>S. aureus</i>	00	00	14
	<i>P. aeruginosa</i>	10	18	20
	<i>E. coli</i>	20	21	30
5f	<i>B. subtilis</i>	12	20	22
	<i>S. aureus</i>	10	12	13
	<i>P. aeruginosa</i>	11	14	19
	<i>E. coli</i>	10	11	19

3.2.5. Combination study

The *in vitro* antibacterial activity of compounds **5e** and **5f** in combination with the traditional antibiotic CIP against all of the aforementioned bacteria was also assessed. In disc diffusion method the compound **5e** showed a 16µg/mL against *E. coli* but after combination with CIP, the MIC value becomes decreased and gives greater activity with 2µg/mL, however against all strains the value also becomes lowered from 32-128µg/mL to 8-32µg/mL (**Table 6**). Like compound **5e**, analog **5f** also showed great inhibition when combined with CIP. The MIC value for compound **5f** was also lowered from 16 to 4µg/mL against *B. subtilis* when combined with CIP suggesting that the mode of interaction is synergistic (**Table 7**). Compound **5e** and **5f** demonstrated enhanced activity against all examined strains when combined with CIP. Compound **5e** exhibited the synergistic mode of interaction against *E. coli* and *P. aeruginosa* ($FICI \leq 0.5$); and is indifferent towards *S. aureus* and *B. subtilis* ($FICI > 0.5$ but < 4), whereas compound **5f** showed the synergistic mode of interaction against all bacteria except *S. aureus*. The outcomes show that compounds **5e** and **5f** work well together with the

widely used drug CIP, suggesting that treating resistant bacterial strains with a combination of procedures may be successful.

Table 6. Combination studies of compound **5e** with standard drug ciprofloxacin (CIP).

Strains	MIC without CIP ($\mu\text{g/mL}$)		MIC with CIP ($\mu\text{g/mL}$)		FICI/ TOI
	5e	CIP	5e	CIP	
<i>B. subtilis</i>	32	1	8	0.5	0.75 / I
<i>S. aureus</i>	128	0.5	32	0.25	0.75 / I
<i>P. aeruginosa</i>	32	2	8	0.125	0.31 / S
<i>E. coli</i>	16	4	2	0.5	0.25 / S

Table 7. Combination studies of compound **5f** with standard drug ciprofloxacin (CIP).

Bacterial strains	MIC without CIP ($\mu\text{g/mL}$)		MIC with CIP ($\mu\text{g/mL}$)		FICI/ TOI
	5f	CIP	5f	CIP	
<i>B. subtilis</i>	16	1	4	0.125	0.37 / S
<i>S. aureus</i>	128	0.5	16	0.5	0.62 / I
<i>P. aeruginosa</i>	32	2	4	0.5	0.37 / S
<i>E. coli</i>	32	4	8	0.25	0.31 / S

I = Indifferent, S = Synergistic; TOI = Type of interaction

3.2.6. Effect on Environmental *E. coli* and MDR isolates

The further study in support of antibacterial activity of compound **5f** was carried out against *E. coli* isolates and Environmental Multidrug-resistant (MDR) bacterial isolates as compare to Ampicillin. The standard drug Ampicillin shows resistant against *E. coli* isolate IA1, IA4, IA12, IA13 and IA22 as compare to compound **5f** which shows considerable zone of inhibition (9-10mm). Compound **5f** doesn't shows any ZOI against IA7, IA15 isolates while rest of the isolates it shows comparable ZOI with

Ampicillin (**Table 8**). In case of MDR isolates compound **5f** shows good ZOI. Against AA200, AA201, AA202, AA216, AA221, AA224, AA269 isolates the compound **5f** shows the ZOI in range of 12-24mm while as in case of the standard drug not obtained

<i>E. coli</i> isolates	5f	Ampicillin
IA 1	10	-
IA 2	12	15
IA 4	10	-
IA 5	10	14
IA 7	-	23
IA 12	9	-
IA 13	10	-
IA 14	11	26
IA 15	-	13
IA 18	9	14
IA 19	11	20
IA 20	10	16
IA 21	9	12
IA 22	10	-
IA 23	10	13
IA 24	10	24
IA 25	10	13

any ZOI against these isolates. With no ZOI compound **5f** against AA243 and AA273 isolates as compare to Ampicillin (**Table 9**). The rest of the MDR isolates shows comparable ZOI with compound **5f** with standard drug Ampicillin.

Table 8: Zone of inhibition (mm) of **5f** against environmental *E. coli* isolates.

MDR isolates	5f	Ampicillin
AA 200	20	-
AA 201	24	-
AA 202	24	-
AA 209	20	30
AA 216	16	-
AA 221	22	-
AA 224	12	-
AA 237	12	26
AA 240	09	23
AA 243	-	20
AA 245	17	18
AA 248	16	25
AA 261	14	25
AA 269	13	-
AA 273	-	15
AA 276	14	22
AA 290	19	-

Table 9: Zone of inhibition (mm) against Environmental Multidrug-resistant bacterial isolates.

3.2.7. Biofilm inhibition assay

Inhibition of Biofilm formation

Biofilms play an important role in virulence and imparting resistance to various bacterial strains and hence, pose a significant hurdle towards treatment of diseases caused by them. The potential of **5f** to inhibit the formation of biofilm by MDR isolates was determined through crystal violet biofilm formation inhibition assay at sub-inhibitory concentrations of $\frac{1}{2}$ MIC, $\frac{1}{4}$ MIC and $\frac{1}{8}$ MIC. It inhibited biofilm formation up to 55% at $\frac{1}{2}$ MIC against AA209 whereas against AA276, inhibition was depicted up to 66%, 15% and 3% at $\frac{1}{2}$ MIC, $\frac{1}{4}$ MIC and $\frac{1}{8}$ MIC respectively (**Figure 3**).

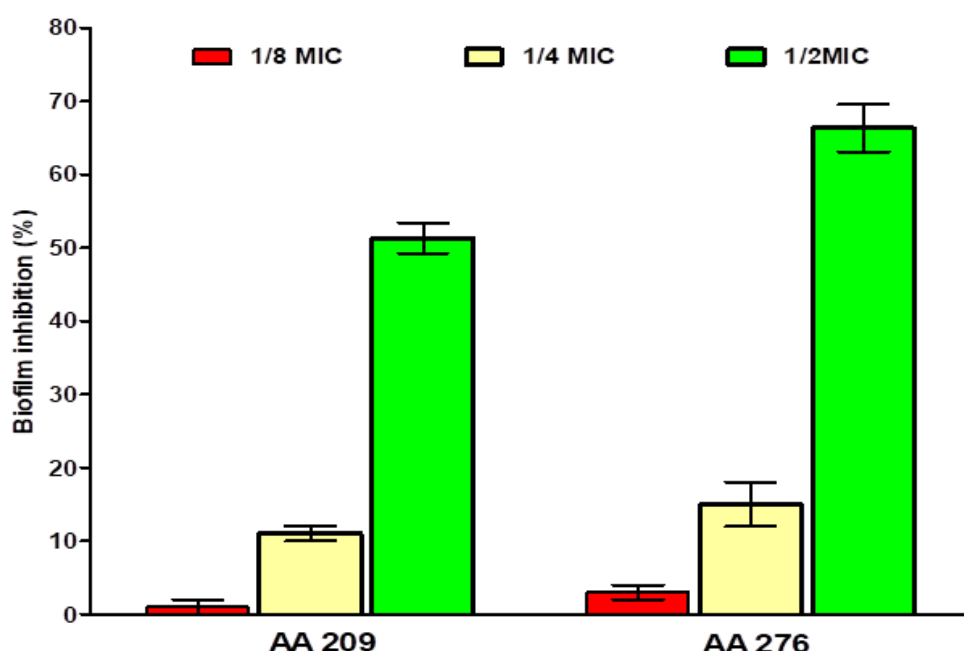
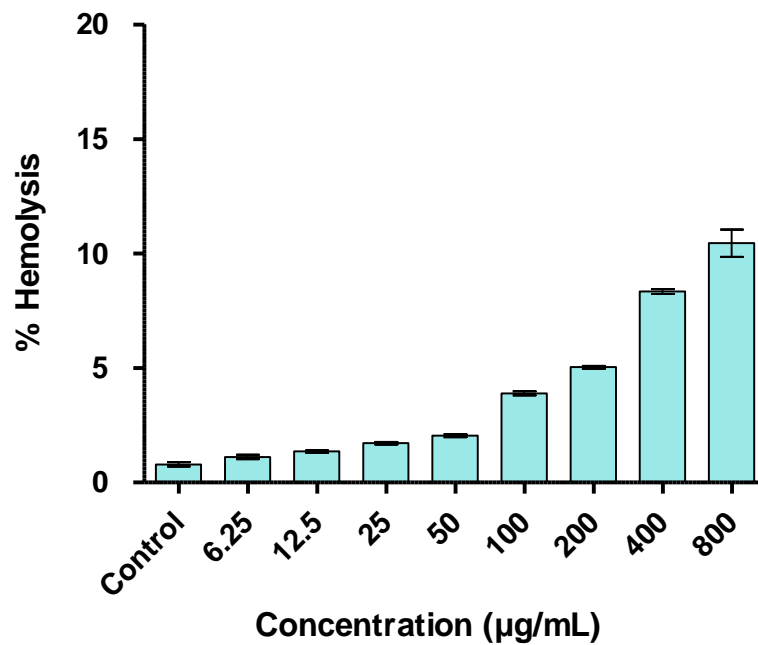


Figure 3: Percent inhibition in biofilm formation against the environmental strain **AA 209** and **AA276**.

3.2.8. Hemolytic assay

Compound **5f** was chosen for the hemolytic assay test based on combination studies. **Figure 4** shows a graphical bar that compares the toxicity of compound **5f** at different concentrations of 6.25, 12.5, 25, 50, 100, 200, 400, and 800 μ g/mL to that of the standard drug CIP (control). Compound **5f** showed less than 10% RBC lyses from 6.25

1 to 400 μ g/mL MIC concentrations due to their low toxicity. Furthermore, compounds
2 **5f** at a higher concentration of 800 μ g/mL showed less than 15% RBC lysis, which could
3 be attributed to their low toxicity. However, at higher concentrations, it was less toxic
4 than ciprofloxacin.
5
6
7
8
9



34 **Figure 4.** Hemolytic assay bar graph to compare compound **5f** to the standard drug CIP.
35
36

37 **3.2.9. MTT Assay of the compound **5f****

38
39
40
41
42
43
44
45
46
47
48
49
50
51
52
53
54
55
56
57
58
59
60
61
62
63
64
65

The outcomes of the MTT assay demonstrated a reduction in cell viability of RAW 264.7 macrophages in a concentration-dependent manner following exposure to **5f**. Specifically, the recorded viability percentages were 96%, 91%, 81%, 54%, and 27% at concentrations of 10, 50, 100, 250, and 500 μ g/mL, respectively (**Figure 5**). Furthermore, it was noted that at a concentration of 100 μ g/mL, the compound exhibited significantly lower toxicity towards the macrophages, suggesting its safety for cellular integrity. We found a concentration-dependent cell viability decrease in RAW 264.7 macrophages following **5f** exposure. However, at lower concentrations (10 and 50 μ g/ml), **5f** exhibits viabilities of 96% and 91%, respectively, suggesting minimal

1
2
3
4
5
6
7
8
9
10
11
12
13
14
15
16
17
18
19
20
21
22
23
24
25
26
27
28
29
30
31
32
33
34
35
36
37
38
39
40
41
42
43
44
45
46
47
48
49
50
51
52
53
54
55
56
57
58
59
60
61
62
63
64
65

cell death. Even at 100 $\mu\text{g}/\text{mL}$, the impact is less severe with 81% cell viability. This implies a safe range for **5f** application, aligning with its Minimum Inhibitory Concentration, 64 $\mu\text{g}/\text{mL}$. Given these results, the utilization of **5f** as an antimicrobial agent seems to have minimal impact on healthy cells, underscoring its potential for therapeutic application with a favorable safety profile.

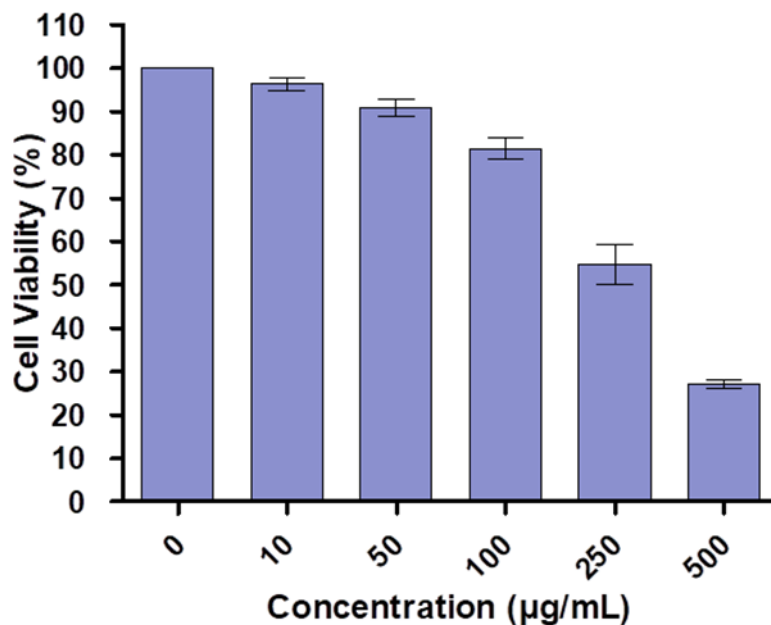


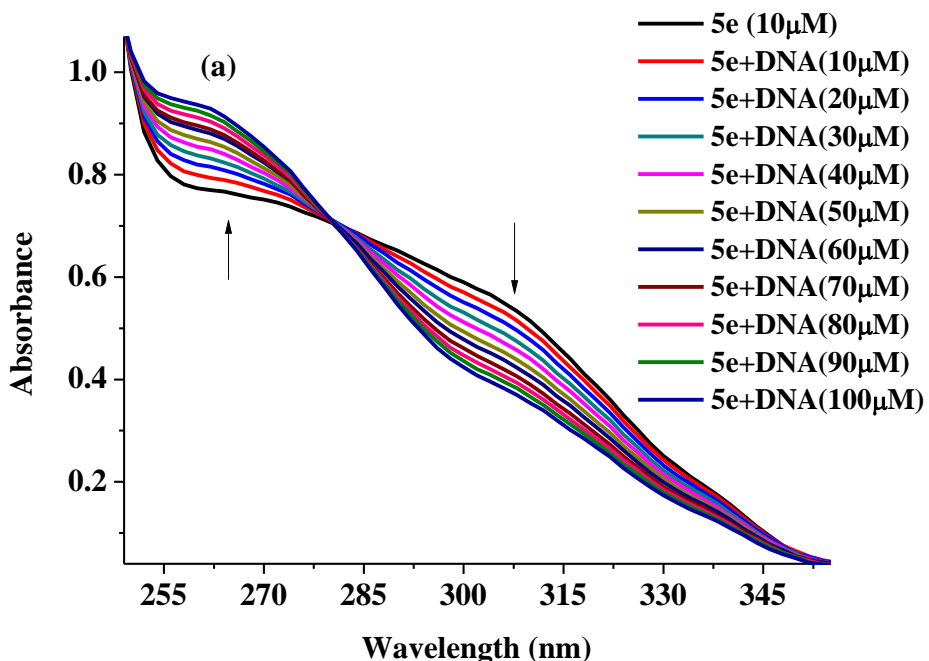
Figure 5: MTT Assay of the compound **5f**

3.3. DNA binding studies

3.3.1. Absorption titration

The analysis of the drug-DNA interaction has been done to comprehend the structural variations in DNA that occurred during the absorption titration in between CT-DNA and compound [33-36]. The absorption spectra of **5e** and **5f** (10 μM) with CT-DNA from 10-100 μM and 10-60 μM , respectively shown in **Figures 6 (a, b)**. In both **Figures 6a** and **6b**, at 260nm wavelength the absorbance peak increases with increase in CT-DNA concentration in both the compounds **5e** and **5f**, while the intensity at 307 and 300nm for compounds **5e** and **5f**, respectively becomes decreased with slight shifting

in wavelength. The decrement in intensity at 307 and 300nm wavelength for compounds **5e** and **5f**, suggests that the compounds and CT-DNA have a binding relationship through intercalation. This hypochromic shift may originate due to $\pi-\pi^*$ transition between the DNA base pair and compound [37]. The data obtained allows for the estimation of the intrinsic efficacy of compounds **5e** and **5f** with CT-DNA. The K_b value of compounds **5e** and **5f** was attained by $[\text{DNA}] / (\varepsilon_a - \varepsilon_f)$ versus $[\text{DNA}]$ plot are shown in **Figure 7 (a, b)**. The K_b values for compounds **5e** and **5f** were found to be 1.07×10^5 and 1.30×10^5 calculated by using Wolf–Shimmer equation.



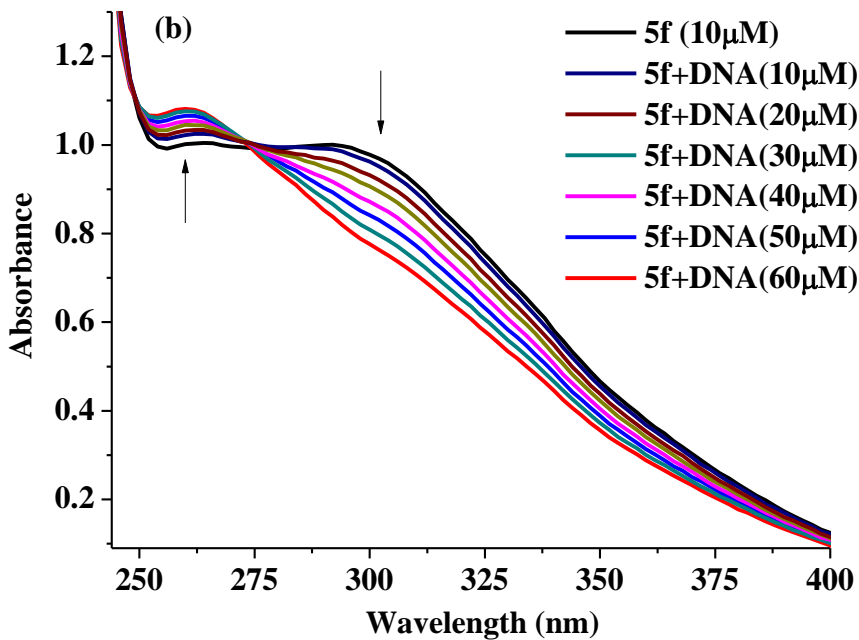
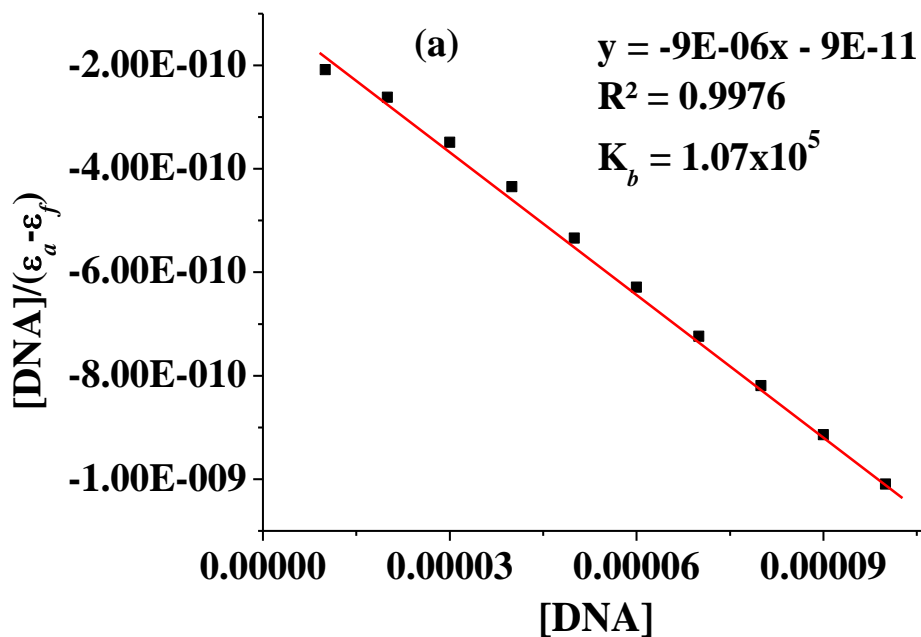


Figure 6. The absorption titration (a) for compound **5e** (10 μ M) and (b) for compound **5f** (10 μ M) with CT-DNA at concentration variation 10-100 μ M and 10-60 μ M, respectively.



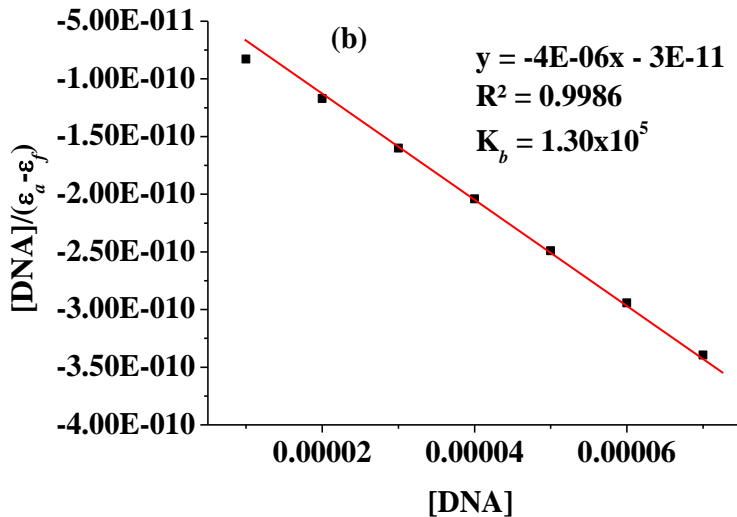


Figure 7. The K_b value (a) for compound **5e** and (b) for compound **5f** by $[\text{DNA}] / (\varepsilon_a - \varepsilon_f)$ vs $[\text{DNA}]$ plot.

3.3.2. Emission studies

Emission spectral analysis is an additional helpful method for the drug binding interaction and CT-DNA [38]. The spectra of emission study of analogs **5e** and **5f**, recorded at varying concentrations with a fixed concentration of CT-DNA (10μM), displayed in **Figure 8 (a, b)**. The titration of compounds **5e** and **5f** (10-90μM) in constant volume of CT-DNA (10 μM) were conducted, and each time the fluorescence intensity in emission peak to be decreased for both the compounds. This study gives the information that after the interaction of compounds with CT-DNA it may be quenching occurs in its internal fluorescence because of the interaction between compound and DNA. For both compounds, a plot of the fluorescence intensity against wavelength in nanometers has been created. The $(F_0 - F)/F$ vs $[C]$ plot gives the slope and intercept value from which we can calculate the K_f value for compounds **5e** and **5f** are 1.84×10^5 and 4.3×10^5 respectively as shown in **Figure 9**.

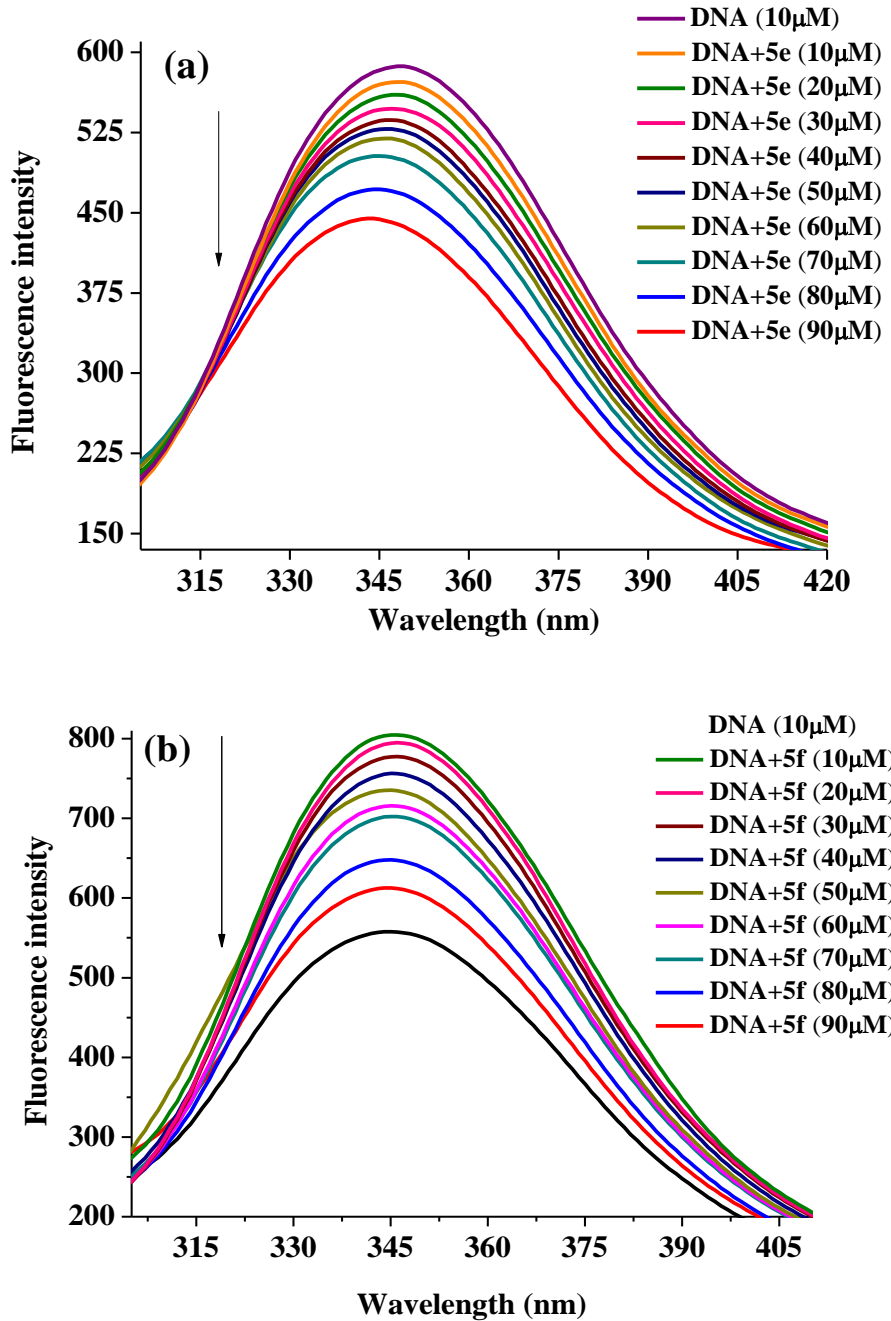


Figure 6. The emission titration study at various concentrations (10-90 μM) of compounds **5e** (a) and **5f** (b) in CT-DNA solutions.

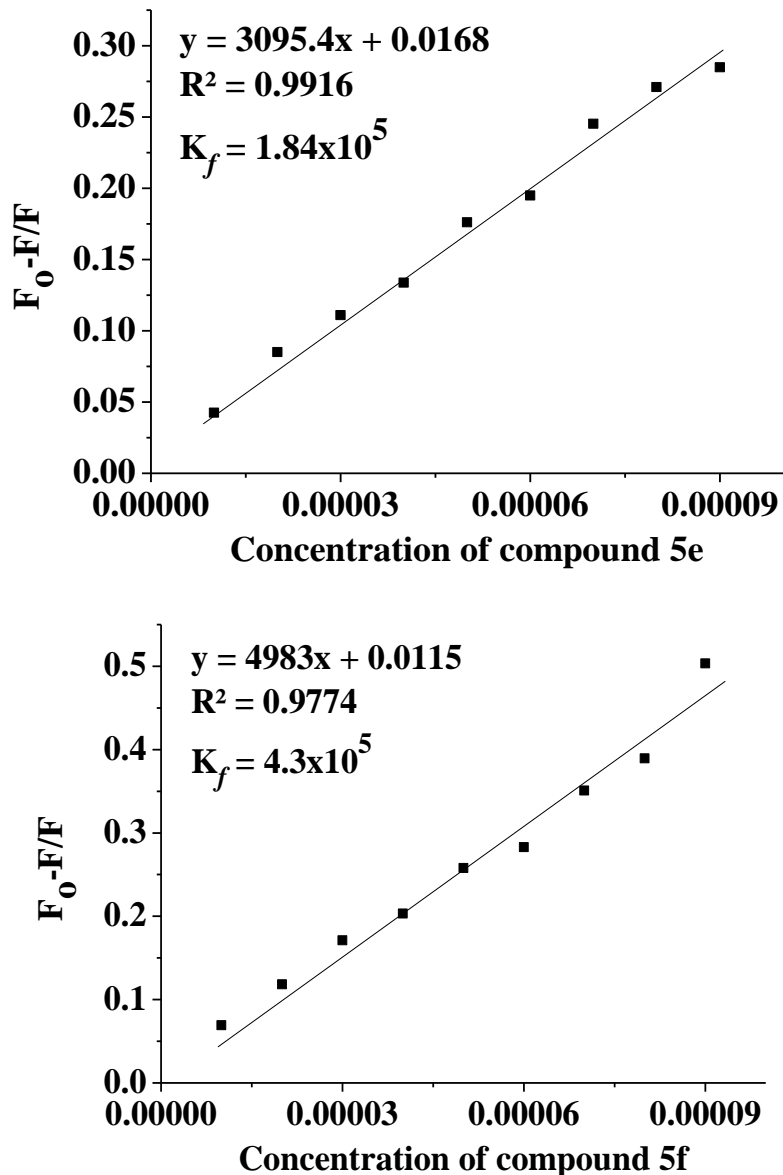


Figure 9. The $(F_0 - F) / F$ vs [C] plot to calculate the K_f value of compound **5e** and **5f**.

3.3.3. Ethidium bromide displacement assay

The intensity of only DNA solution in emission spectrum was found to be very. After the addition of EtBr solution in DNA it showed an intense emission peak at 610 nm wavelength due to the substantial intercalation with CT-DNA's neighbouring base pairs. The literature states that when a compound is added, EtBr/DNA's enhanced fluorescence value can be eliminated because EtBr will have competition to connect to CT-DNA [39-41]. **Figure 10 (a, b)** depicts the binding pattern which is competitive of

1 compounds **5e** and **5f** with ethidium bromide in the 500-750nm region. The obtained
2 diagram shows that the fluorescence emission intensity of EtBr-DNA reduces with the
3 addition of varying concentrations of compounds **5e** (10.0-80.0 μ M) and **5f** (10.0-
4 90.0 μ M). The quenched emission peak shows that both the compound **5e** and **5f**
5 replaced the EtBr at the DNA binding site. The slope determined from Stern-Volmer's
6 equation band gives the K_{sv} value seen in **Figure 11a and 11b** for compounds **5e** and
7 **5f**. From the value of K_{sv} , the K_q value (biomolecular rate constant) was determined.
8 Two mechanisms: static and dynamic quenching are used to describe the behavior of
9 fluorescence quenching based on the values of the limiting diffusion rate constant (K_d
10 = 2.0×10^{10} Lmol $^{-1} \cdot s$) and K_q of the biomolecule. The mechanism should be static
11 quenching, if the $K_q > K_d$ value; else, dynamic quenching occurs [42]. **Table 10** displays
12 the computed K_{sv} and K_q values for compounds **5e** and **5f**. **Table 10** that $K_q > K_d$,
13 indicates that EtBr/DNA fluorescence has been quenched by a static quenching
14 mechanism that has been controlled.

33
34
35 **Table 10.** The values of the bimolecular rate constant (K_q) and the stern-Volmer
36 constant (K_{sv}) for compounds **5e** and **5f**.

Compounds	Stern-volmer constant (K_{sv})	Bimolecular rate constant (K_q)
5e	$7.65 \times 10^4 \text{ M}^{-1}$	$3.3 \times 10^{12} \text{ Lmol}^{-1} \cdot s$
5f	$5.36 \times 10^4 \text{ M}^{-1}$	$2.3 \times 10^{12} \text{ Lmol}^{-1} \cdot s$

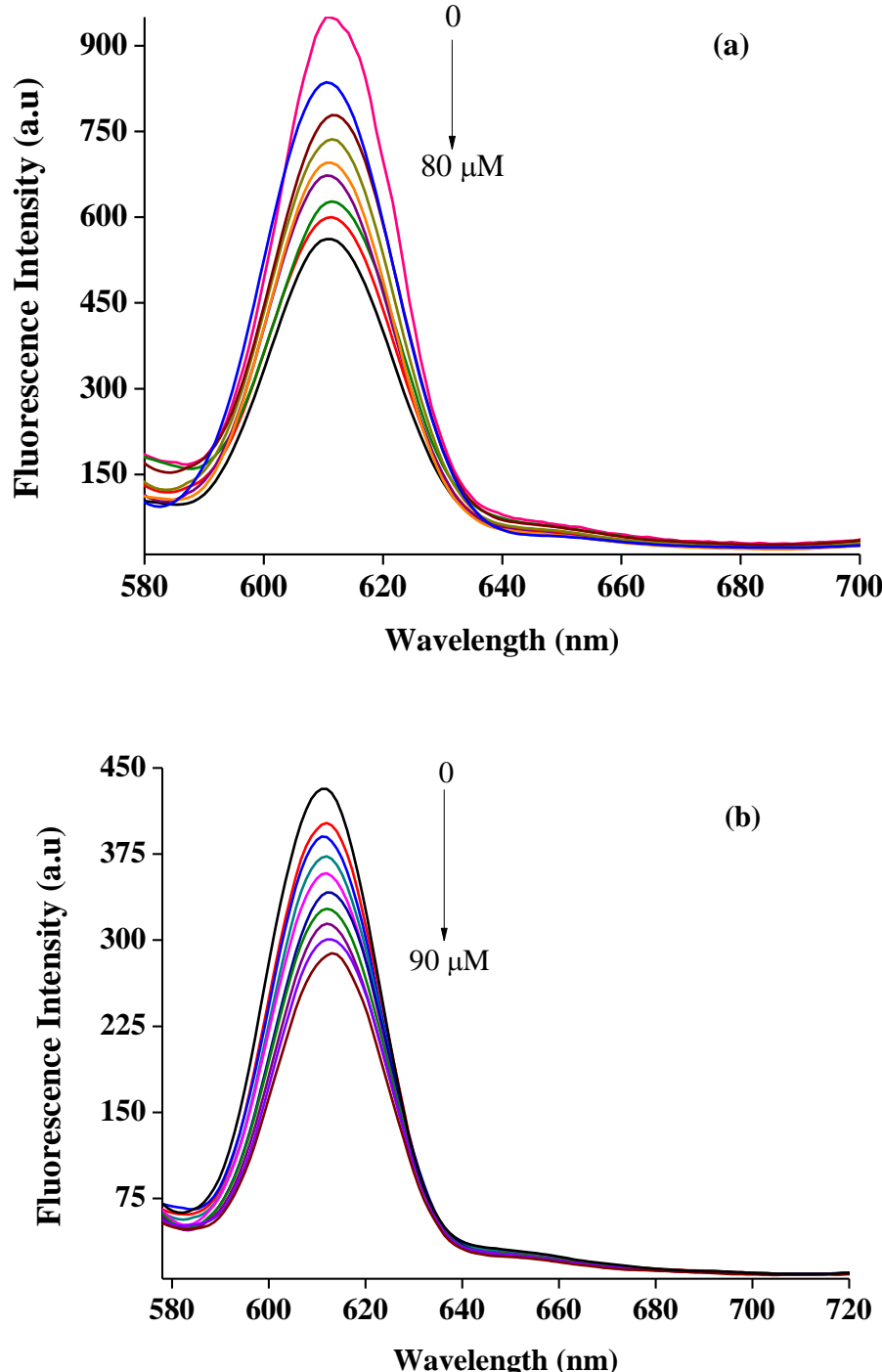


Figure 10. Competitive binding study **(a)** for compound **5e** at 10-80 μ M and **(b)** for compound **5f** at 10-90 μ M in the presence of EtBr/DNA solution.

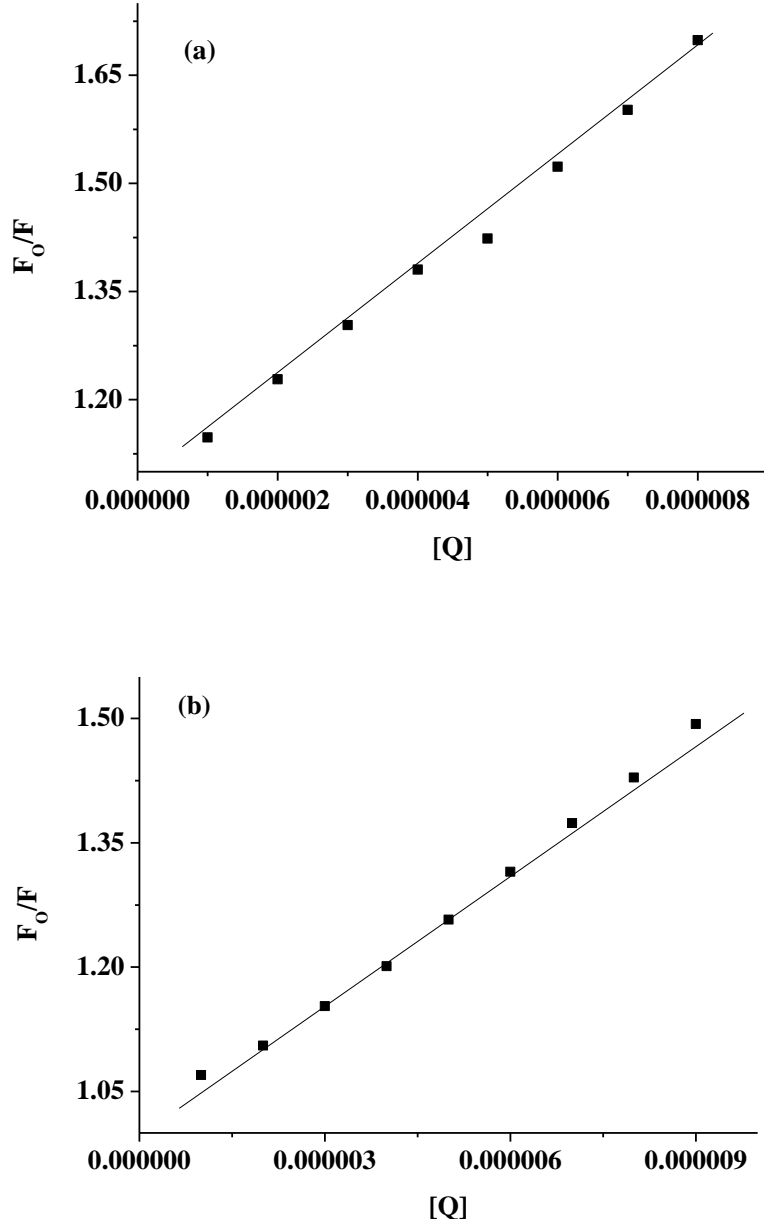
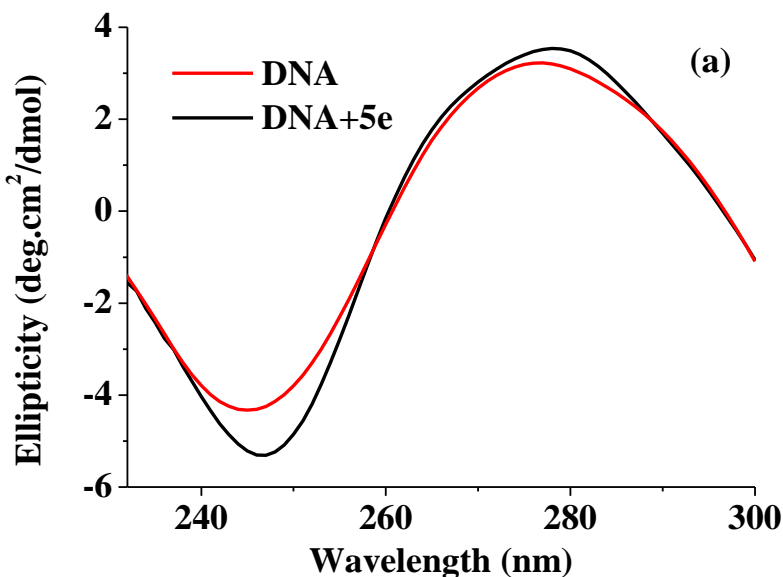


Figure 11. The K_{sv} values (a) for compound **5e** and (b) for compound **5f** by the plot of F_0/F vs $[Q]$.

3.3.4. Circular dichroism studies

The CD spectrum of DNA is known to be highly sensitive to variations in its secondary structures, we can use this technique to investigate conformational changes during binding, as well as the DNA-lead compound binding mode. The positive and negative band at 275 nm and 242 nm, respective, becomes altered after the addition of a

compound to CT-DNA in two ways: first, intercalation, which is caused by a deviation from the nucleotide sequence of DNA; second, slight variation in the 2^0 structure of CT-DNA is caused by electrostatic or groove binding [43-44]. According to **Figure 12 (a, b)**, the addition of compound **5e** and **5f** to CT-DNA resulted in disruptions to the nucleotide base sequences, indicating changes in DNA conformation. DNA base pairs and conformation were shown to alter throughout the binding process between compounds **5e** and **5f**. Additionally, there was a shift in the wavelength-dependent intensity of both positive and negative bands, indicating that the binding mechanism may be either electrostatic or groove-based.



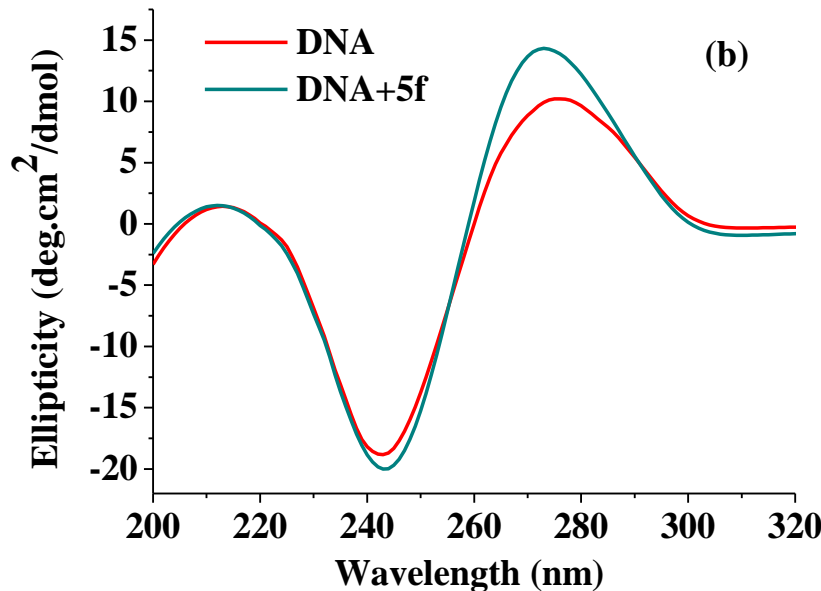


Figure 12. The circular dichroism spectra (**a**) for compound **5e** and (**b**) for compound **5f** with CT-DNA.

3.3.5. Cyclic voltammetric

The cyclic voltammetric (CV) study, providing further validation in the corroboration of the above methodologies. The oxidation-reduction process is used in cyclic voltammetric measurements. The variation in the potential and current peak position confirms the binding of molecule-DNA [45]. **Figure 13 (a, b)** depicts the cyclic voltammograms of compounds **5e** and **5f** with and without DNA. We may conclude from the results that the decrease in current value may be related to the formation of drug-DNA complexes when compound concentration decreases.

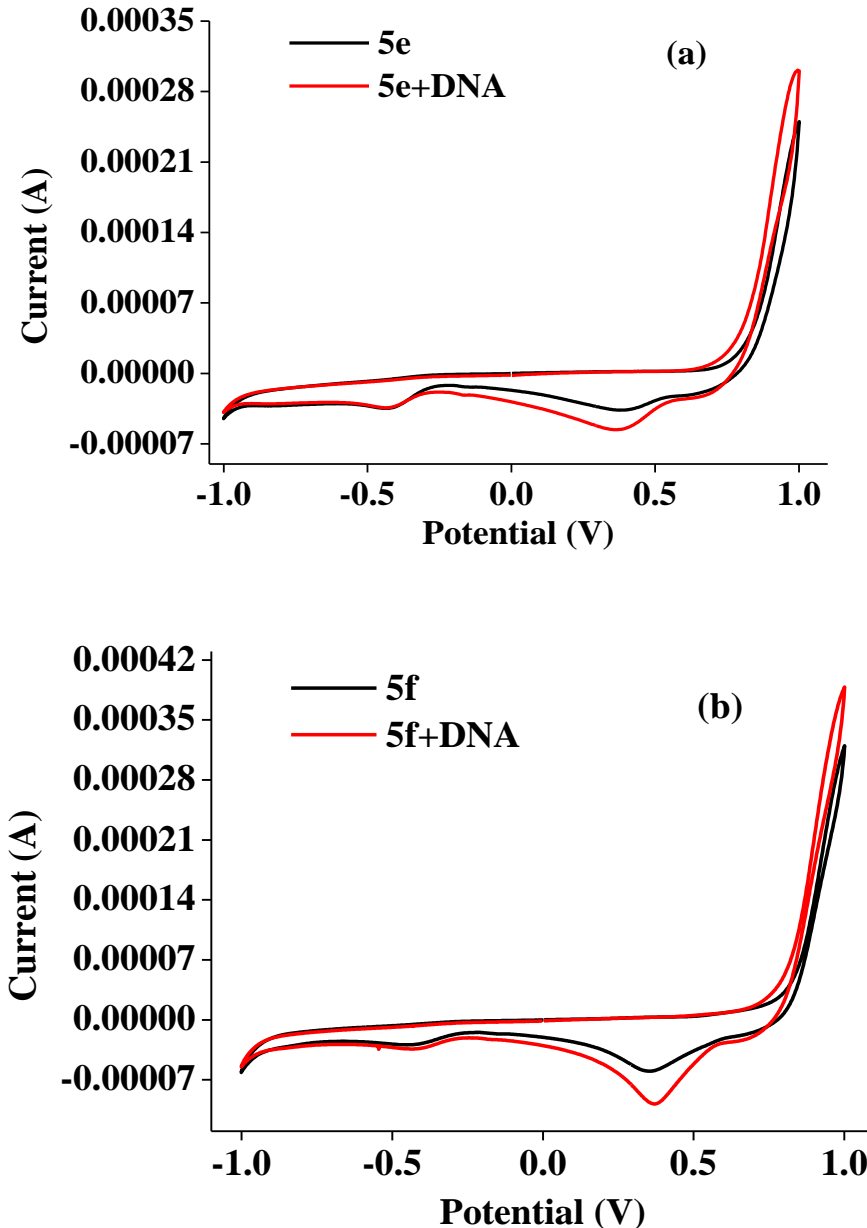


Figure 13. Cyclic voltammogram **(a)** for compound **5e** and **(b)** for compound **5f** with and without CT-DNA.

3.4. Molecular docking

This molecular docking studies can help us to develop ligands that bind to specific proteins and DNA, as well as contribute to our comprehension of the nature of binding [46-48]. To assess the compounds' binding mechanisms, all of the synthesized derivatives **5a–5p** were docked into the DNA gyrase protein's active site (PDB ID:

1 2XCT and PDB ID: BNA). The molecular docking scores and their interactions like
 2 van der Waals, Hydrogen bond (H-bond), Carbon-Hydrogen bond (C-H bond), Pi-
 3 alkyl/alkyl, Pi-Pi T-shaped/stacked of all the compounds **5a–5p** range from -7.8 to -
 4 11.5 kcal/mol for 2XCT and from -6.8 to -9.5 kcal/mol for 1BNA, respectively shown
 5 in **Tables 11 and 12**. The lead compounds **5e** and **5f** exhibit van der Waals interactions
 6 with DC9, DA18, DC15, and DA17 and DG12, DG14, DC11, DC15, DC9, DA17, and
 7 DT19 with docking scores of -9.5 and 9.3 kcal/mol for 1BNA, respectively. DG10 and
 8 DG16 demonstrated the H-bond interaction between compounds **5e** and **5f**. The
 9 compound **5e** tends to interact with SER1084, GLY436, GLY459, ASP437, DT10, and
 10 DC12 in van der Waal mode, with a docking score of -11.5 kcal/mol and a Pi-Pi T-
 11 shaped/stacked direction towards DG9, DT8, and DA13. The second lead compound **5f**
 12 with docking score -11.5 kcal/mol. towards 2XCT was analysed. The compound **5f** was
 13 involved in the formation of three van der Waal interactions with SER1084, DG7, and
 14 DT10; H-bond with DA13; and a Pi-Pi T-shaped/stacked interaction with DG9, DT8,
 15 and PHE1123. **Figure 14** shows the interaction of active compounds **5e** and **5f** with
 16 PDB: 1BNA, and **Figure 15** shows for PDB: 2XCT.
 17

18 **Table 11.** Docking score and interaction mode of compounds **5a–5p** with PDB code:
 19 2XCT.
 20

Comp ound	Binding score (kcal/mol)	2XCT Interaction					
		van der Waals	H-bond	C-H bond	Pi-alkyl/ alkyl	Pi- Cation/ Anion	Pi-Pi T- shaped/ stacked
5a	-11.5	SER1085, SER1084, ARG1122	DG9, GLY 459	ASP437, GLY436, GLY459, DC12	ARG458, DT8	-	DG9, DT8, PHE1123, DA13

1								
2								
3								
4								
5								
6								
7								
8								
9								
10								
11								
12								
13								
14								
15								
16								
17								
18								
19								
20								
21								
22								
23								
24								
25								
26								
27								
28								
29								
30								
31								
32								
33								
34								
35								
36								
37								
38								
39								
40								
41								
42								
43								
44								
45								
46								
47								
48								
49								
50								
51								
52								
53								
54								
55								
56								
57								
58								
59								
60								
61								
62								
63								
64								
65								
	5b	-11.0	ARG458, SER1084, SER1085, DG7, PHE1123, GLY1082, HIS1081	DA13, DG9, DG6, ARG11 22	-	DT8, DA13, DG9	GLU10 88	DC12, DA13, DG9
	5c	-11.4	ASP508, GLY436, ASP437, GLY459, DT 10	-	DC12, DA 13, SER 1084, ARG 1122	DG9, ARG458, PHE 1123	-	DG9, DT8, PHE 1123
	5d	-11.2	ASP 508, GLY 436, GLY 459, DT 10	-	ARG 1122, DG9, DC12, DA 13	ARG 458, PHE 1123	ASP437	DT8, PHE 1123
	5e	-11.5	SER1084, GLY436, GLY459, ASP 437, DT10, DC12	-	ARG458	PHE1123, ARG458	-	DG9, DT8, DA13
	5f	-11.5	SER1084, DG7, DT10	DA13	GLY459, ASP437, GLY436, DC12	DT8, PHE1123, ARG458, DG9	-	DG9, DT8, PHE1123
	5g	-11.5	ARG458, DT10, GLY459, GLY436	SER108 4, GLY 1082	ARG1122, DG9	-	ARG11 22	DG9, DT8, PHE1123
	5h	-11.3	GLY459, GLY436, ASP 437, DC12, DT10	DA13, DG9	-	PHE1123, DT8, ARG458	-	DT8, PHE1123, DG9, DA13
	5i	-11.2	GLY459, ASP437, GLY436, SER1084, DT10	DA13	-	PHE1123, DT8, DG9, ARG 458	-	DC12, PHE1123, DT8, DG9
	5j	-10.7	DG6, DG7, DC12, SER1084, GLY1082, PHE1123	DG9, DA13, ARG11 22	-	ARG458	GLU10 88	DA13, DG9
	5k	-10.9	DT10, DA11, ASP437, DC12, GLY436, GLY459, PHE1123, ARG1122, GLU1088	DG9	DT8	ARG458	ARG45 8	DA13, DG9

1	5l	-11.5	GLY459, ASP437, DT10, GLY436, SER1084	DA13	-	PHE1123, ARG458	-	DA13 DG9, DT8, PHE1123
2	5m	-7.8	GLY1082, ARG1122, GLY459,	DG9	DA13, DC12	DT8	-	DG9, DA13, DT8
3	5n	-8.1	ARG1122	GLY459	DA13, DC12	DT8	-	DA13, DG9, DT8
4	5o	-7.8	ARG1122, SER1084, DC12, GLY459	-	ASP437, DG9, DA13, DT8	DG9, ARG458	-	DT8, DG9, DA13
5	5p	-9.0	SER1084, GLY1082, ARG1122, PHE1123, ARG458	DT8, DA13	DG9	DT8	-	DG9

Table 12. Docking score and interaction of compounds **5a-5p** with PDB code: 1BNA.

Comp ound	Binding score (kcal/m ol)	1BNA Interaction				
		van der Waals	H-bond	C-H bond	Pi-Cation/ Anion	Pi- sigma
5a	-9.3	DG14, DC11, DC15, DG12, DA17, DC9, DT19	DG16	-	DA18, DG10	DA18
5b	-9.0	DG12, DG14, DC11, DC15, DC9, DA17, DT19	DG16	-	DA18, DG10	-
5c	-9.2	DG12, DG14, DC11, DC15, DC9, DA17, DT19	DG16	-	DA18, DG10	DA18
5d	-8.6	DC15, DG14, DC9, DA18	DG16	DA17, DT19, DC11, DG12	DT19, DG10	-
5e	-9.5	DC9, DA18, DC15, DA17	DG10	DC11, DG16, DG12	DT19	-
5f	-9.3	DG12, DG14, DC11, DC15, DC9, DA17, DT19	DG16	-	DA18, DG10	DA18
5g	-8.6	DC15, DG14, DC9, DA18	DG16	DA17, DT19, DC11, DG12	DG10, DT19	-
5h	-9.4	DC15, DG14, DC9, DA18	DG10	DG16, DC11, DA17	DG12	-
5i	-9.4	DA17, DA18, DC9, DC15, DG14	DG10	DG16, DC11	DG12	-
5j	-9.2	DG14, DC15, DC11, DG12, DA17	DG16	DC9, DT19, DA18	DA18, DG10	DA18
5k	-9.4	DC11, DG12, DA17, DG14, DC9, DC15, DT19	DG16	-	DA18, DG10	DA18
5l	-9.2	DT19, DC9, DA17, DG12, DG14, DC15, DC11	DG16	-	DA18, DG10	DA18
5m	-6.8	DA18, DC9, DT19, DC11, DA17	DG10	DG16	-	-
5n	-6.9	DA18, DG12, DA17, DC15, DC11	DG10	DG16	-	-
5o	-7.1	DC15, DA17, DA18, DC11	DG10, DG14	DG16, DC11, DG12	-	-
5p	-8.0	DC9, DC15, DG14, DA17, DG12, DA18, DC11	DG10, DG16	DG10	-	-

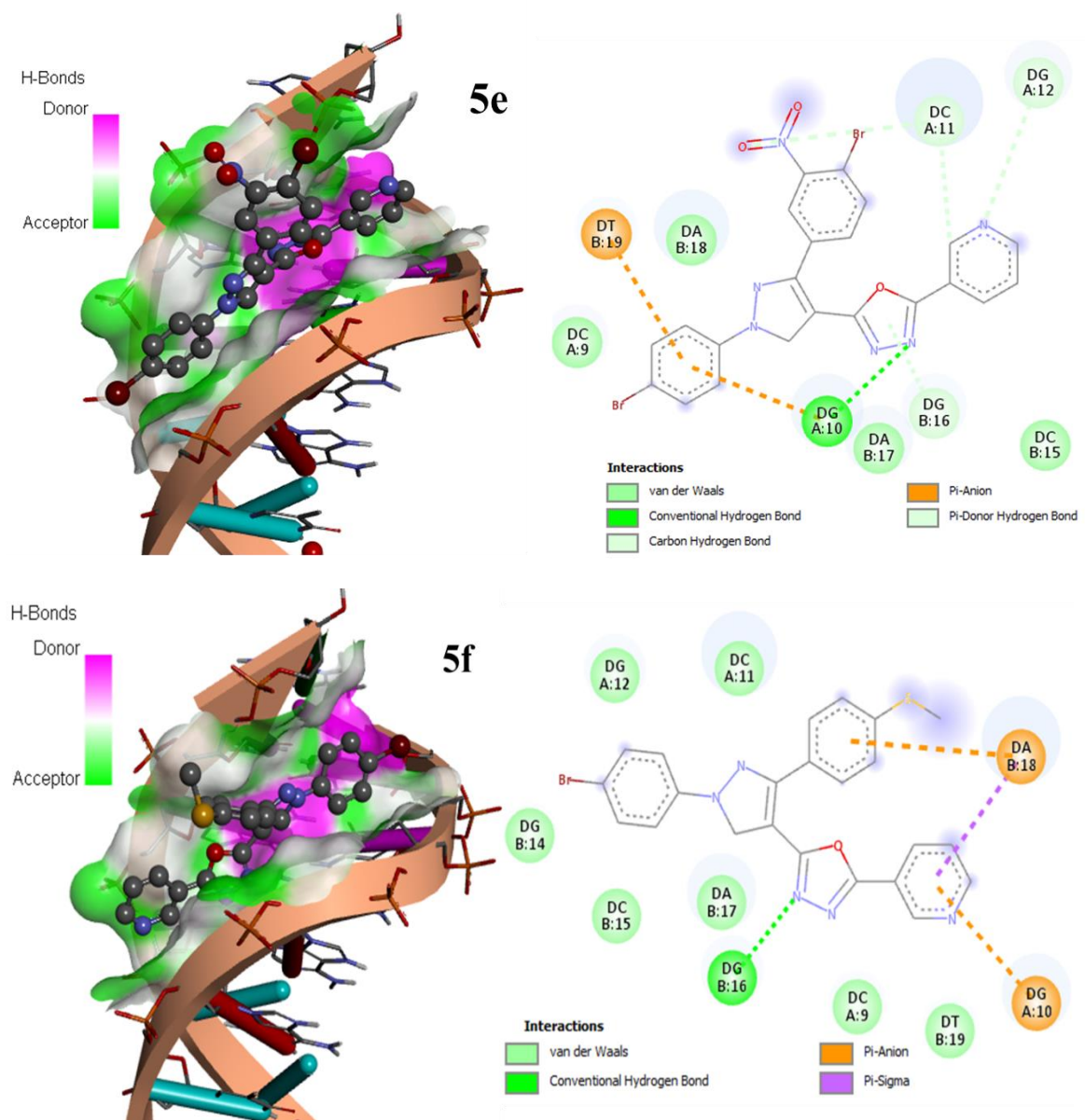


Figure 14. Docking pose and 2D interactions of compound **5e** and **5f** with PDB ID: 1BNA.

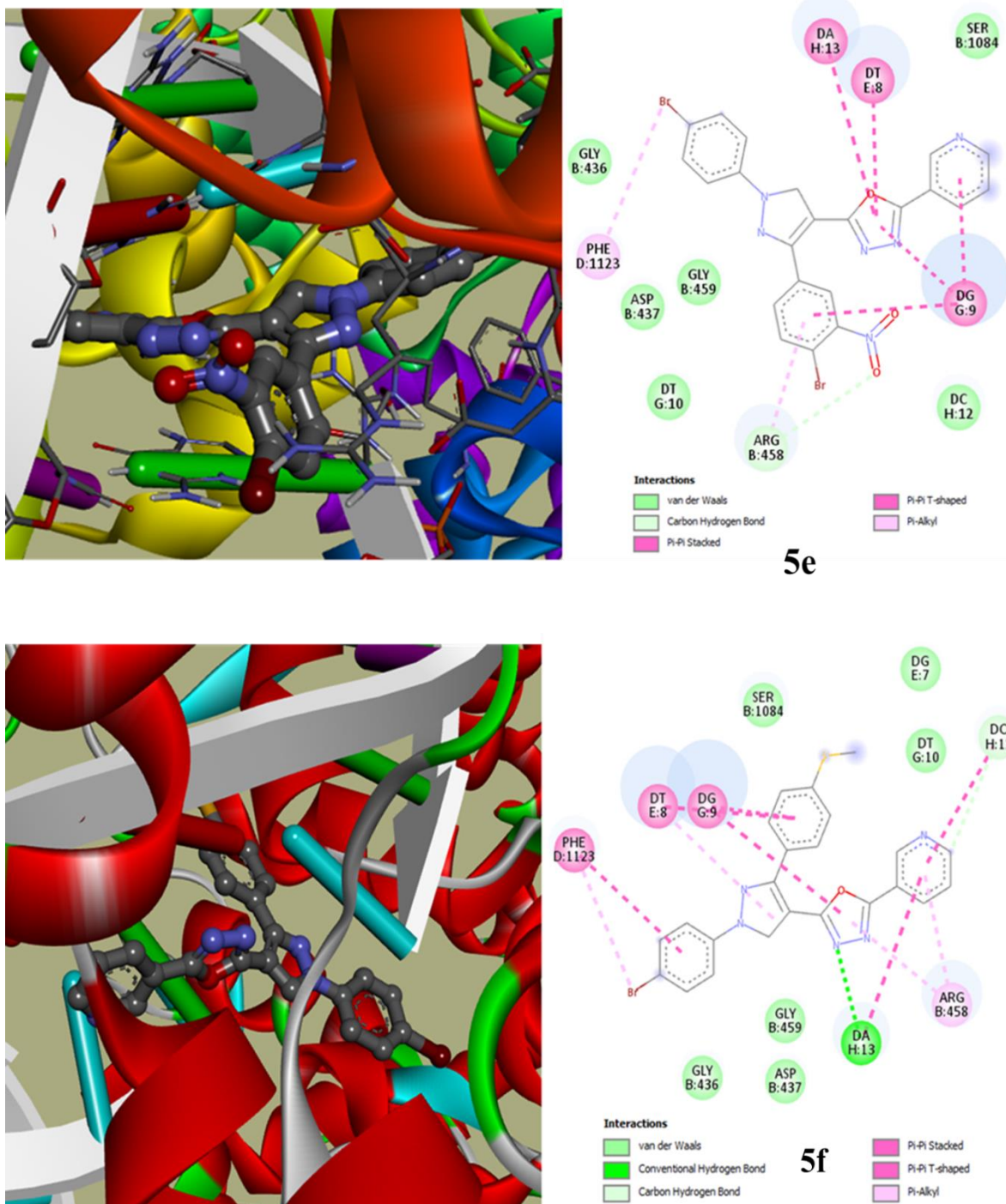


Figure 15. Docking pose and 2D interactions of compound **5e** and **5f** with PDB: 2XCT.

3.5. Molecular modelling

Figure 16 represents the schematic of compound **5e** interaction with the DNA Gyrase amino acid residues. The plot shows the interactions that occurred more than 30% of the overall simulation time (from 0 to 100 nanosecond). Glu435 and Asp508 of DNA gyrase showed the maximum interaction with **5e**.

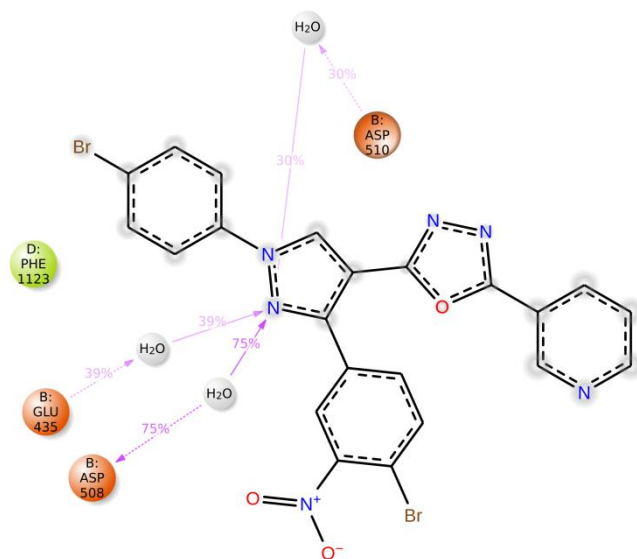


Figure 16. Showing the ligand interaction diagram of DNA Gyrase (PDB ID: 2XCT) with **5e**.

The RMSF (root mean square fluctuations) was used to determine the local changes along the DNA gyrase. **Figure 17 (A)** depicts the peaks that indicate the areas of DNA gyrase that fluctuated the most during simulation. Upon binding with **5e**, mostly the fluctuations were within a certain range i.e., up to 3.0 Å. Only the residues in the range of 600-800 of the residue indices showed the higher fluctuations. Further, the RMSD (root mean square deviation) was employed to calculate an average variation in the atoms of DNA gyrase and **5e** with respect to the DNA gyrase (**Figure 17 B**). RMSD values of both the ligand and the protein are found to be almost similar with only minor

1
2
3
4
5
6
7
8
9
10
11
12
13
14
15
16
17
18
19
20
21
22
23
24
25
26
27
28
29
30
31
32
33
34
35
36
37
38
39
40
41
42
43
44
45
46
47
48
49
50
51
52
53
54
55
56
57
58
59
60
61
62
63
64
65
differences. This indicated that **5e** did not diffuse away and remained in the binding pocket of the protein.

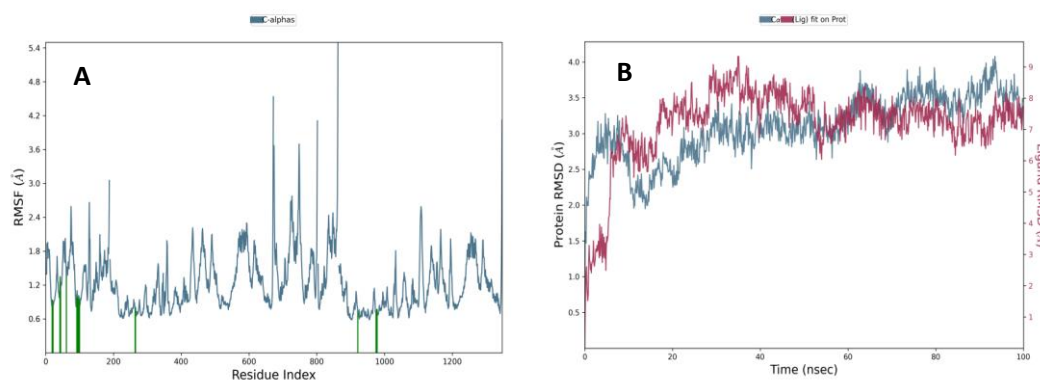


Figure 17. Showing the **A**) RMSD plot of DNA Gyrase protein (blue) and ligand (**5e**) (red) and **B**) RMSF plot of protein (Å) (blue) and ligand contact with the amino acids (green).

Similarly, in case of ligand **5f**, it was observed that **5f** could maintain interaction only with Arg1122 residue of the protein for about 48% of the simulation time (**Figure 18**). Moreover, upon **5f** contact, the RMSF values of the protein showed almost similar pattern that of **5e** (**Figure 19 A**). However, the RMSD values of **5f** (**Figure 19 B**) showed a significant difference. The decreased values indicate formation of more stable complex with ligand binding stably in the protein's pocket.

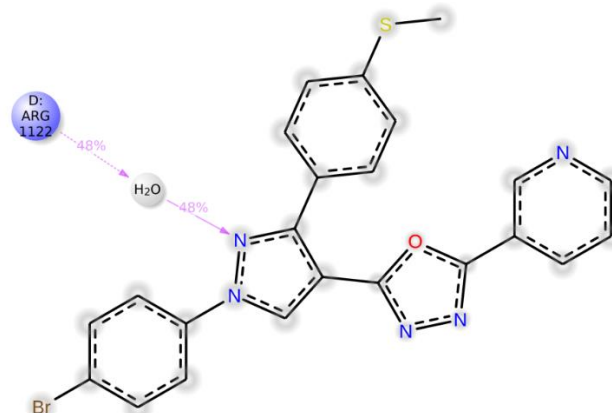


Figure 18. Showing the ligand interaction diagram of DNA Gyrase (PDB ID- 2XCT) with **5f**.

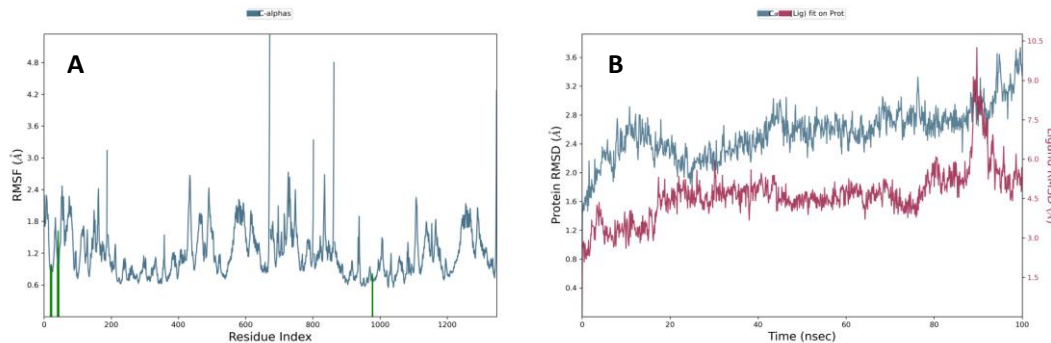


Figure 19. Showing the **A)** RMSD plot of DNA Gyrase protein (blue) and ligand (**5f**) (red) and **B)** RMSF of protein (Å) (blue) and ligand contact with the amino acids (green)

3.6. Pharmacokinetics properties

The pharmacological characteristics and ADME assay of all the synthetic compounds **5a–5p**, were examined using the Swiss ADME and mol inspiration online software by calculating lipophilicity (logP), skin permeability (logK_p), number of donor and acceptor H-bonds and topological polar surface areas (TPSA). **Table 13** summarises the drug likeness properties and ADME data of synthesized analogs. According to the obtained properties, synthesized derivatives physicochemical properties were found to be within an acceptable range.

Table 13. The pharmacological properties of synthesized compounds **5a-5p**.

Compound	Mol Wt. ^a	n O N ^b	nO HN H ^c	Nrot b ^d	iLogP ^e	WlogP (lipophilicity)	TPSA ^f	Volume (^o A ³)	Synthe- tic Accessi- bility	Lipin- ski violat- ion	Absorption			Metabolism					Fraction Csp3
											Log S ^g	GI ^h	log Kp ⁱ	1A2	2C1 9	3A4	2 D 6	2 C 9	
5a	489.29	9	0	5	4.72	5.32	115.47	361.21	3.53	0	-5.81	Low	-6.33	N	N	Y	N	Y	0
5b	489.29	9	0	5	4.75	5.32	115.47	361.21	3.48	0	-5.81	Low	-6.33	N	N	Y	N	Y	0
5c	478.74	6	0	4	5.47	6.07	69.64	351.41	3.36	1	-6.35	High	-5.71	N	N	N	N	Y	0
5d	474.32	7	0	5	4.84	5.42	78.88	363.42	3.47	0	-5.83	High	-6.14	N	N	Y	N	Y	0.04
5e	568.18	9	0	5	5.49	6.08	115.47	379.09	3.55	1	-6.72	Low	-6.32	N	N	N	N	Y	0
5f	490.39	6	0	5	5.22	6.14	69.64	372.56	3.51	1	-6.27	Low	-5.85	N	N	Y	N	Y	0.04
5g	489.29	9	0	5	4.50	5.32	115.47	361.21	3.48	0	-5.81	Low	-6.33	N	N	Y	N	Y	0
5h	489.29	9	0	5	4.75	5.32	115.47	361.21	3.44	0	-5.81	Low	-6.33	N	N	Y	N	Y	0
5i	478.74	6	0	4	5.25	6.07	69.64	351.41	3.31	1	-6.35	High	-5.71	N	N	N	N	Y	0
5j	474.32	7	0	5	4.63	5.42	78.88	363.42	3.42	0	-5.83	High	-6.14	N	N	Y	N	Y	0.04
5k	568.18	9	0	5	5.27	6.08	115.47	379.09	3.51	1	-6.72	Low	-6.32	N	N	N	N	Y	0
5l	490.39	6	0	5	5.22	6.14	69.64	372.56	3.46	1	-6.27	Low	-5.85	N	N	Y	N	Y	0.04
5m	207.26	4	2	2	1.85	2.05	64.95	174.69	2.38	0	-2.57	High	-6.44	Y	N	N	N	N	0.11

5n	207.19	6	3	2	0.75	1.04	94.41	173.56	2.32	0	-1.96	High	-7.08	N	N	N	N	N	0.11
5o	221.22	6	2	3	1.46	1.34	83.42	191.09	2.66	0	-2.16	High	-6.93	Y	N	N	N	N	0.20
5p	227.22	5	3	1	2.31	2.19	85.17	192.00	2.57	0	-3.07	High	-6.29	Y	N	N	N	N	0

^a Molecular Weight \leq 500 (gm/mol), ^b nON \leq 10 (Hydrogen Bond Acceptor), ^c n-OHNN \leq 5 (Hydrogen Bond Donor), ^d Nrotb \leq 10 (No. of Rotatable Bonds), ^e iLogP \leq 5, ^f Total Polar Surface Area \leq 140 ($^{\circ}$ A²), ^g Water Solubility range (-0.5 to -6.5 mol/L), ^h Gastrointestinal absorption (High/Low), ⁱ Skin permeability $>$ -2.5 (cm/s) considered to be permeable. Y = Yes; N = No; Synthetic Accessibility = 1 (very easy) to 10 (very difficult).

1
2
3
Conclusion
4
5
6
7
8
9
10
11
12
13
14
15
16
17
18
19
20
21
22
23
24
25
26
27
28
29
30
31
32
33
34
35
36
37
38
39
40
41
42
43
44
45
46
47
48
49
50
51
52
53
54
55
56
57
58
59
60
61
62
63
64
65

The oxadiazole based pyrazole derivatives **5a-5l** and oxadiazole derivatives **5m-5p** were synthesized, characterized and evaluated for their antibacterial activity against a panel of bacterial strains. The most active analogs **5e** and **5f** showed potent antibacterial activity, with 16 µg/mL MIC values against *B. subtilis* and *E. coli*. The further studies of compound **5f** with *E. coli* and MDR isolates was carried out. The biofilm inhibition assay gives the information that the compound **5f** inhibited biofilm formation up to 55% at $\frac{1}{2}$ MIC against AA209 whereas against AA276, inhibition was depicted up to 66%, 15% and 3% at $\frac{1}{2}$ MIC, $\frac{1}{4}$ MIC and $\frac{1}{8}$ MIC respectively. The lead analogs **5e** and **5f** were considered to investigate for their interaction ability with CT-DNA by various techniques and the results were found to be intercalation mode of binding. The analysis of compounds **5e** and **5f** using *in silico* molecular docking was performed towards PDB ID: 1BNA and 2XCT. The docking score and the interactions like van der Walls, conventional H-bonding, and Pi-Pi stacking/T-shaped were observed. The *S. aureus* DNA gyrase action matched the computational findings from studies using molecular docking and MD simulation. The physicochemical properties results found to be within an acceptable range for the drug-likeness properties of all the synthesized molecules.

41
42
Acknowledgement
43
44
45
46
47
48
49
50
51
52
53
54

The authors thank Prof. Nahid Nishat, Head, Department of Chemistry and Incharge, Central Instrumentation Facility (CIF), Jamia Millia Islamia, New Delhi for providing instrumentation facility.

55
56
57
Conflict of interest
58
59
60
61
62
63
64
65

There are no conflicts to declare.

References

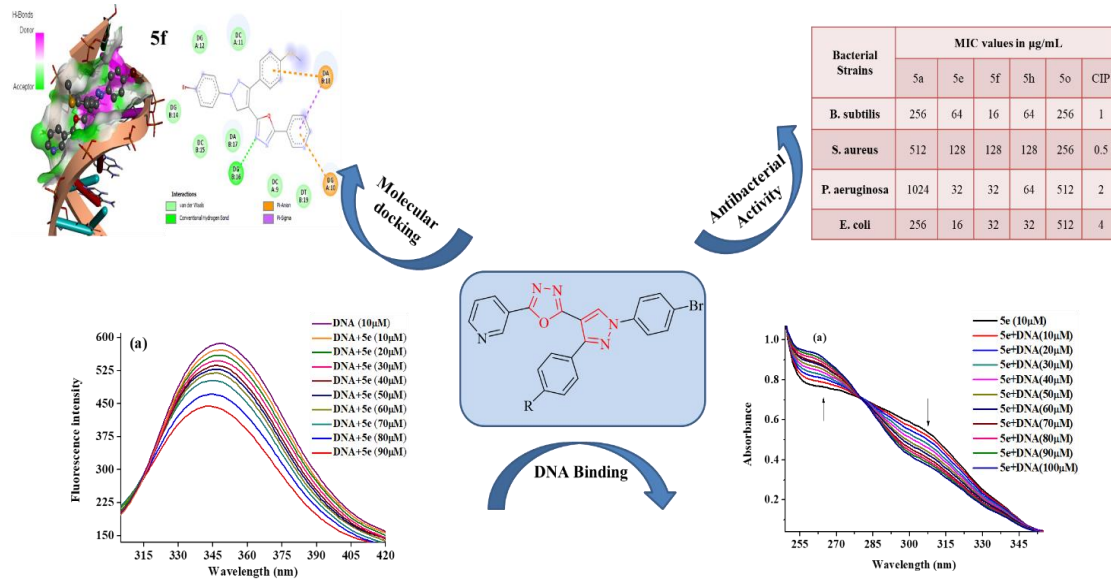
1. H. Yuan, F. Liu, J. Long, G. Duan, H. Yang, *Int. J. Biol. Macromol.*, 2023, **244**, 125391.
2. C.J.L. Murray, K.S. Ikuta, F. Sharara, L. Swetschinski, G.R. Aguilar, A. Gray, *Lancet*,
3. 2022, **399**, 629-655.
4. G. Mancuso, A. Midiri, E. Gerace, C. Biondo, *Pathogens*, 2021, **10**, 1310.
5. C. Llor, L. Bjerrum, *Ther Adv Drug Saf.*, 2014, **5**, 229–241.
6. M. M. Heravi, V. Zadsirjan, *RSC Adv.*, 2020, **10**, 44247–44311.
7. S. Gupta, K. Paul, *Eur. J. Med. Chem.*, 2023, **258**, 115551.
8. F.-Fen Li, W.-Hao Zhao, V. K. R. Tangadanchu, J.-Ping Meng, C.-He Zhou, *Eur. J. Med. Chem.*, 2022, **239**, 114521.
9. Y. Kanzouai, M. Chalkha, H. Hadni, M. Laghmari, R. Bouzammit, A. Nakkabi, T. Benali, B. Tüzün, M. Akhazzane, M. El Yazidi, G. Al Houari, *J. Mol. Struct.*, 2023, **1293**, 136205.
10. A. Saeed, A.M. Soliman, K. M. Al-Taisan, E. Abdel-Latif, A. A.A. Ahmed, Z.M. Alaizeri, H. A. Alhadlaq, *J. Mol. Struct.*, 2023, **1289**, 135763.
11. C. E. Theodore, A. M. Anusuya, G. Sivaiah, R. Jain, C.S. A. Kumar, S. B. B. Prasad, M.S. Raghu, F. A. Alharti, M. K. Prashanth, Byong-Hun Jeon, *J. Mol. Struct.*, 2023, **1288**, 135765.
12. K. Karrouchi, S. Fettach, Ö. Tamer, D. Avci, A. Başoğlu, Y. Atalay, Z. Ayaz, S. Radi, H. A. Ghabbour, Y. N. Mabkhot, M. El A. Faouzi, M. Ansar, *J. Mol. Struct.*, 2022, **1248**, 131506.
13. A. Gupta, S. Gawandi, Vandna, I. Yadav, H. Mohan, V. G Desai, S. Kumar, *Virus Res.*, 2023, **323**, 198955.
14. E. H.-Vázquez, S. S.-Barrera, J. J. R.-Espinosa, S. E.-Soto, F. H.-Luis, *Bioorganic Med. Chem. Lett.*, 2016, **24**, 2298-2306.

14. M. J. Naim, O. Alam, M. J. Alam, M. Q. Hassan, N. Siddiqui, V.G.M. Naidu, M. Iqbal
1
2
3
4
5
6
7
8
9
10
11
12
13
14
15
16
17
18
19
20
21
22
23
24
25
26
27
28
29
30
31
32
33
34
35
36
37
38
39
40
41
42
43
44
45
46
47
48
49
50
51
52
53
54
55
56
57
58
59
60
61
62
63
64
65
Alam, *Bioorg. Chem.*, 2018, **76**, 98-112.
15. J. Boström, A. Hogner, A. Llinàs, E. Wellner, A. T. Plowright, *J. Med. Chem.*, 2012, **55**,
1817–1830.
16. A. A. Othman, M. Kihel, S. Amara, *Arab. J. Chem.*, 2019, **12**, 1660-1675.
17. A. Siwach, P. K. Verma, *BMC Chem.*, 2020, **14**, 70.
18. H. A. Hofny, M. F.A. Mohamed, H. A.M. Gomaa, S. A. Abdel-Aziz, B. G.M. Youssif,
N. A. El-koussi, A. S. Aboraia, *Bioorg. Chem.*, 2021, **112**, 104920.
19. R. Hussain, W. Rehman, F. Rahim, S. Khan, M. Taha, Y. Khan, A. Sardar, I. Khan, S.
A. Ali Shah, *J. Mol. Struct.*, 2023, **1293**, 136185.
20. A. A. Upare, P. K. Gadekar, H. Sivaramakrishnan, N. Naik, V. M. Khedkar, D.Sarkar,
A. Choudhari, S. M. Roopan, *Bioorg. Chem.*, 2019, **86**, 507-512.
21. U. A. Çevik, I. Celik, A. Işık, R. R. Pillai, T. E. Tallei, R.Yadav, Y.Özkay, Z. A.
Kaplancıklı, *J. Mol. Struct.*, 2022, **1252**, 132095.
22. S. Wang, H. Liu, X. Wang, K. Lei, G. Li, J. Li, R. Liu, Z. Quan, *Eur. J. Med. Chem.*,
2020, **206**, 112672.
23. S. V. Bhandari, O. G. Nagras, P. V. Kuthe, A. P. Sarkate, K. S. Waghmare, D. N.
Pansare, S. Y. Chaudhari, S. N. Mawale, M. C. Belwate, *J. Mol. Struct.*, 2023, **1276**,
134747.
24. I. Khan, T. Ganapathi, M. M. Rehman, M. Adil Shareef, C. G. Kumar, A. Kamal,
Bioorg. Med. Chem. Lett., 2021, **44**, 128094.
25. Y. U. Cebeci, H. Bayrak, Y. Şirin, *Bioorg. Chem.*, 2019, **88**, 102928.
26. R. Kotla, A. C. Murugulla, R. Ruddaraju, M. V. B. Rao, P. Aparna, S. Donthabakthuni,
Chem. Data Collect., 2020, **30**, 100548.

- 1 27. B. B. Kashid, P. H. Salunkhe, B. B. Dongare, K. R. More, V. M. Khedkar, A. A.
2 Ghanwat, *Bioorg. Med. Chem. Lett.*, 2020, **30**, 127136.
3
4
5 28. R. Sultana, A. Ali, C. Twala, R. Mehandi, M. Rana, D. Yameen, M. Abid, Rahisuddin
6
7 *J. Biomol. Struct. Dyn.*, 2023, 1-28.
8
9
10 29. R. Sultana, R. Arif, M. Rana, S. Ahmed, R. Mehandi, Akrema, N. Manzoor,
11 Rahisuddin, *Luminescence*, 2022, **37**, 408–421.
12
13
14 30. G. D. Christensen, W. A. Simpson, J. J. Younger, M. Larry, F. F. Barrett, D. M. Melton,
15 E. H. Beachey, *J. Clin. Microbiol.*, 1985, **22**, 996–1006.
16
17
18 31. A. J. Hedges, *Int. J. Food Microbiol.*, 2002, **76**, 207–214.
19
20
21 32. M. Y. Vaidya, A. J. McBain, J. A. Butler, C. E. Banks, K. A. Whitehead, *Sci. Rep.*,
22 2017b, **7**, 5911.
23
24
25 33. R. Kaushal, M. Kaur, Sheetal, J. Sharma, K. Nehra, *J. Mol. Struct.*, 2023, **1295**, 136788.
26
27
28 34. S. Ponkarpagam, K. N. Vennila, K. P. Elango, *Spectrochim. Acta A Mol. Biomol.*
29 *Spectrosc.*, 2022, **278**, 121351
30
31
32 35. F. T. Elmali, *J. Mol. Struct.*, 2022, **1261**, 132900.
33
34
35 36. S. Gurusamy, K. Krishnaveni, M. Sankarganesh, R. N. Asha, A. Mathavan, *J. Mol. Liq.*,
36 2022, **345**, 117045
37
38 37. M. Mohideen, N. A. Kamaruzaman, M. A. Hamali, M. N. Mordi, S. M. Mansor, A. F.
39 M. M. Rahman, *J. Mol. Struct.*, 2021, **1243**, 130771.
40
41
42 38. G.S. Amitha, S. Vasudevan, *Polyhedron*, 2020, **190** 114773.
43
44
45 39. E. Oguzcan, Z. Koksal, T. Taskin-Tok, A. Uzgoren-Baran, N. Akbay, *Spectrochim. Acta*
46 *A Mol. Biomol. Spectrosc.*, 2022, **270**, 120787.
47
48
49 40. J. B. Lepecq, C. Paoletti, *J. Mol. Biol.*, 1967, **27**, 87–106.
50
51
52 41. E. A. Lafayette, S. M. V. de Almeida, R. V. Cavalcanti Santos, J. F. de Oliveira, C. A.
53 da C. Amorim, R. M. F. da Silva, M. G. da R. Pitta, I. da R. Pitta, R. O. de Moura, L. B.
54
55
56
57
58
59
60
61
62
63
64
65

- 1 de Carvalho Júnior, M. J. B. de Melo Rêgo, M. do C. A. de Lima, *Eur. J. Med. Chem.*,
2 2017, **136**, 511–522.
3
4 42. X. Xu, Y. Wang, H. Wang, H. Su, X. Mao, L. Jiang, M. Liu, D. Sun, S. Hou, *J. Mol.*
5
6 *Liq.*, 2016. **220**, 14–20.
7
8 43. M. N. Ahamad, M. Shahid, Ansari, Azaj, M. Kumar, I. M. Khan, M. Ahmad,
9 Rahisuddind, R. Arif, *New J. Chem.*, 2019, **43**, 7511-7519,
10
11 44. A. J. Miles, R. W. Janes, B. A. Wallace, *Chem. Soc. Rev.*, 2021, **50**, 8400-8413.
12
13 45. A. Barmpa, A. G. Hatzidimitriou, G. Psomas, *J. Inorg. Biochem.*, 2021, **217**, 111357.
14
15 46. H. Yang, P. Tang, B. Tang, Y. Huang, X. Xiong, H. Li, *RSC Adv.*, 2017, **7**, 10242–
16
17 10251.
18
19
20
21
22
23
24
25
26
27
28
29
30
31
32
33
34
35
36
37
38
39
40
41
42
43
44
45
46
47
48
49
50
51
52
53
54
55
56
57
58
59
60
61
62
63
64
65

Graphical Abstract





Synthesis of oxadiazole derivatives: Anti-bacterial, DNA binding and *in silico* molecular modelling approaches

Razia Sultana^a, Asghar Ali^b, Manish Rana^{c*}, Iqbal Ahmad^d, Mohan Kamthan^b, Haider Thaer Abdulhameed Almuqdati^e, Nouman^a, Rabiya Mehandi^a, Mohammad Abid^e, Zeinhom M. El-Bahy^f, Rahisuddin^{a*}

^aMolecular and Biophysical Research Laboratory (MBRL), Department of Chemistry, Jamia Millia Islamia, New Delhi 110025, India

^bClinical Biochemistry lab, Department of Biochemistry, School of Chemical and Life Sciences, Jamia Hamdard, New Delhi-110062, India

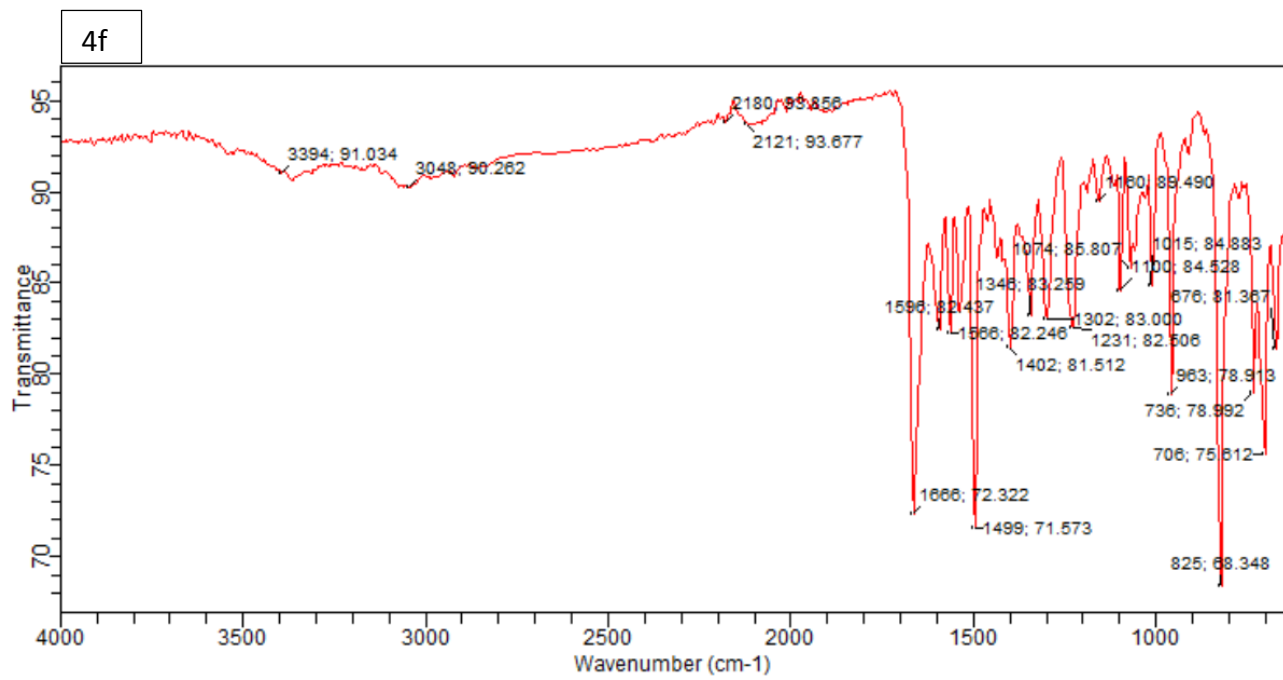
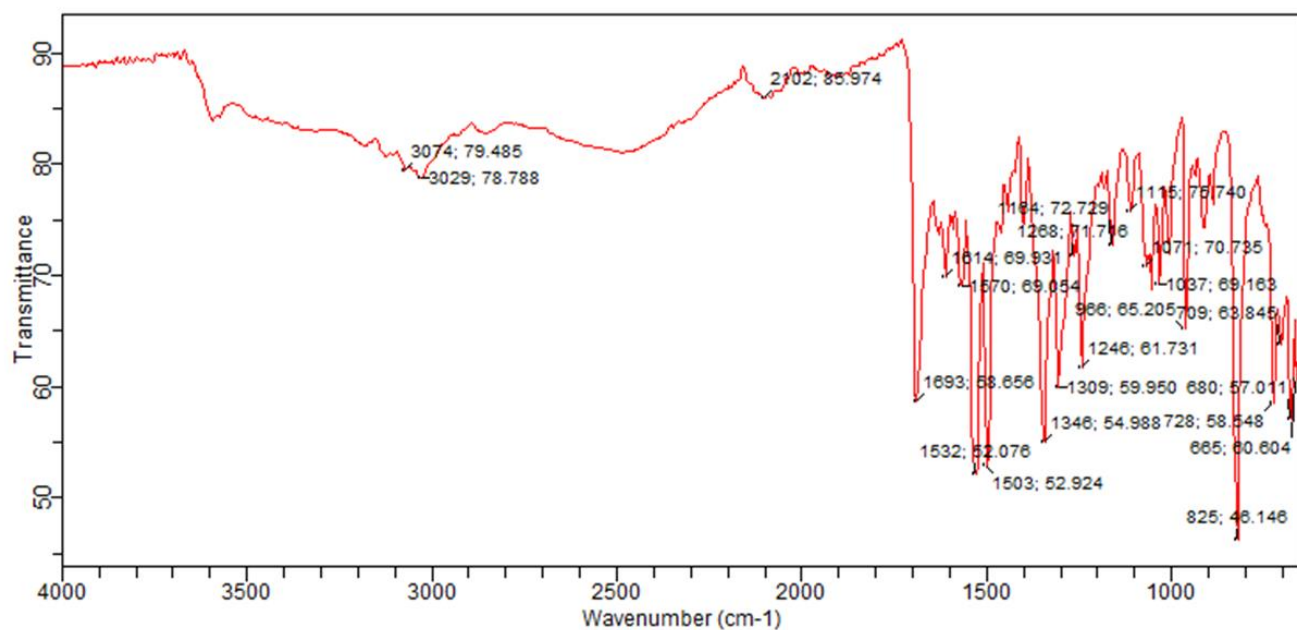
^cDepartment of Chemistry, Ramjas College, University of Delhi, Delhi 110007, India

^dDepartment of Agricultural Microbiology, Faculty of Agricultural Sciences, Aligarh Muslim University, Aligarh (UP), 202002, India.

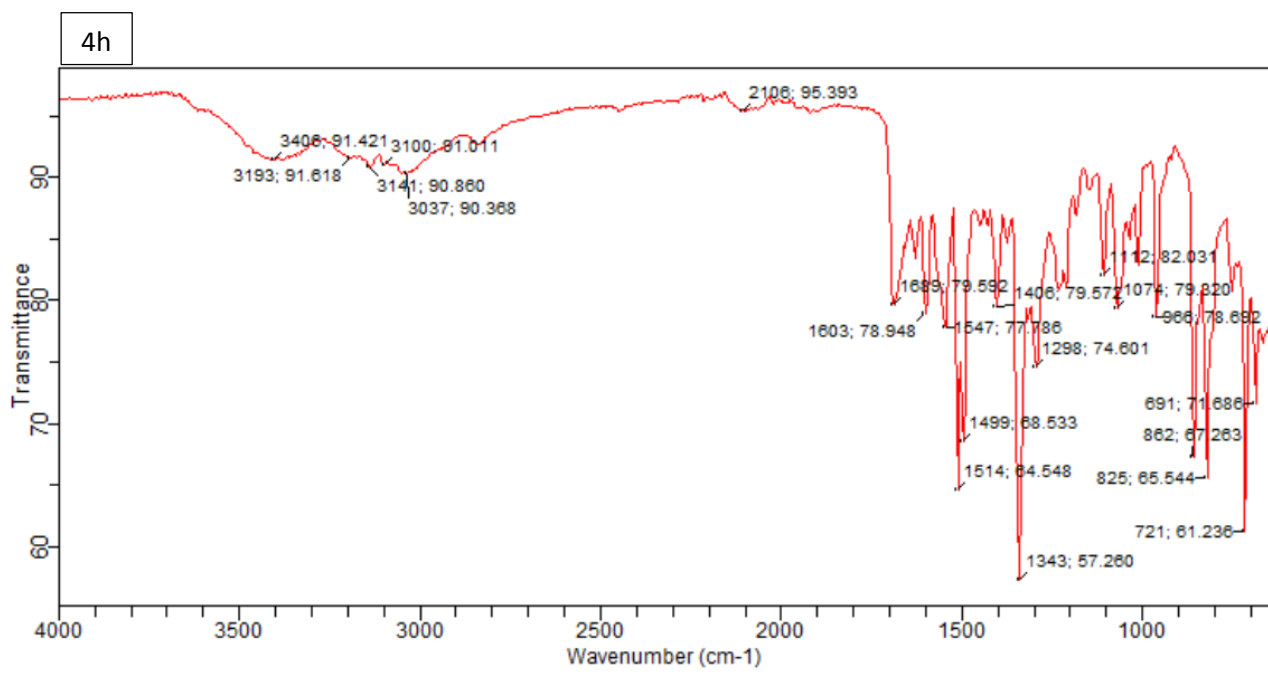
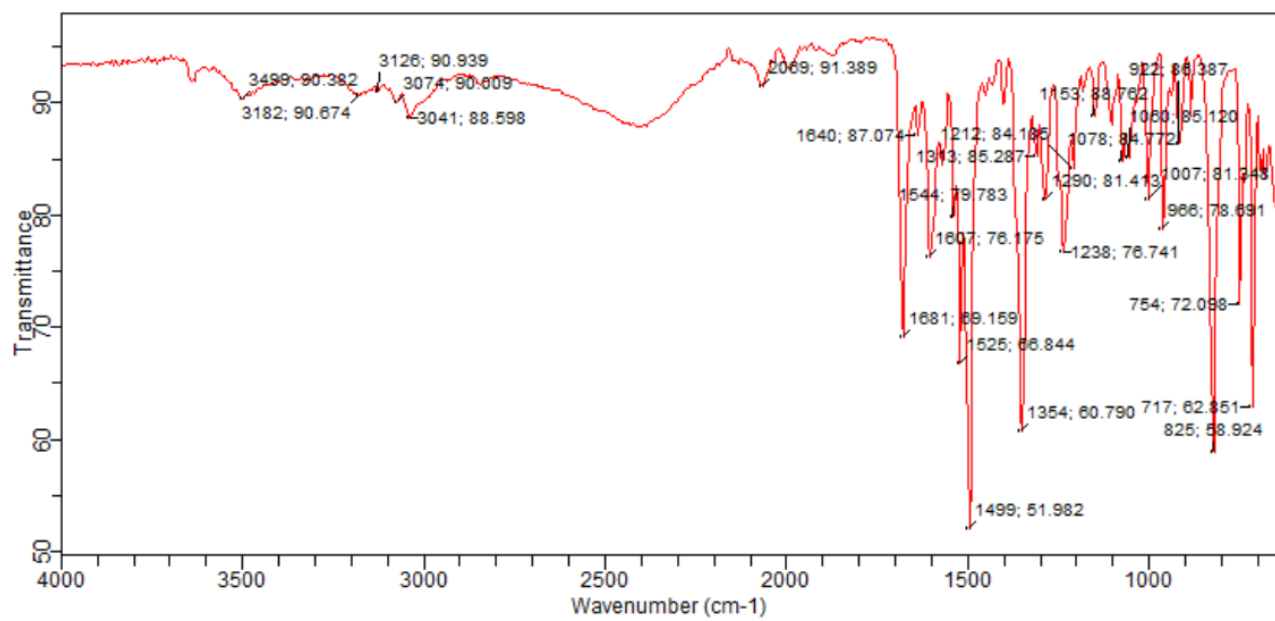
^eDepartment of Biosciences, Jamia Millia Islamia, New Delhi 110025, India

^fDepartment of Chemistry, Faculty of Science, Al-Azhar University, Nasr City 11884, Cairo, Egypt

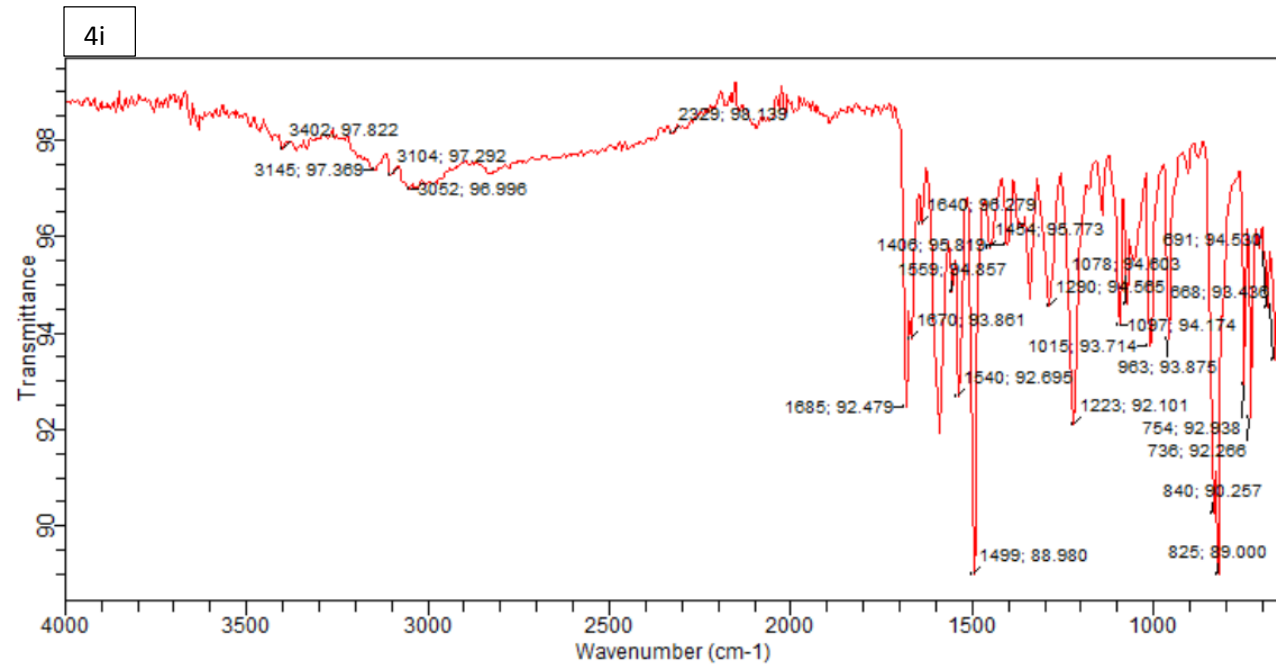
* Corresponding author:
[rahisuddin@jmi.ac.in \(Rahisuddin\)](mailto:rahisuddin@jmi.ac.in)



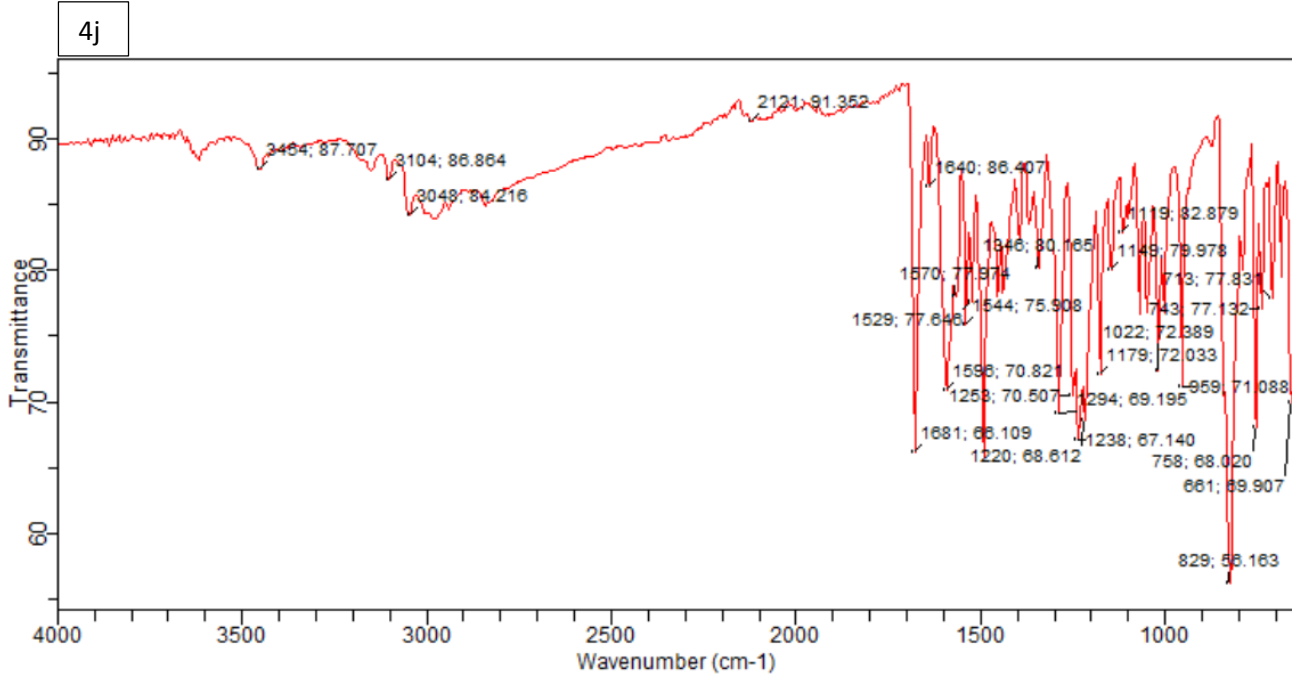
4g



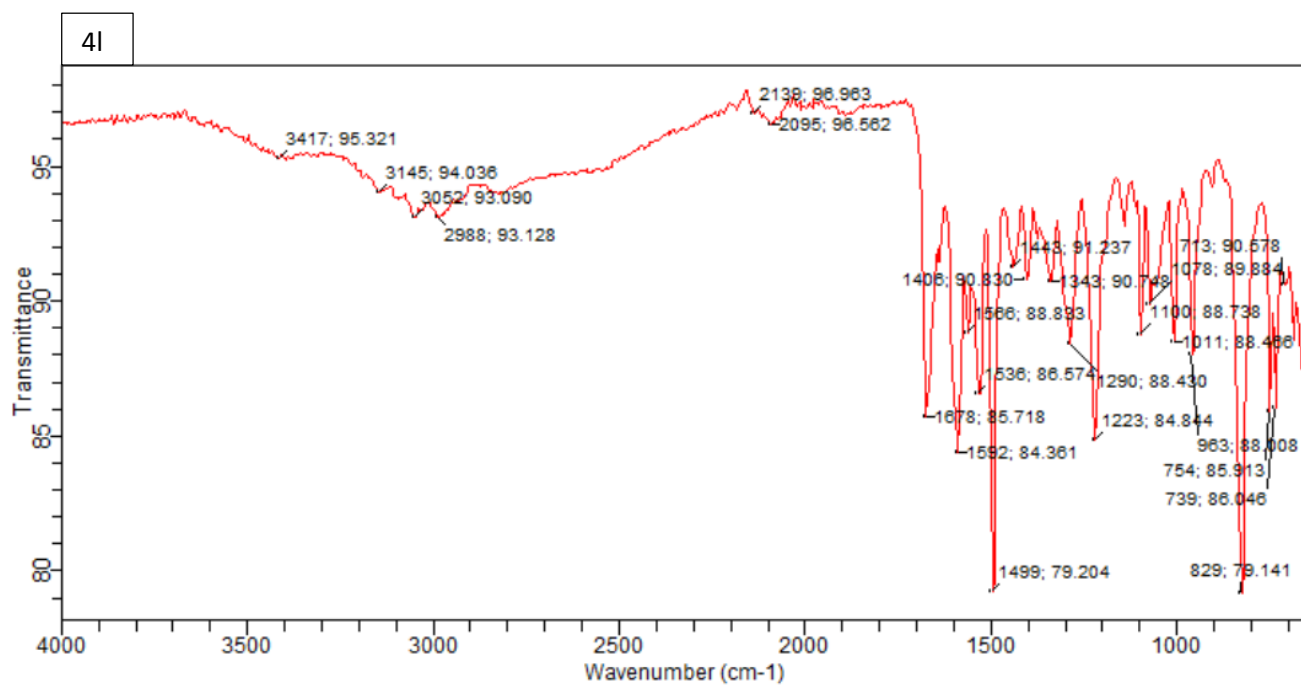
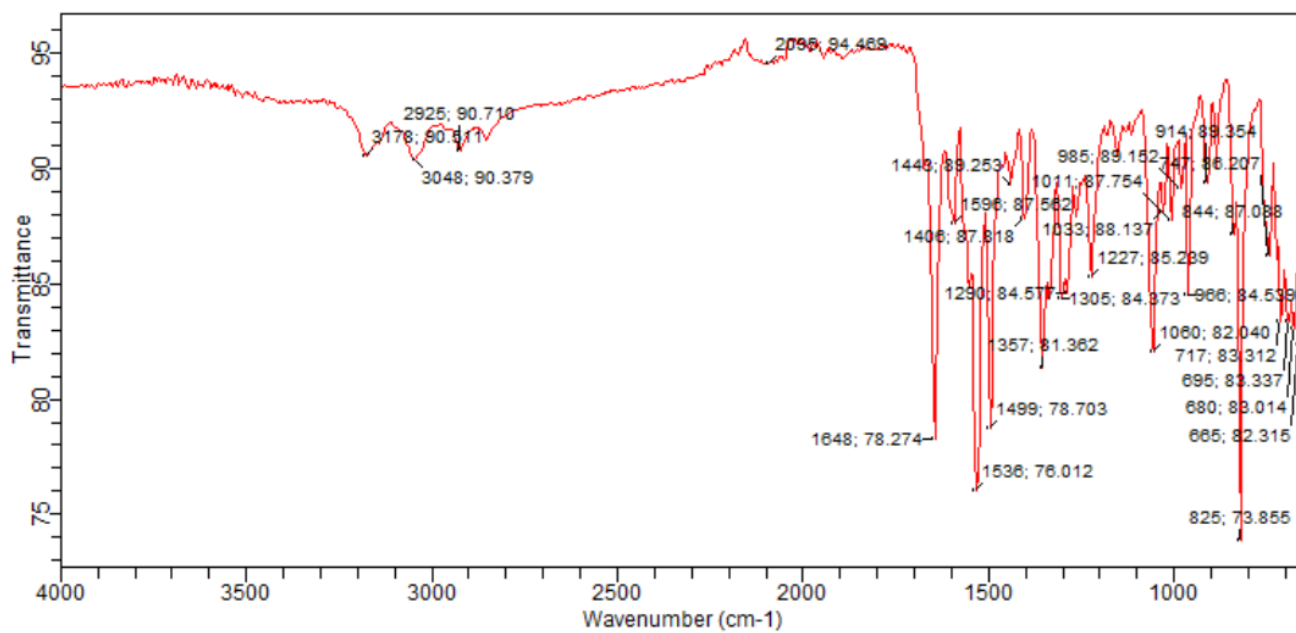
4i



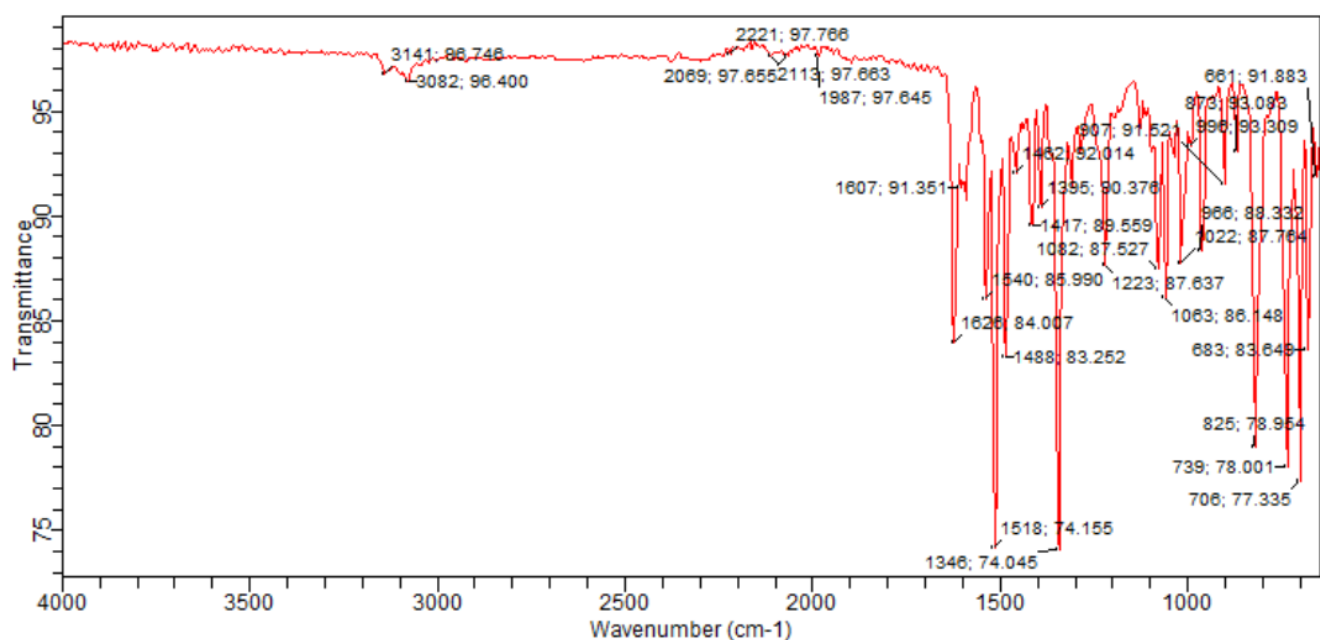
4j



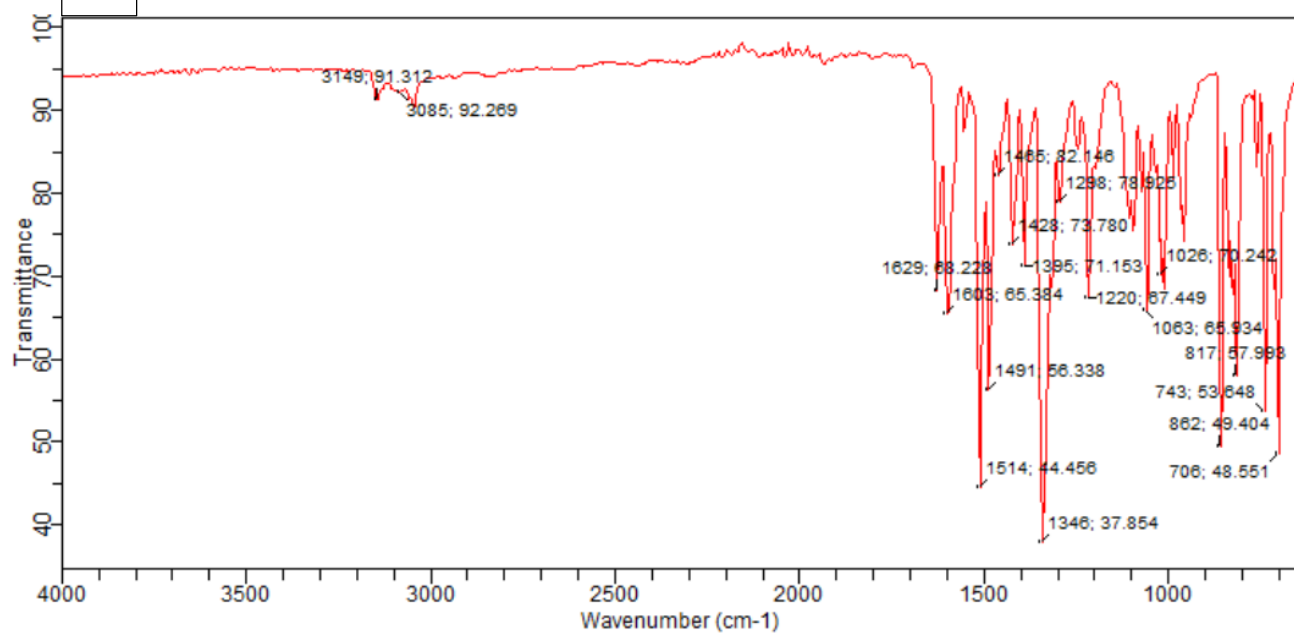
4k



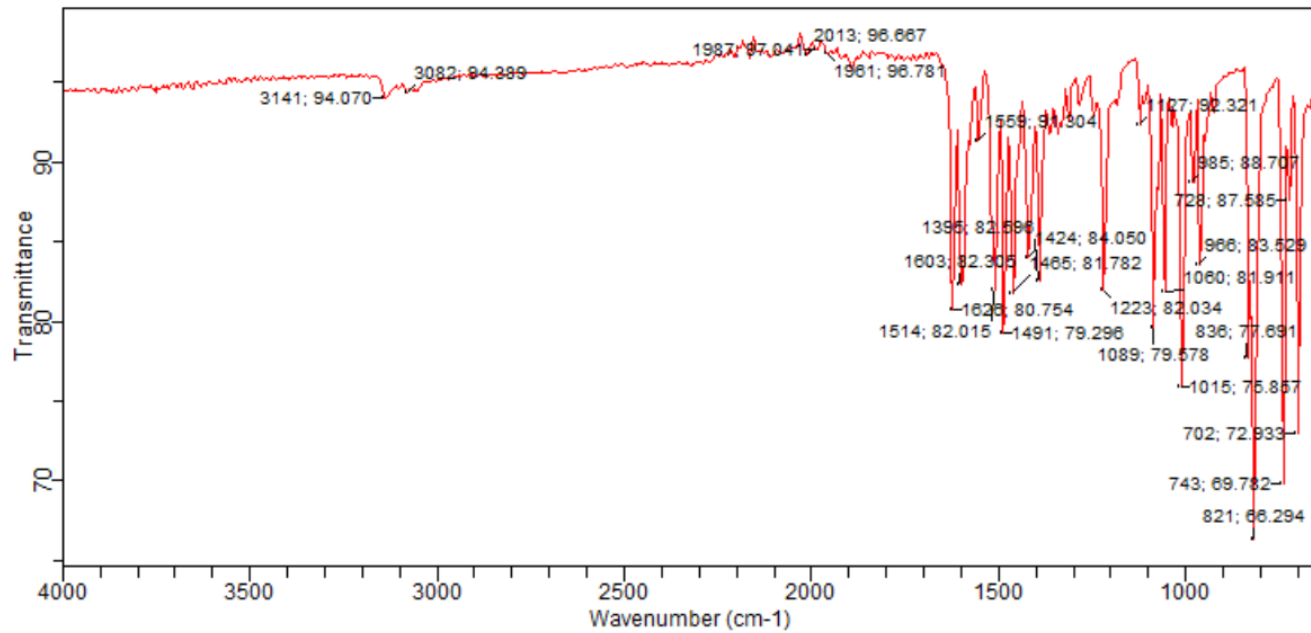
5a



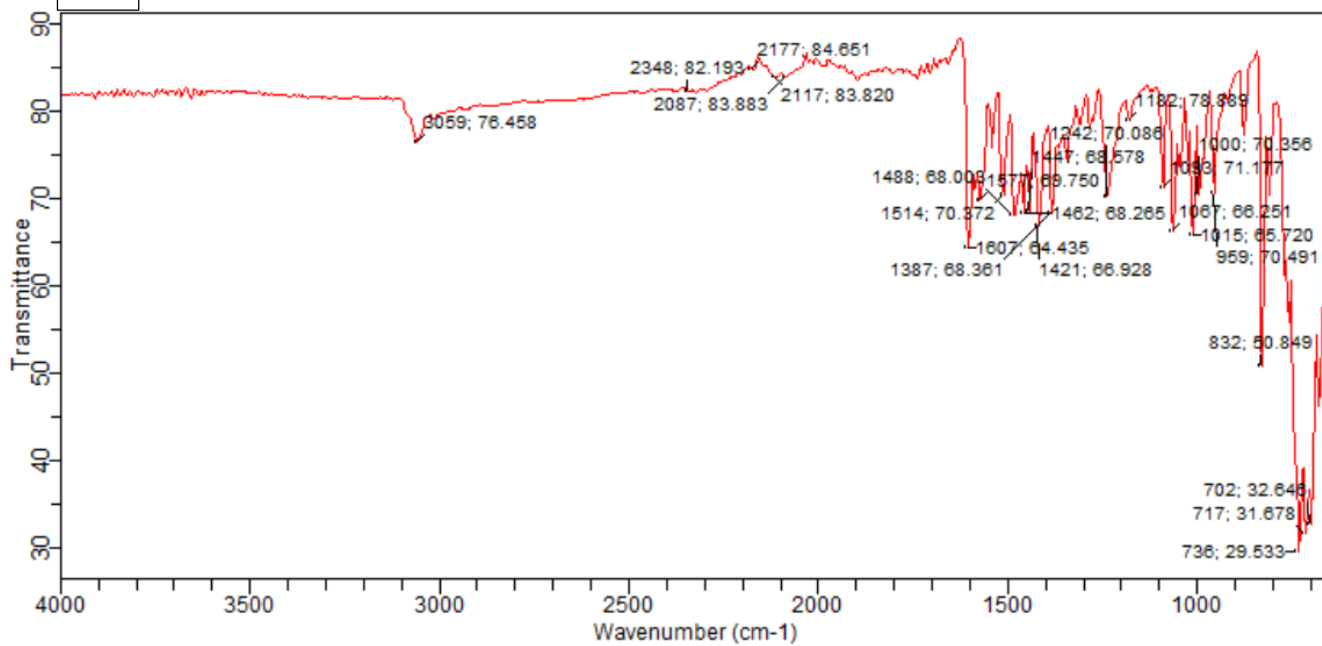
5b



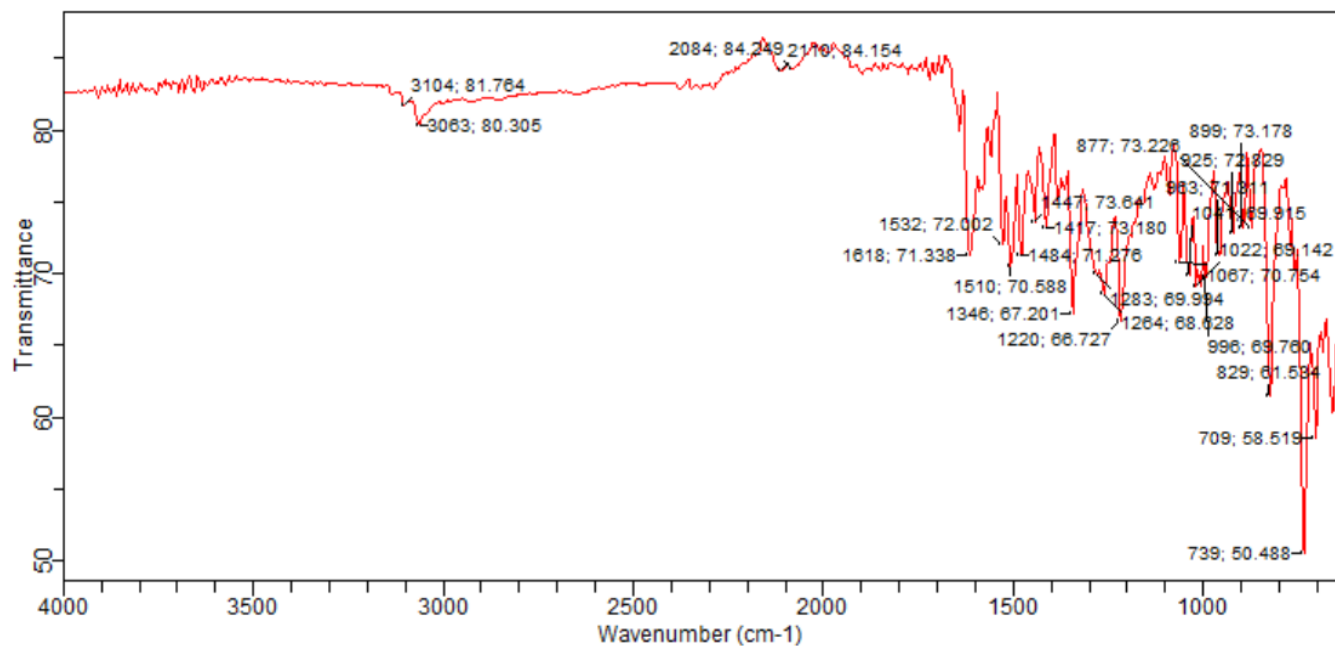
5c



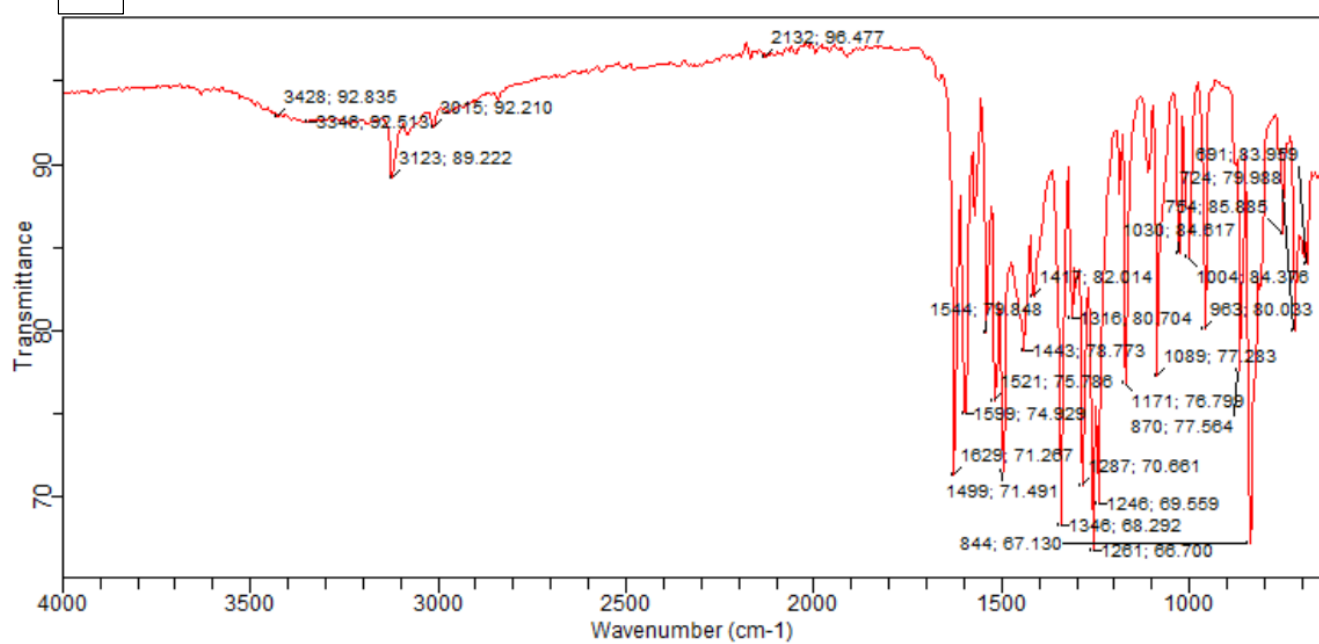
5d



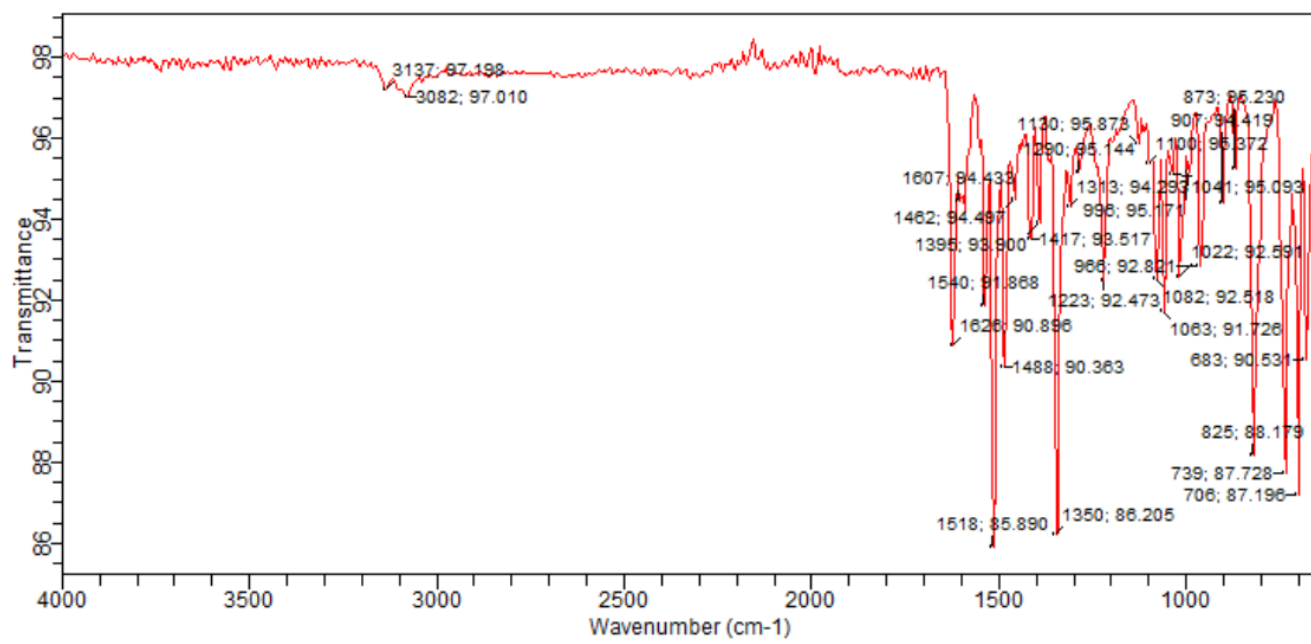
5e



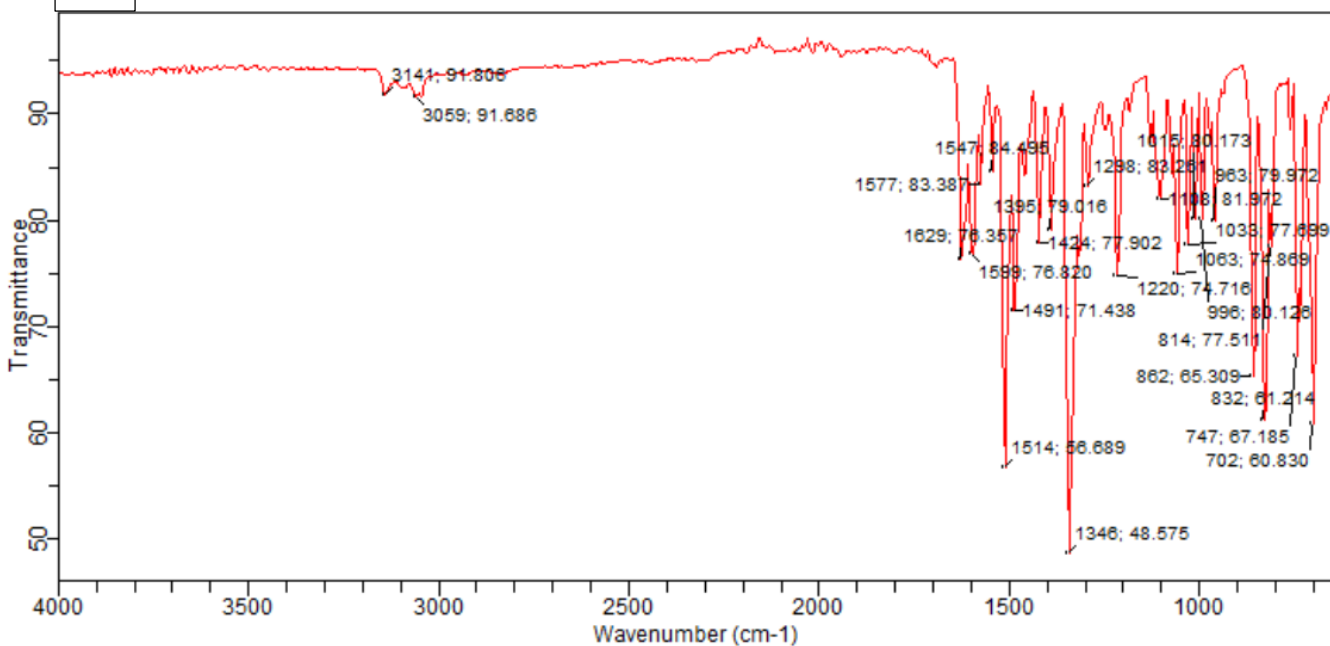
5f



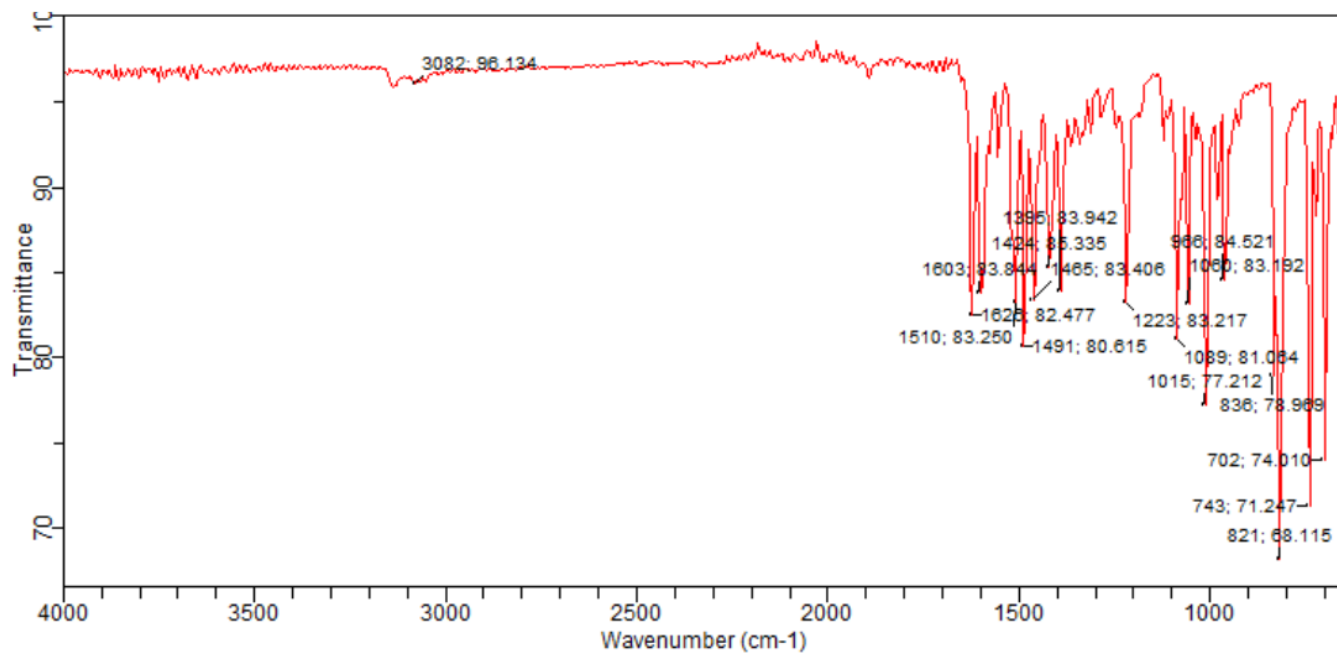
5g



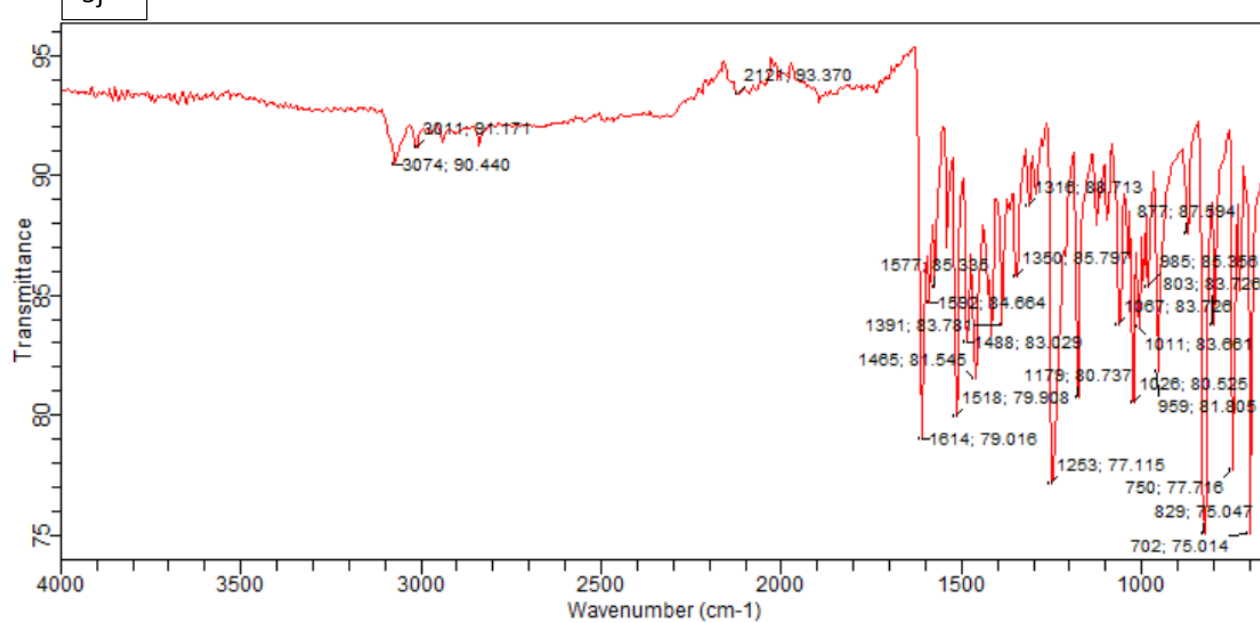
5h



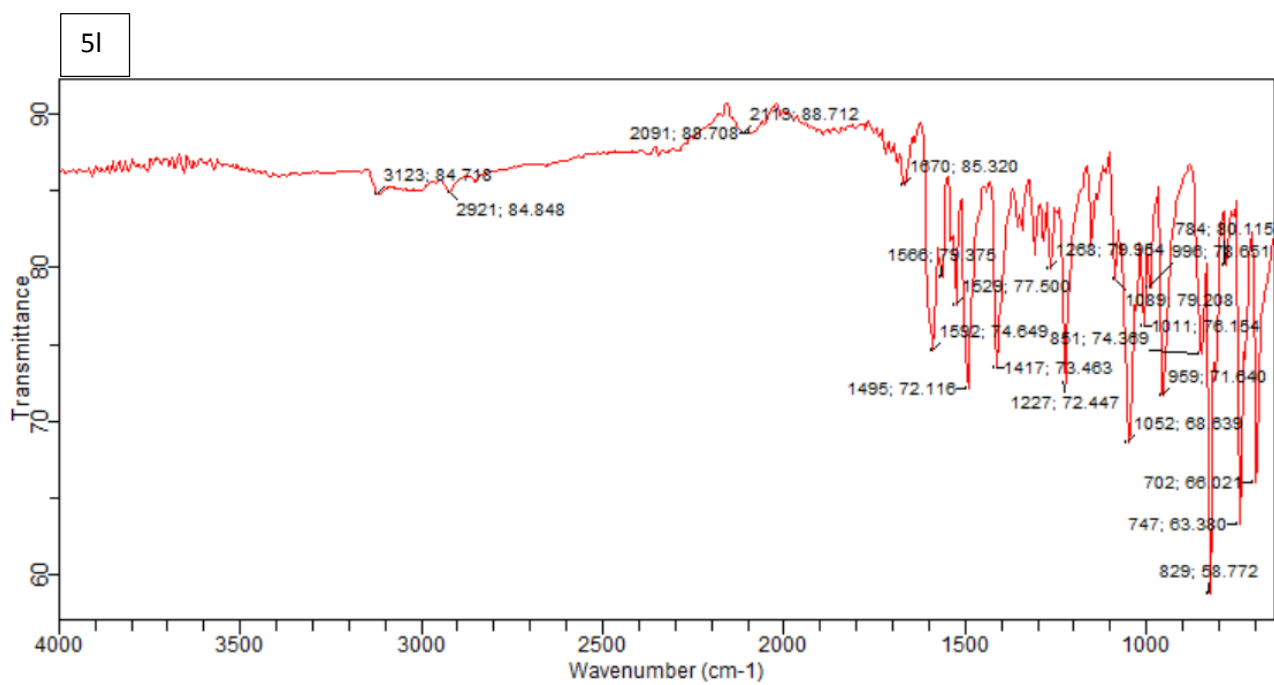
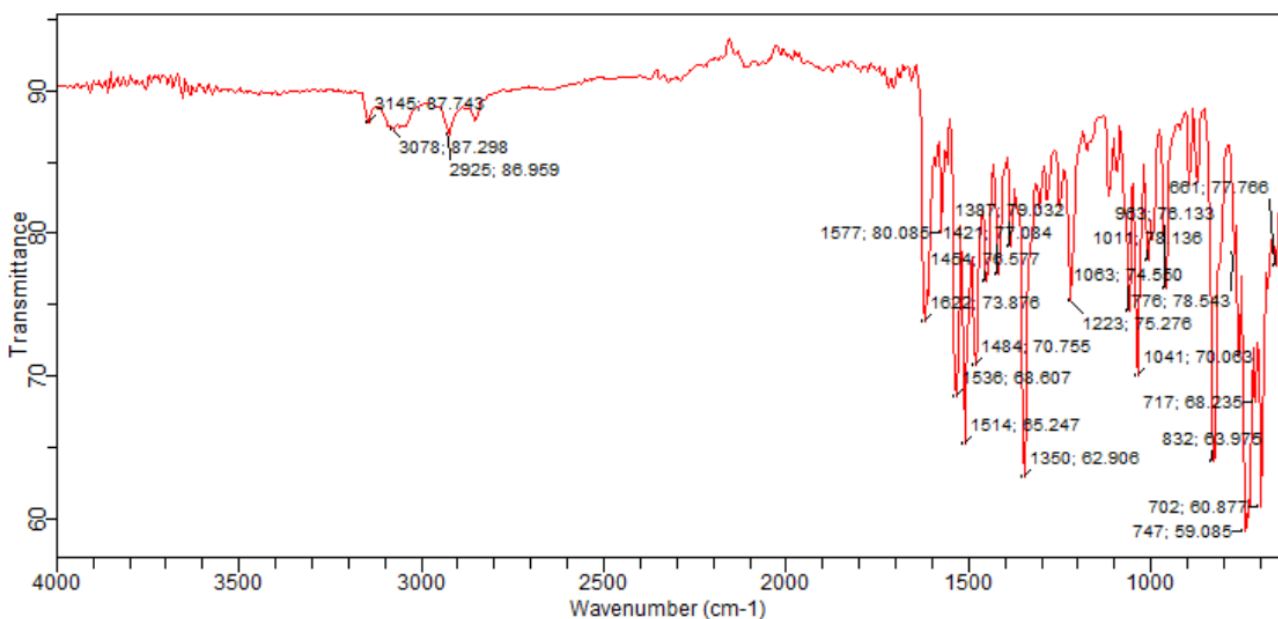
5i

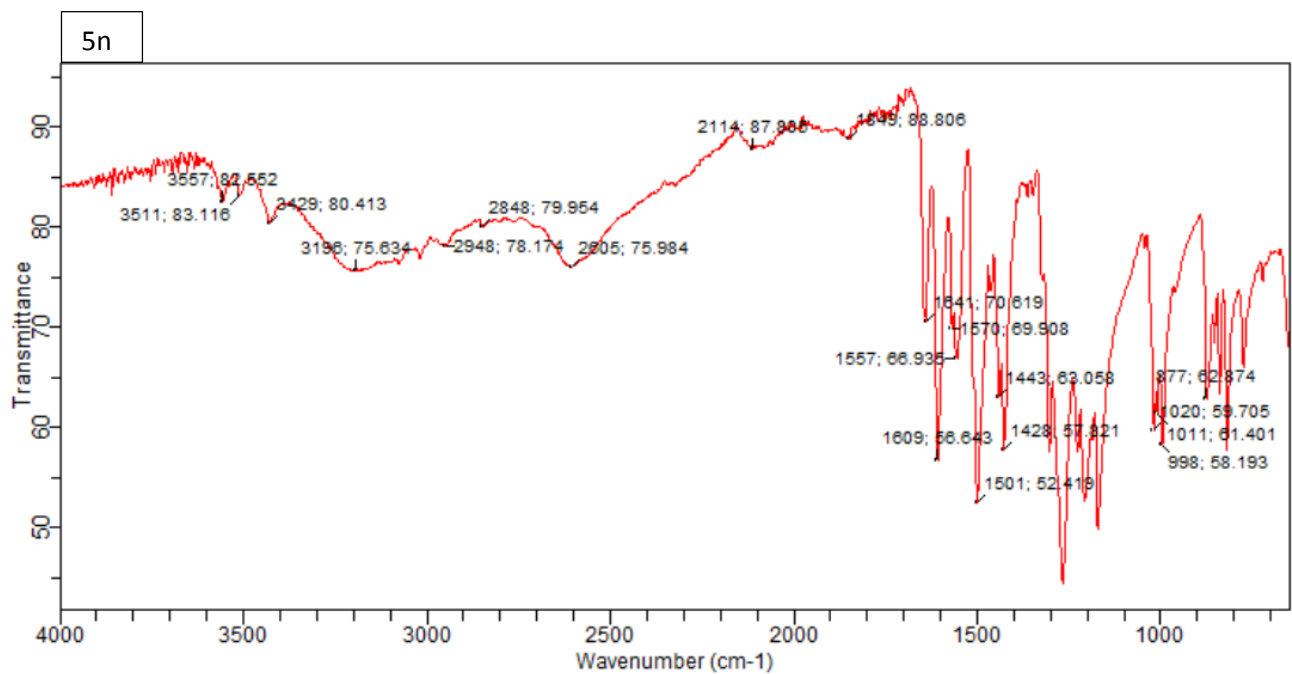
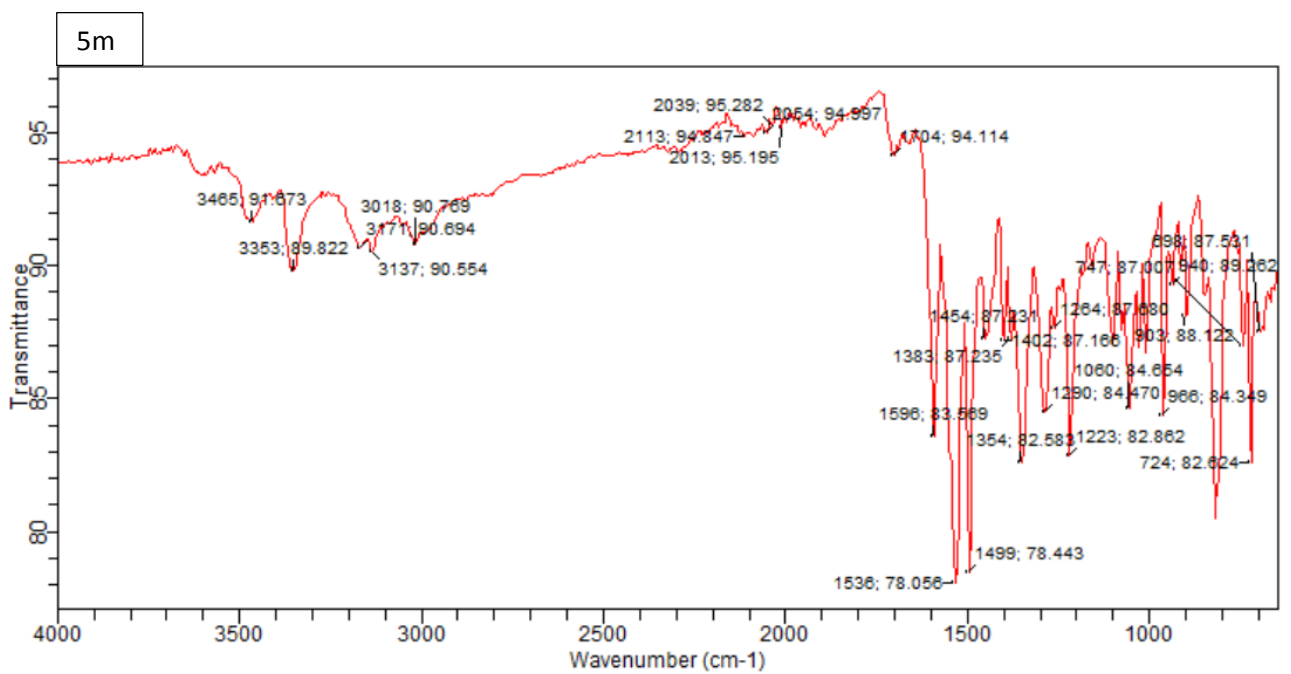


5j



5k





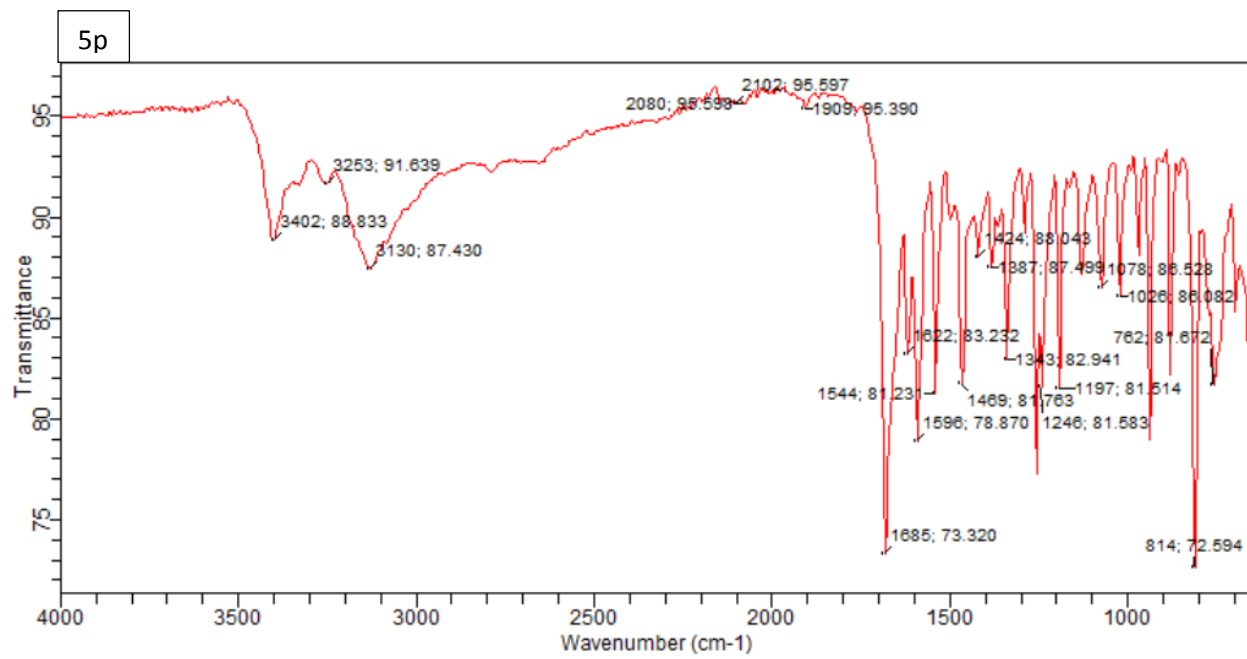
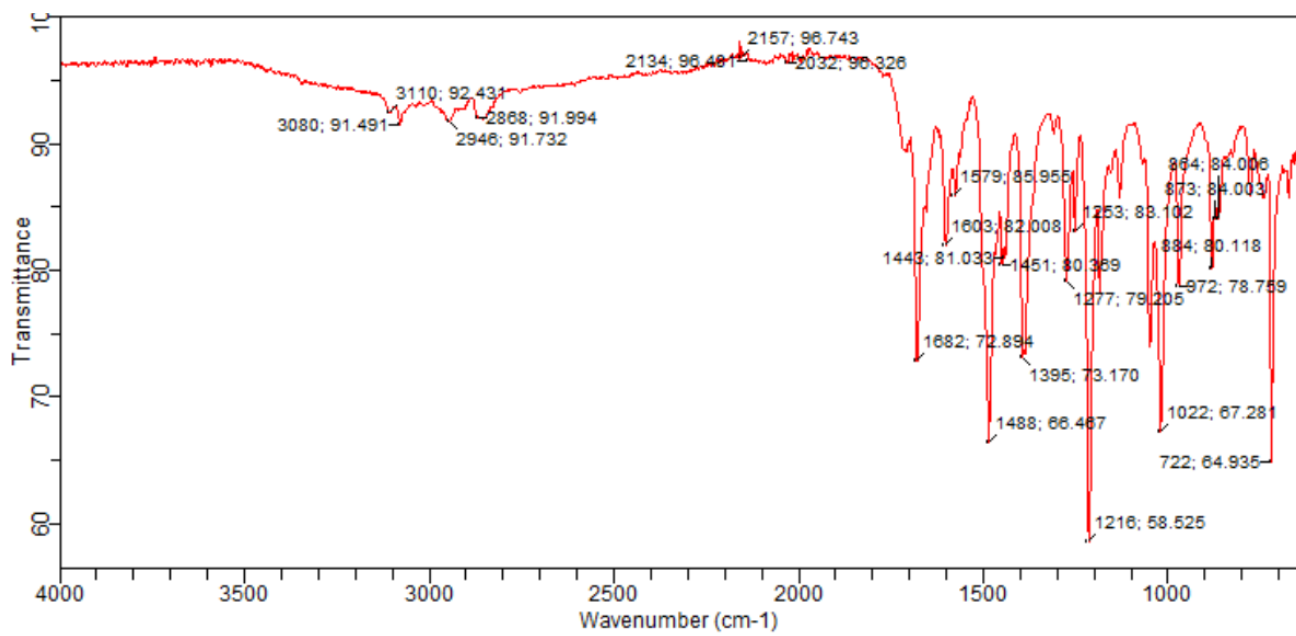
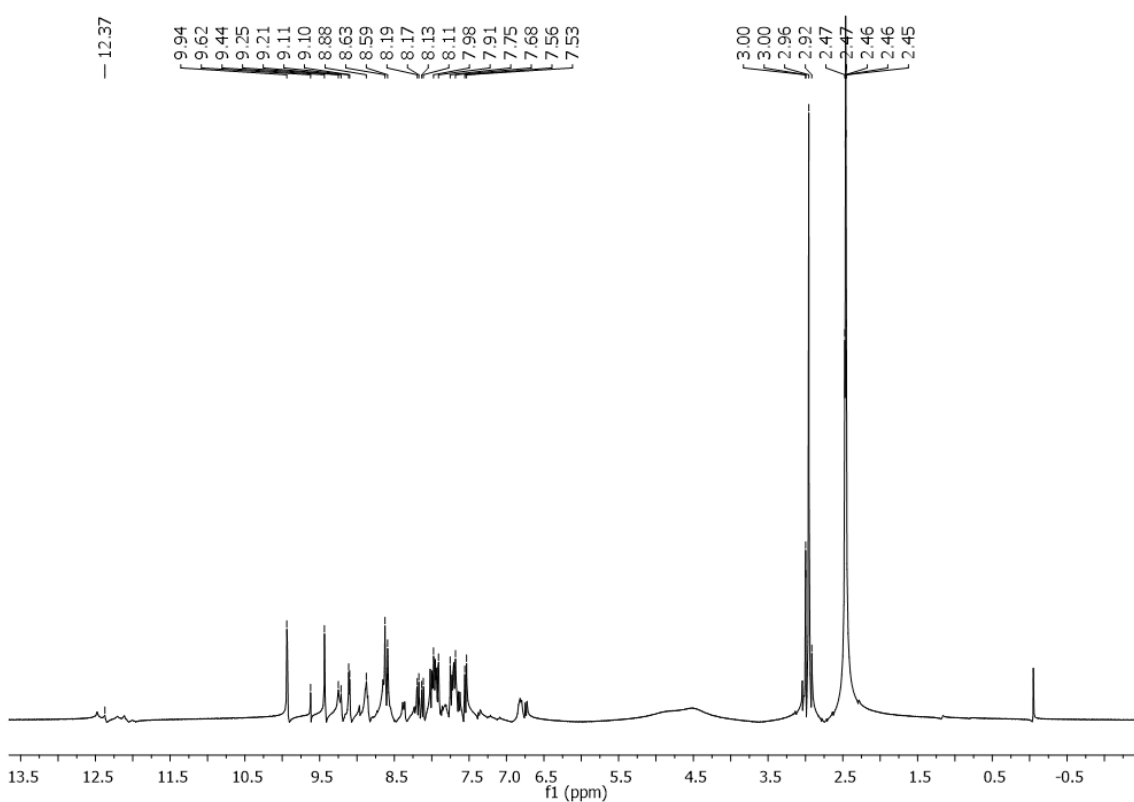
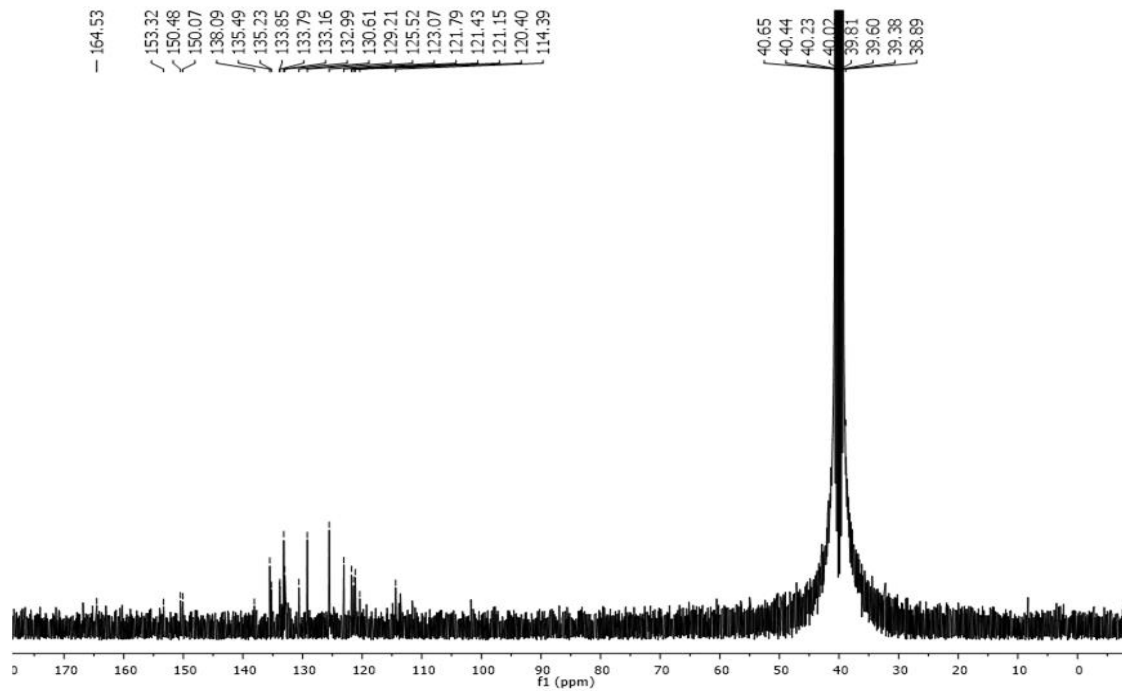


Fig. S1: FT-IR spectra of heterocyclic derivatives **4e-4l**, and **5a-5p**.

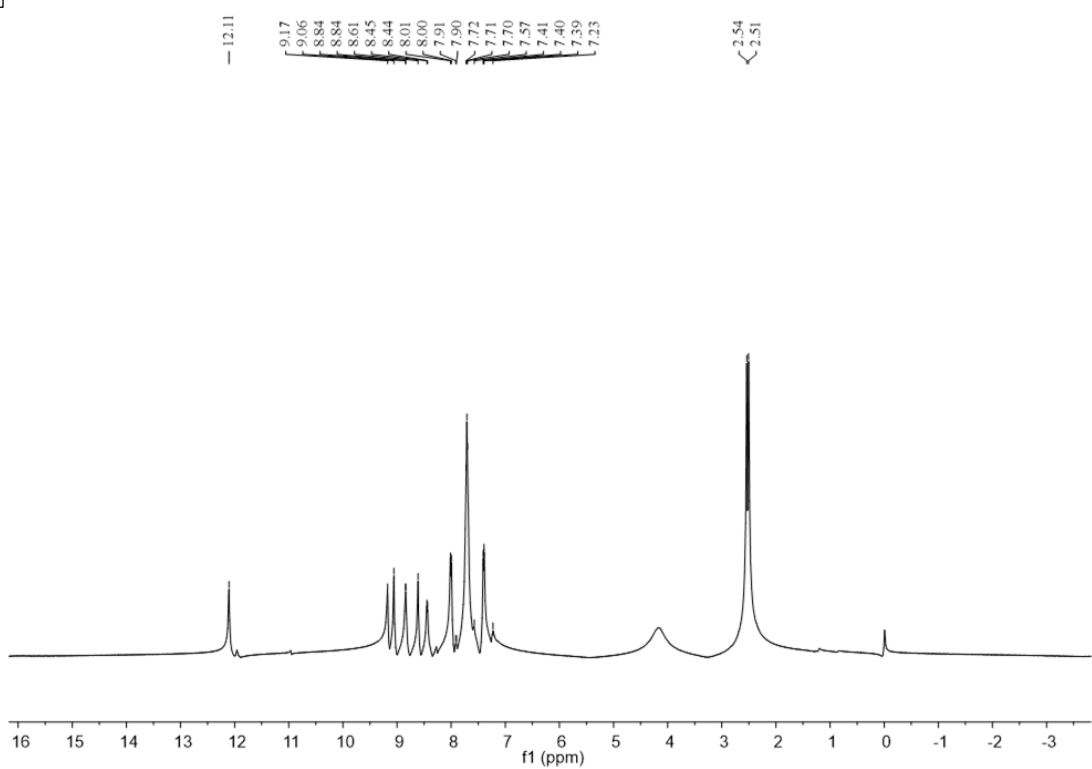
4e



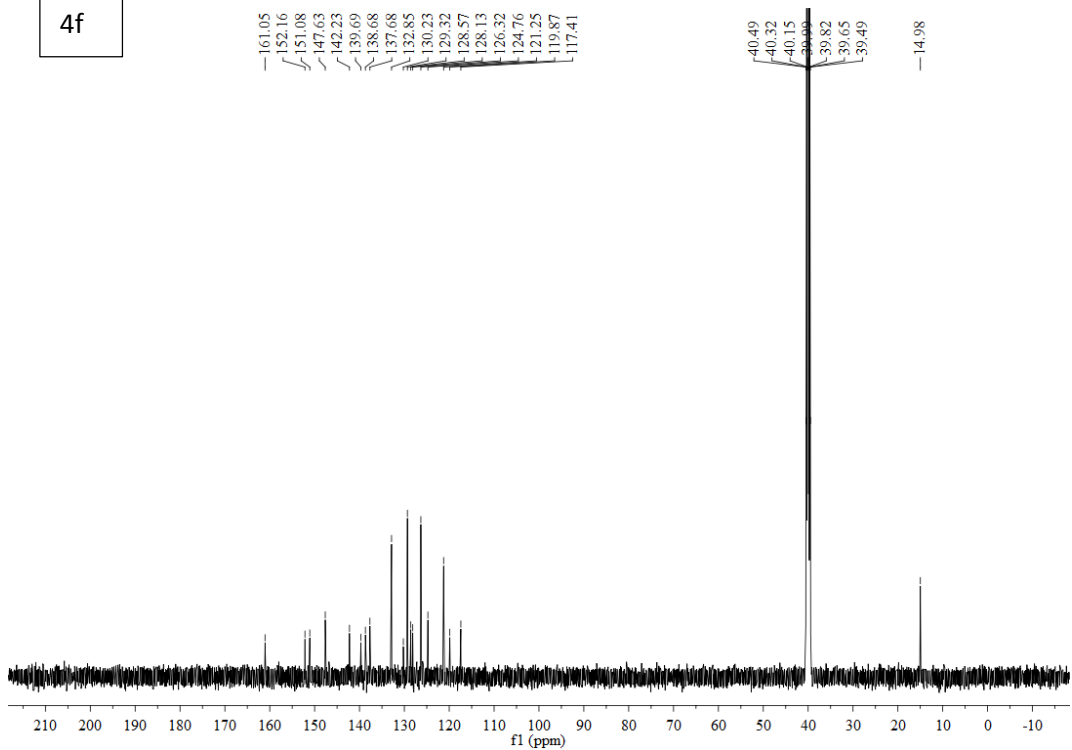
4e



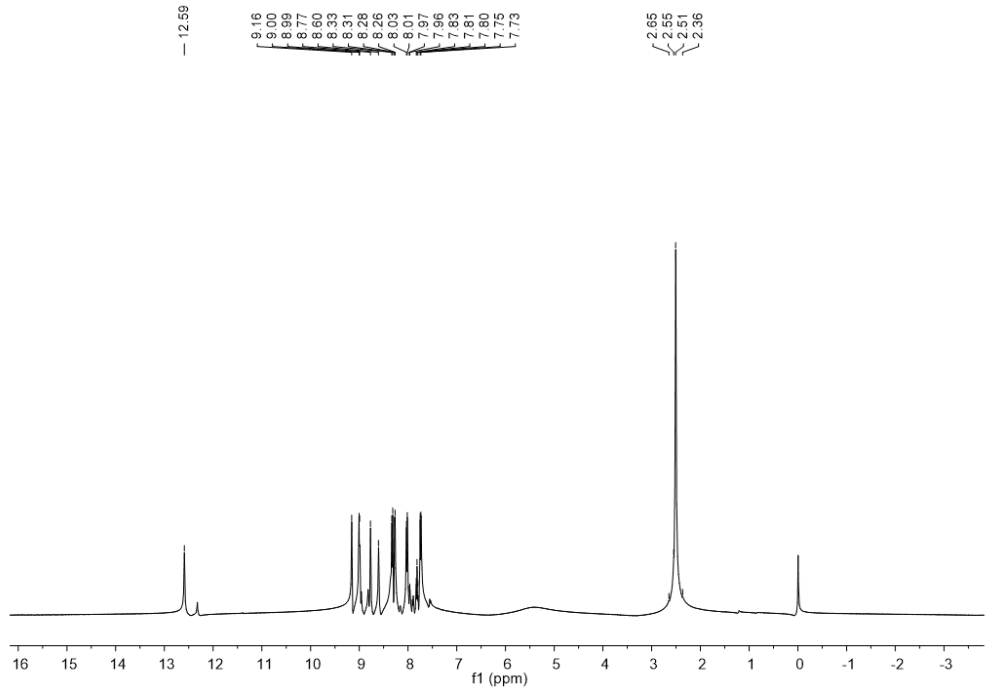
4f



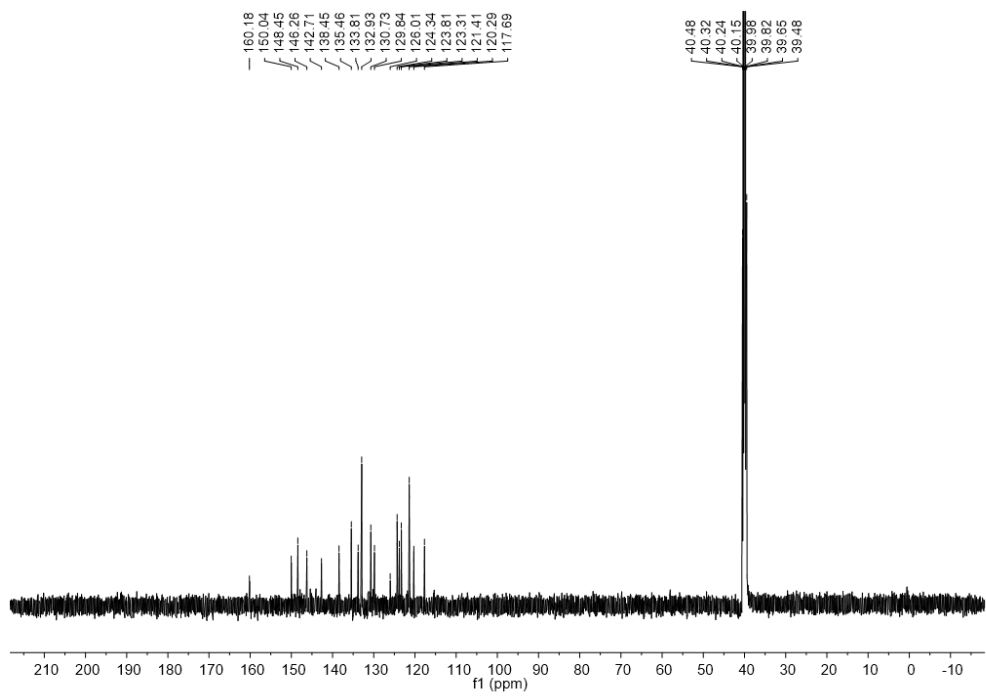
4f



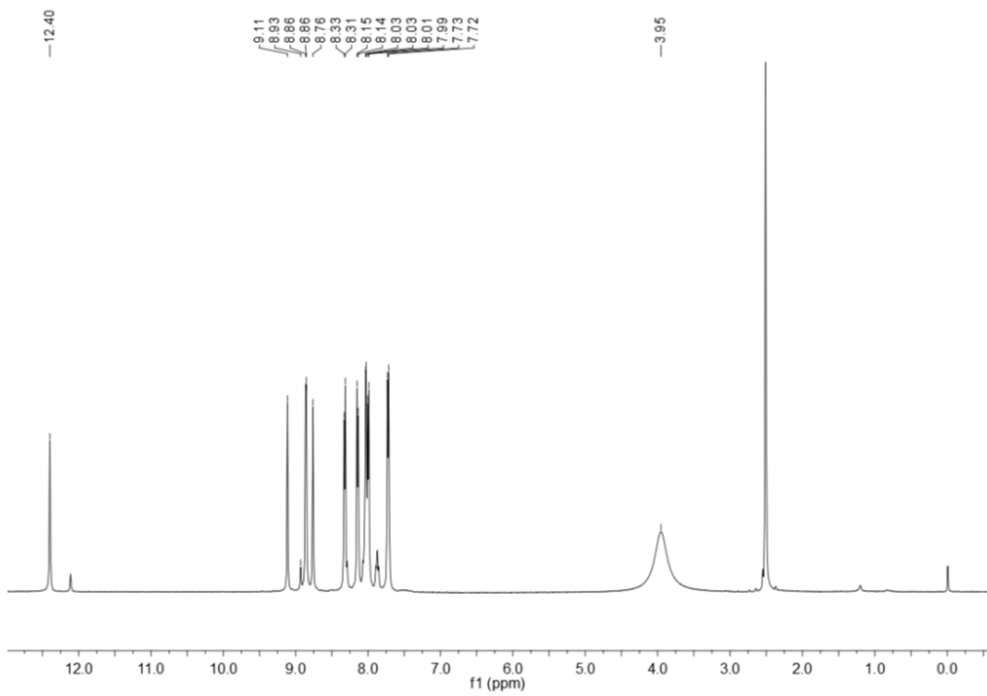
4g



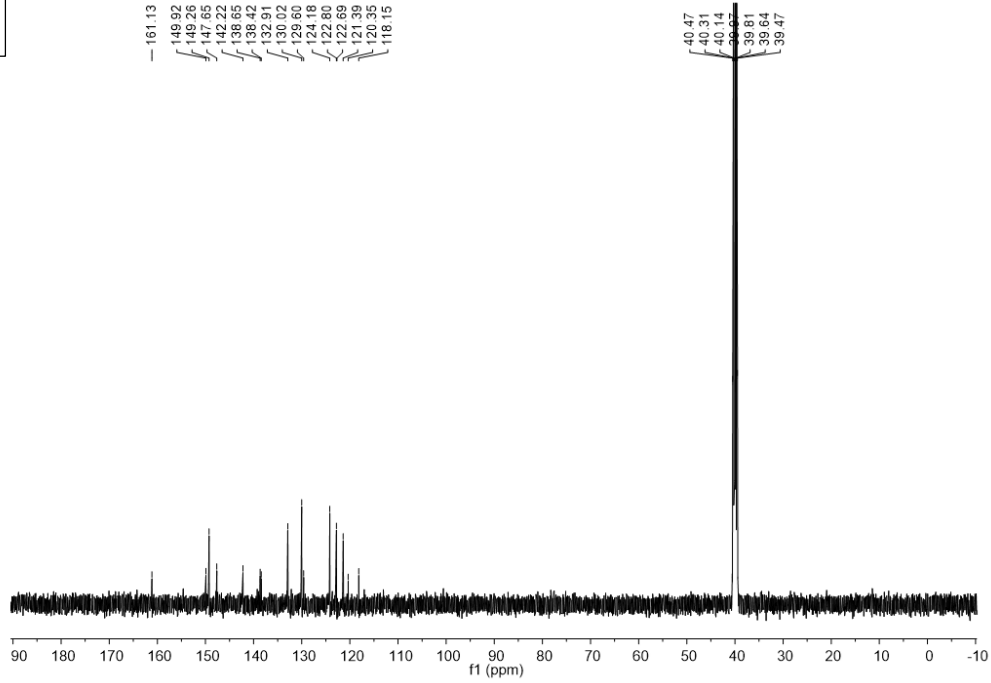
4g



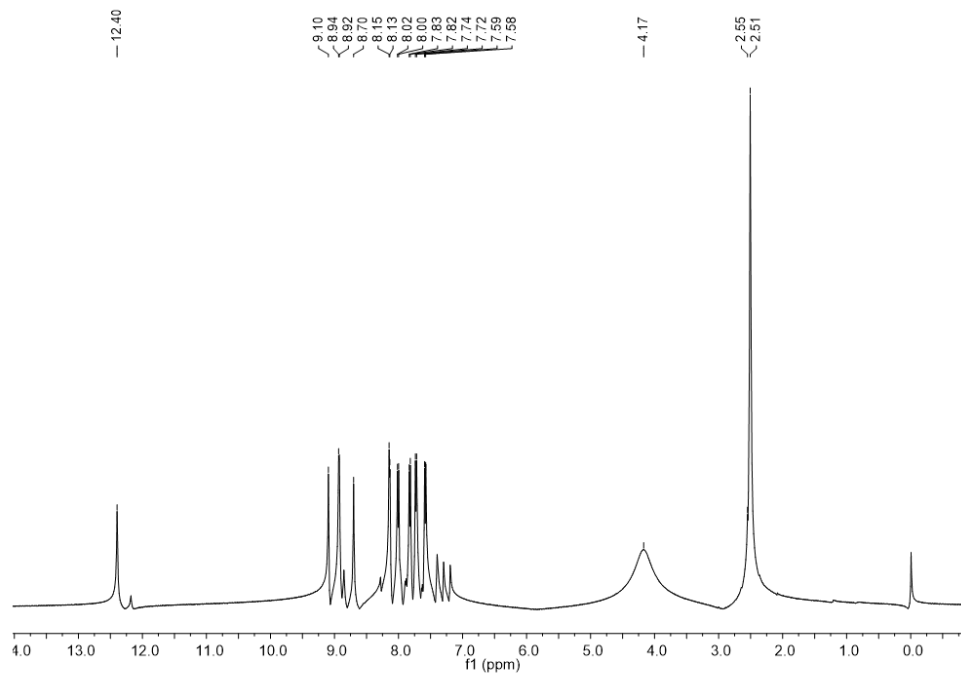
4h



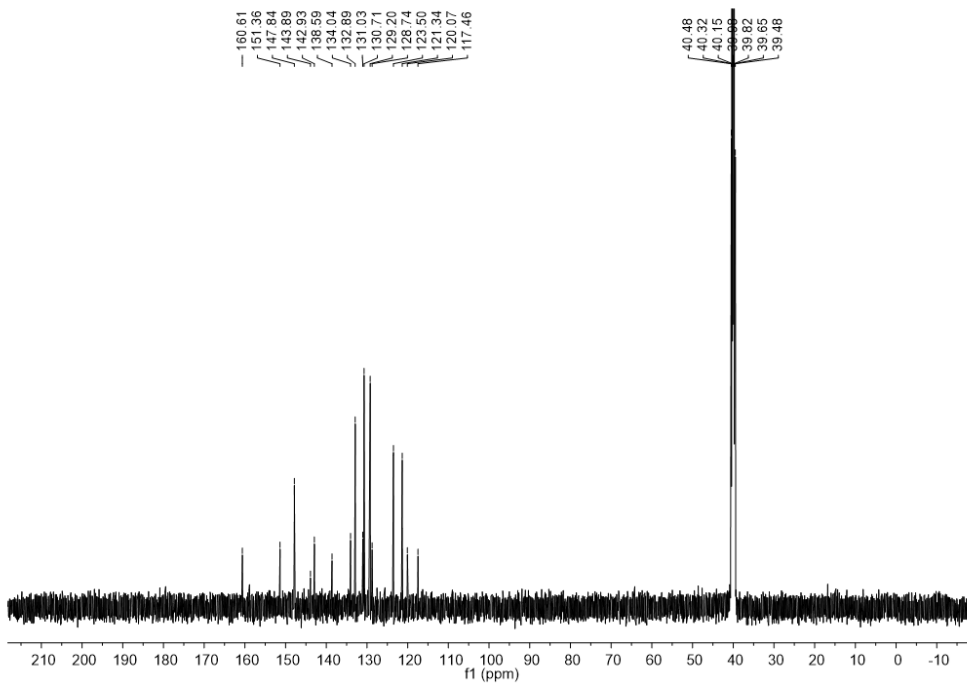
4h

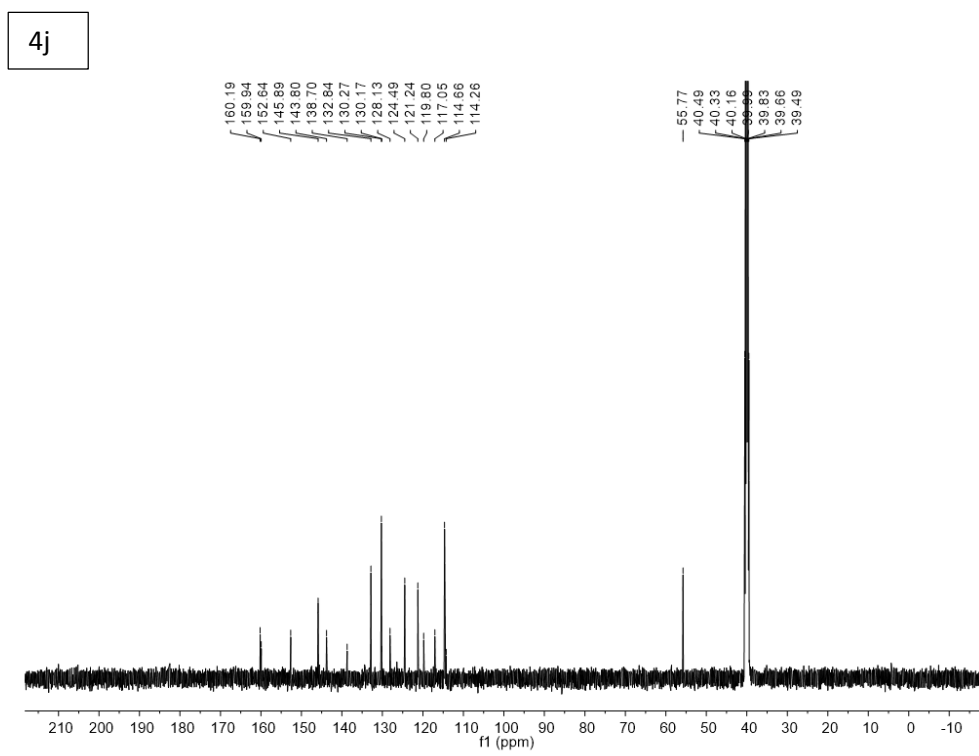
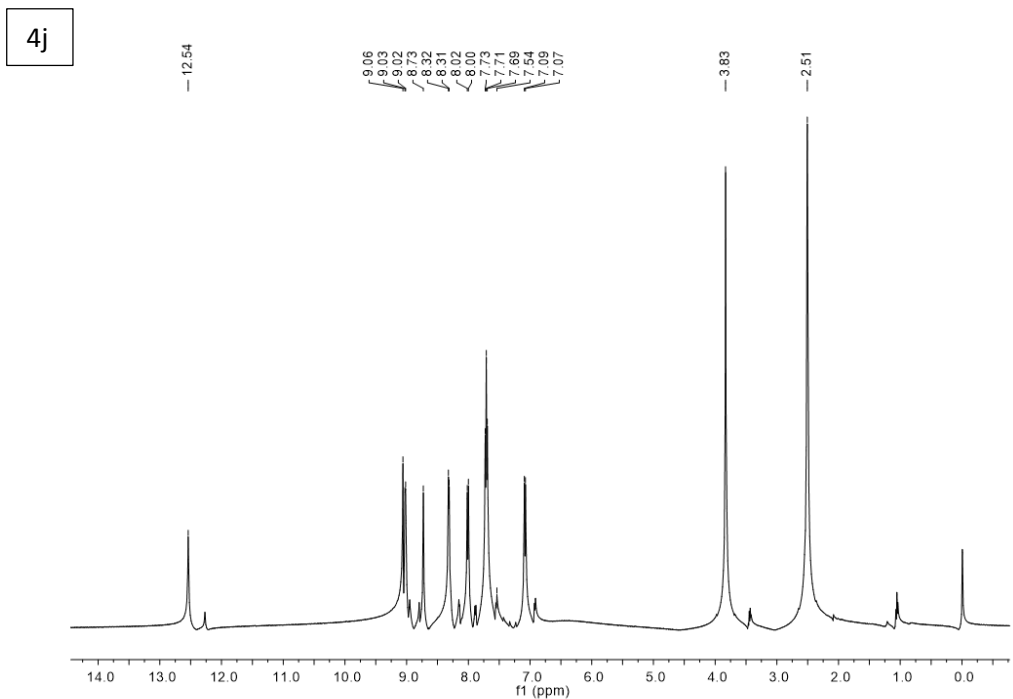


4i

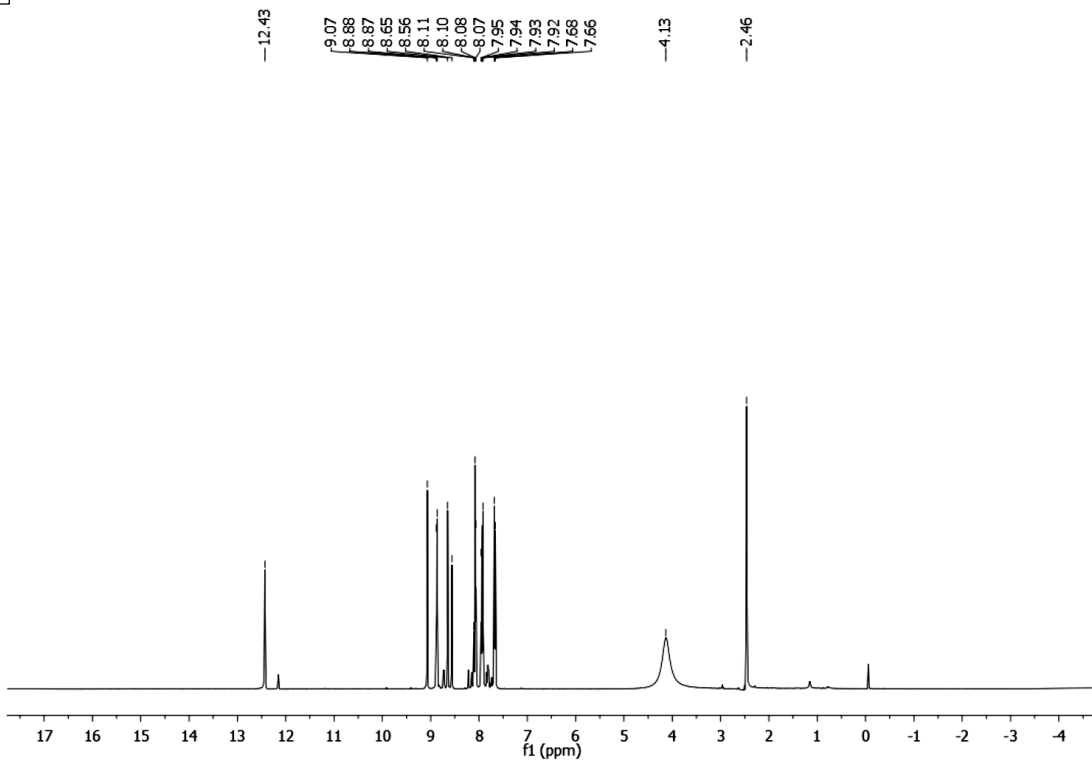


4i

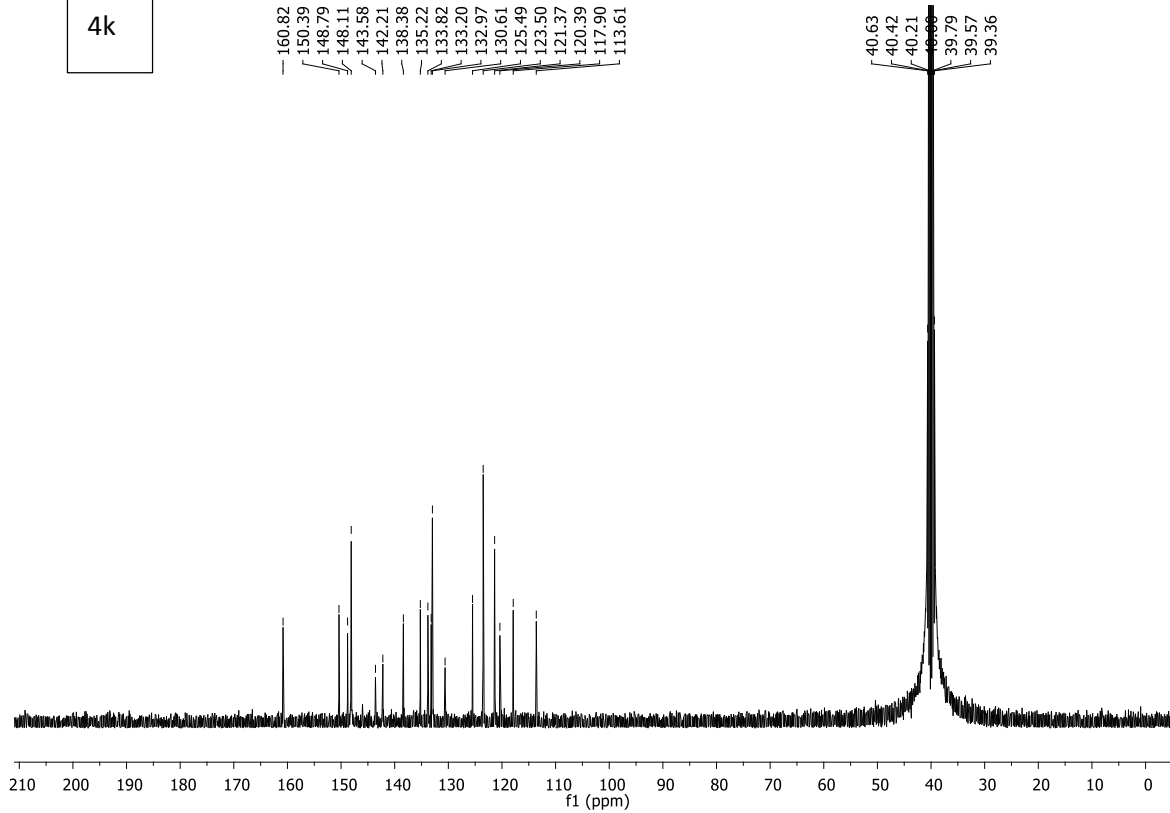




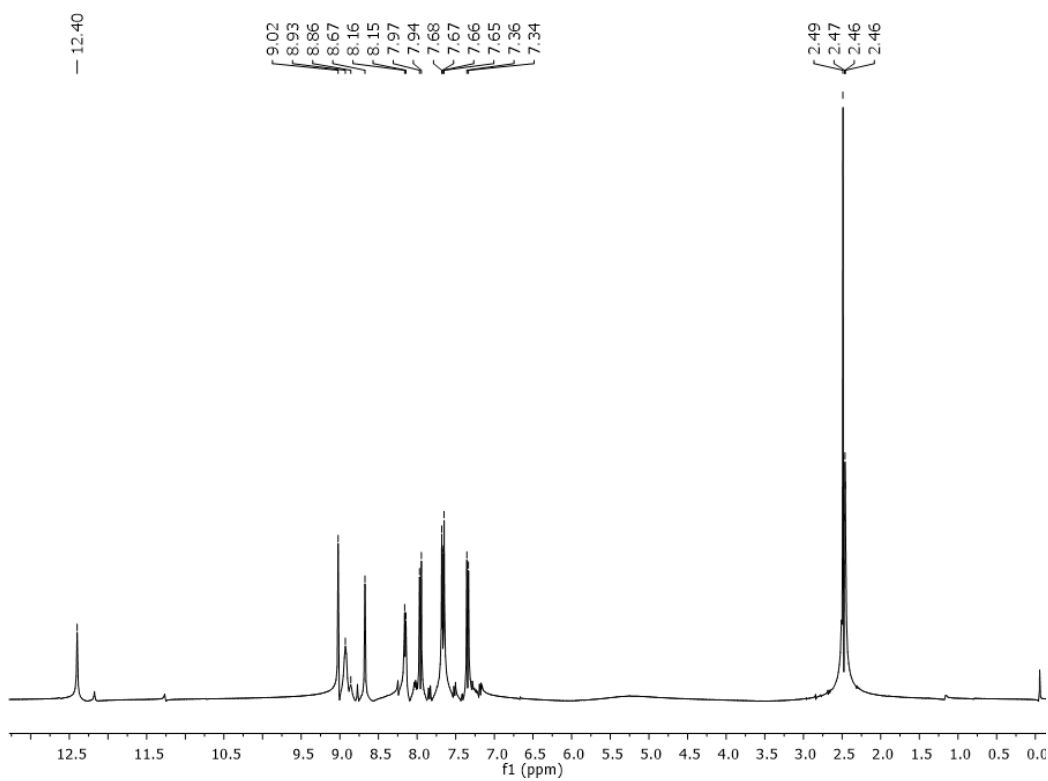
4k



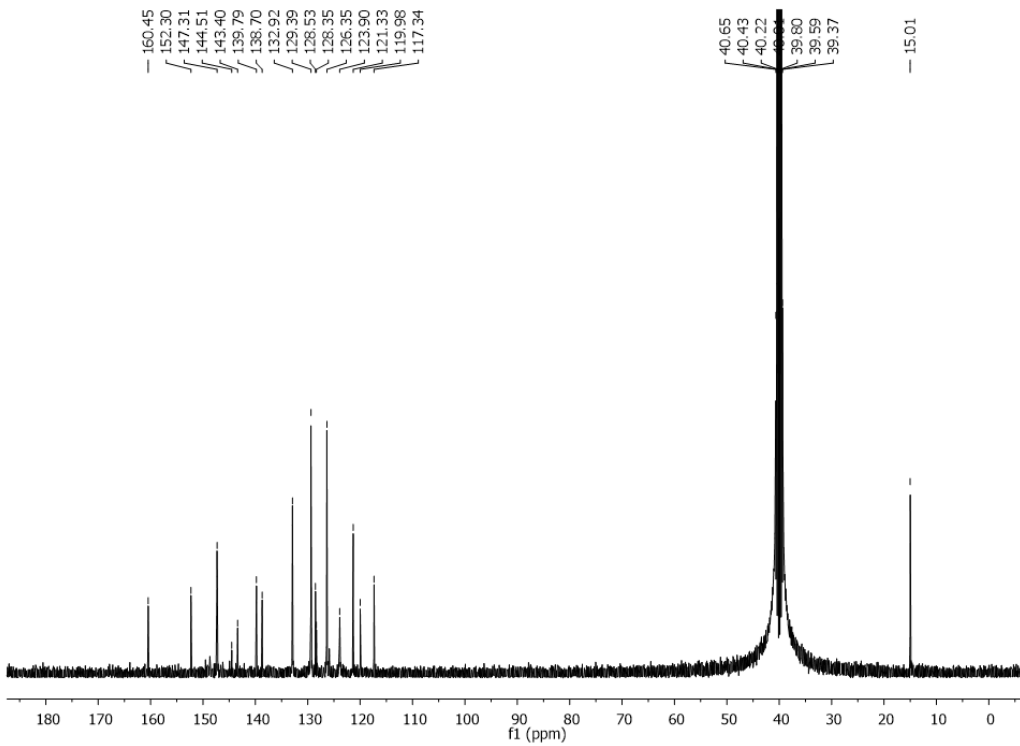
4k



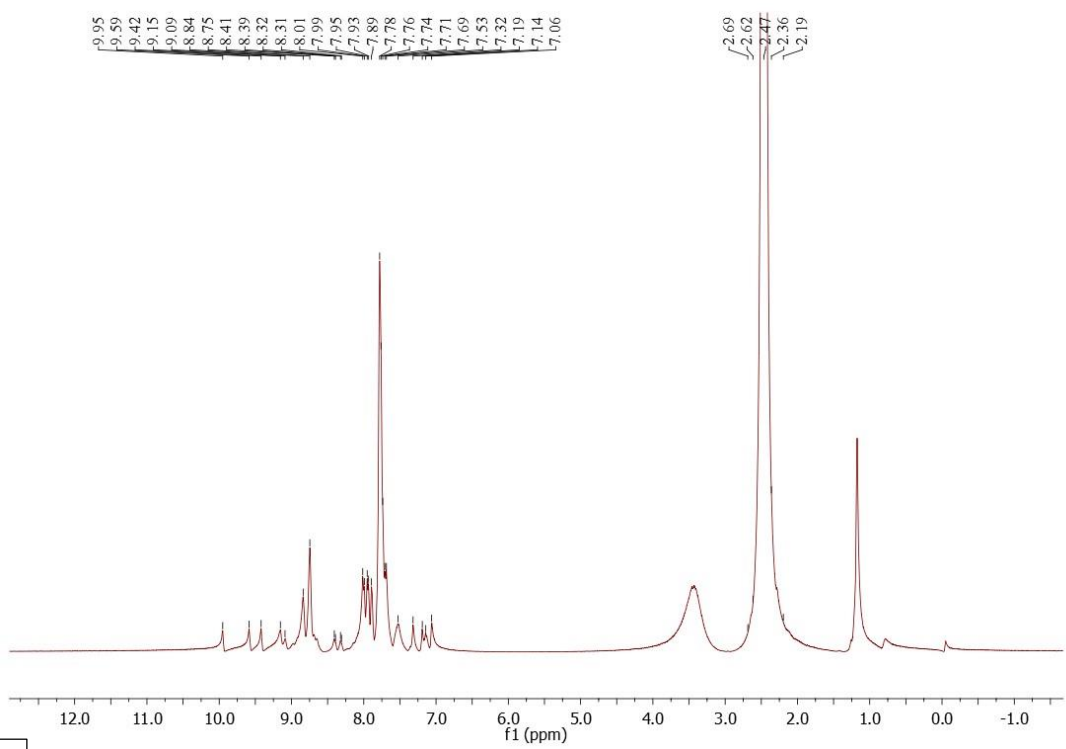
4l



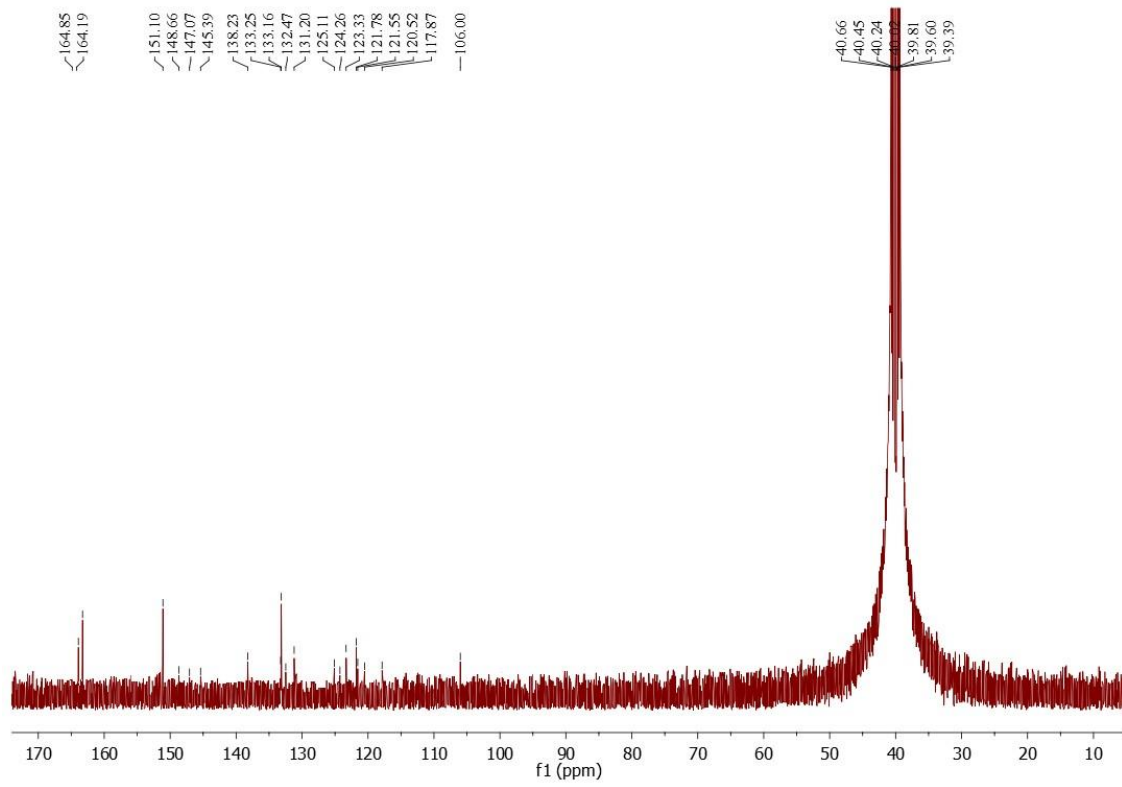
4l



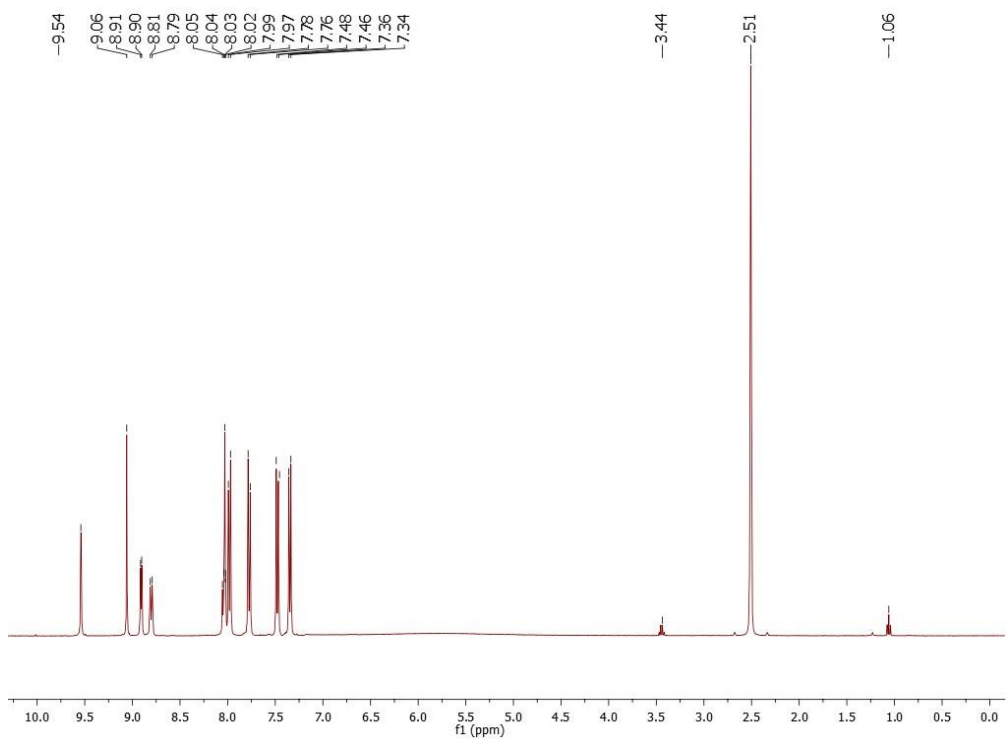
5a



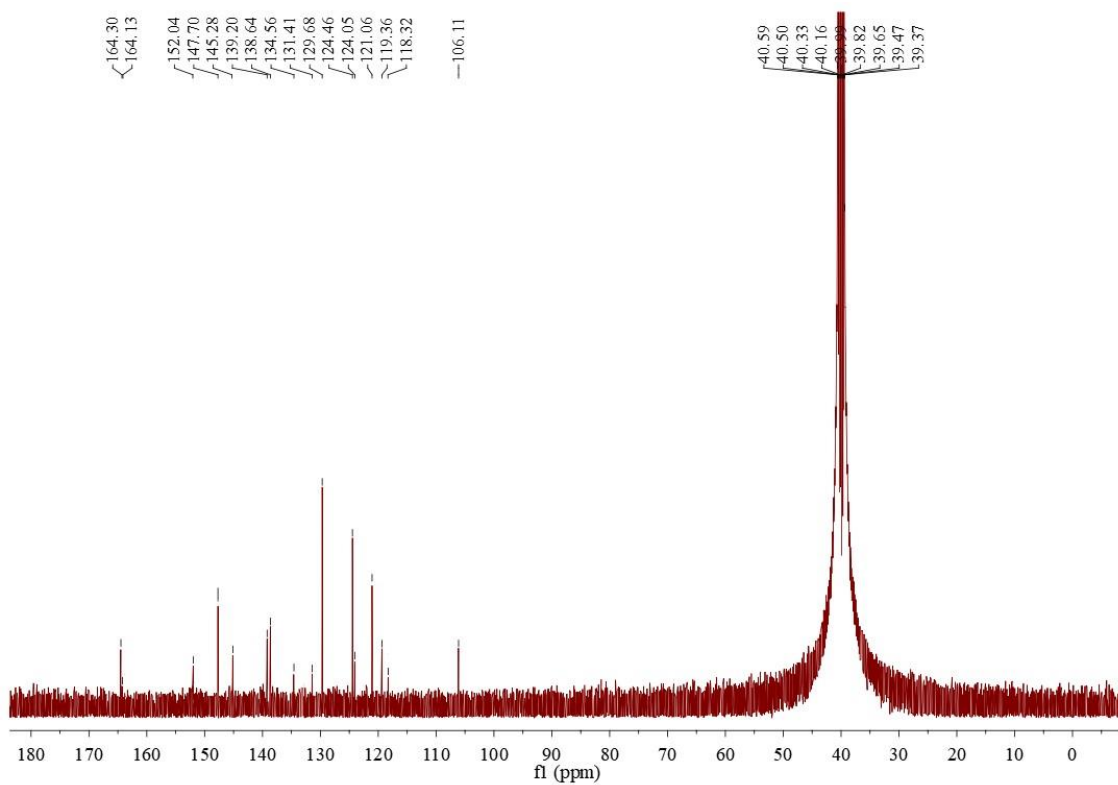
5a



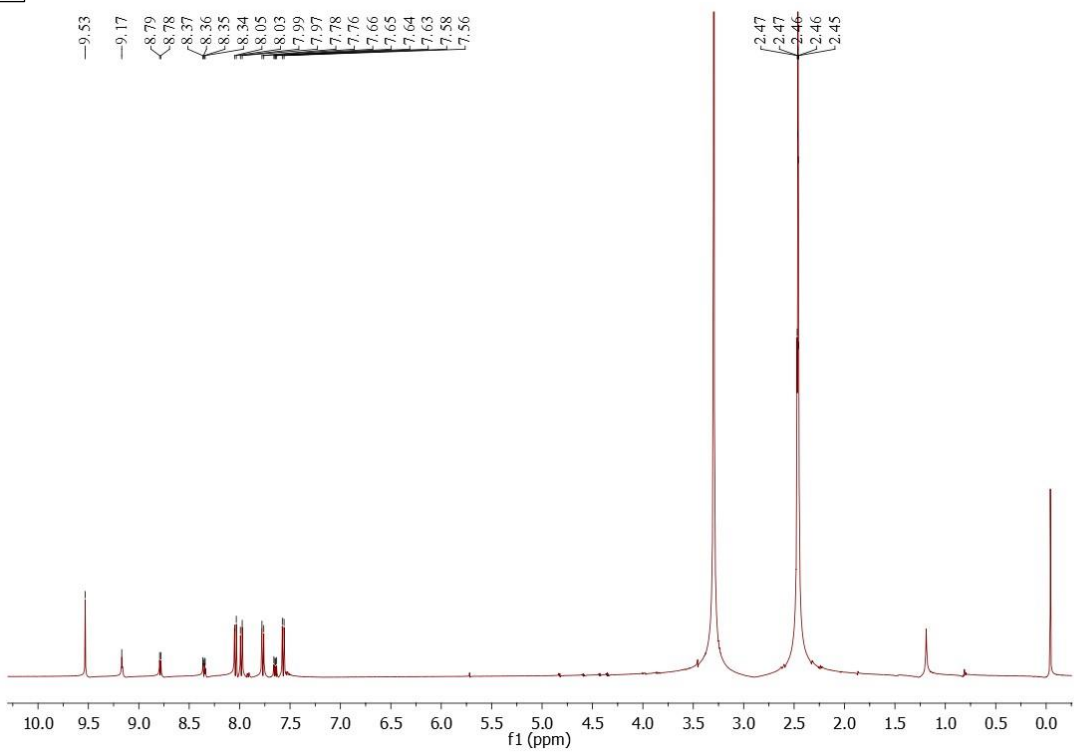
5b



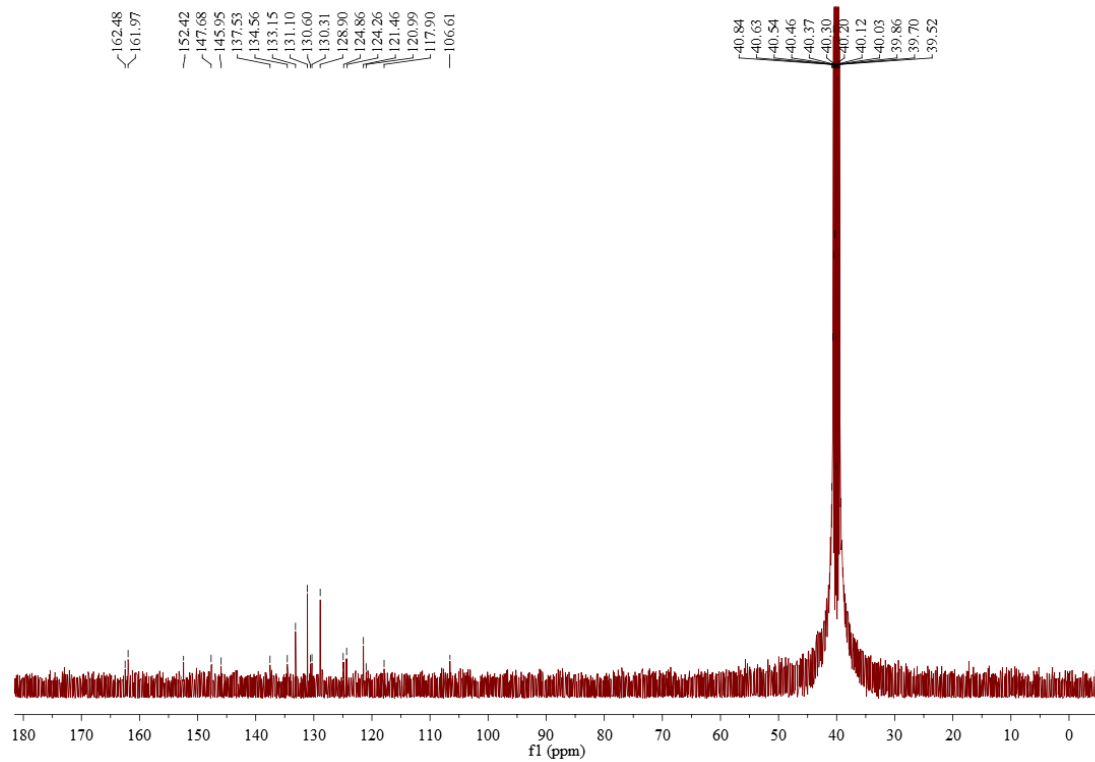
5b



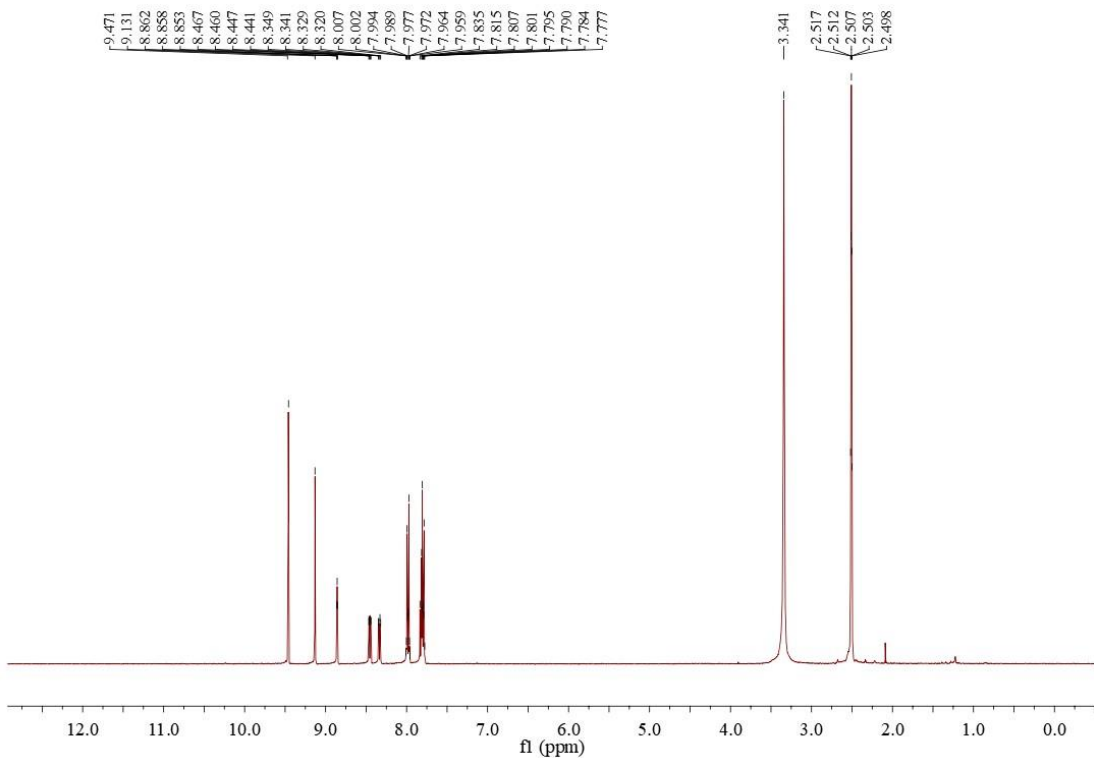
5c



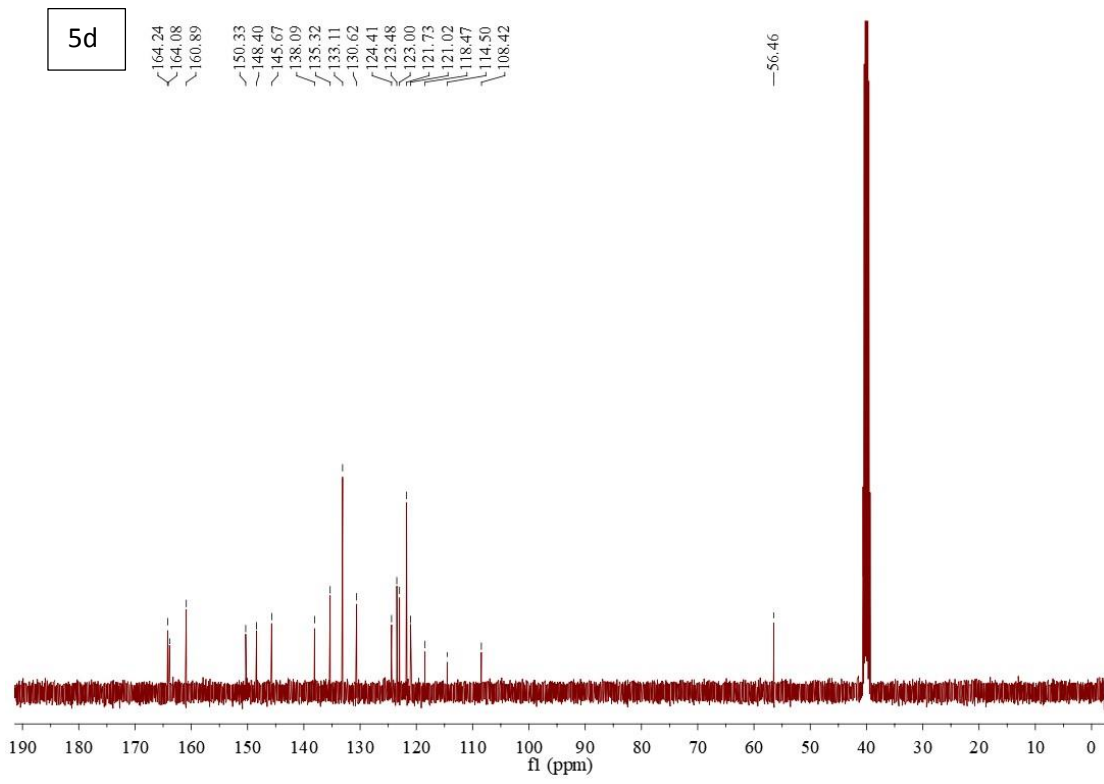
5c



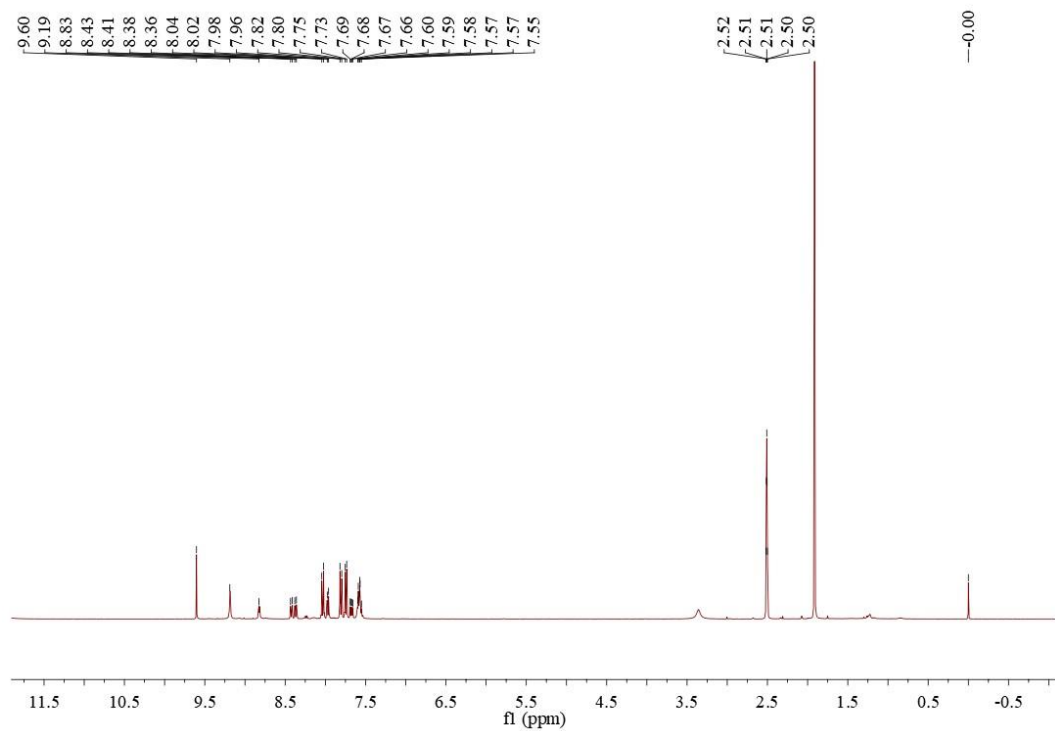
5d



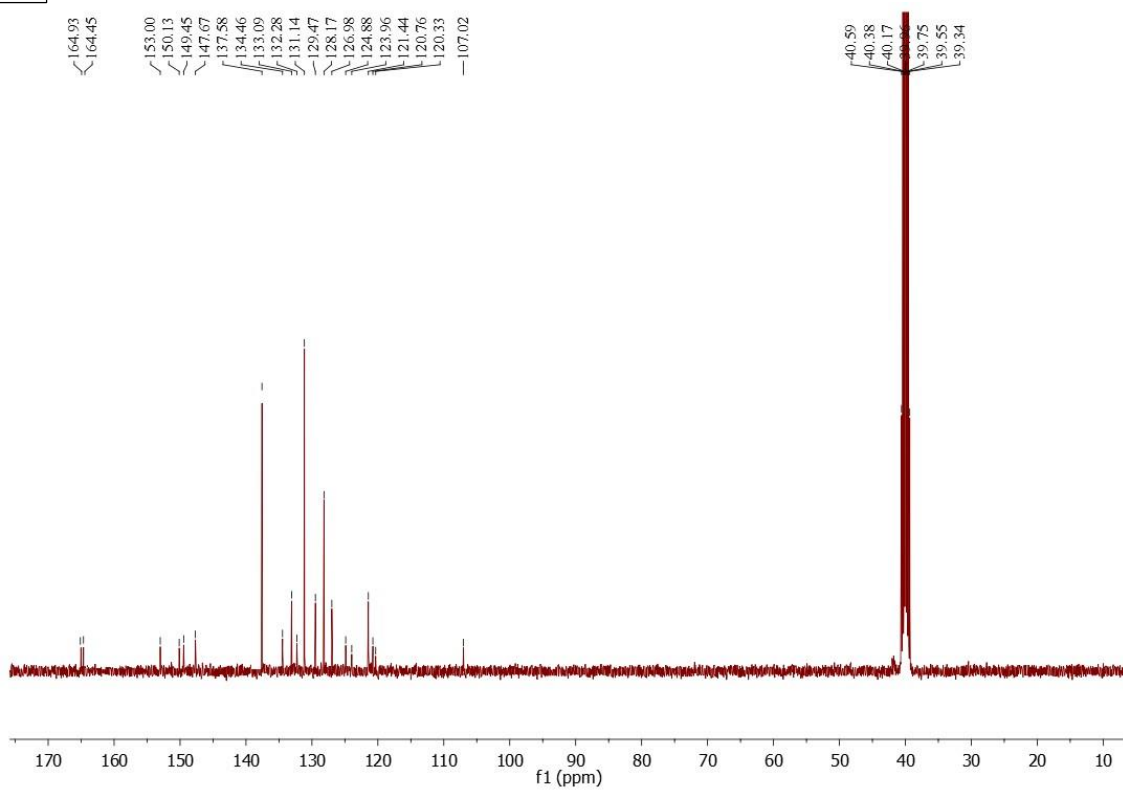
5d



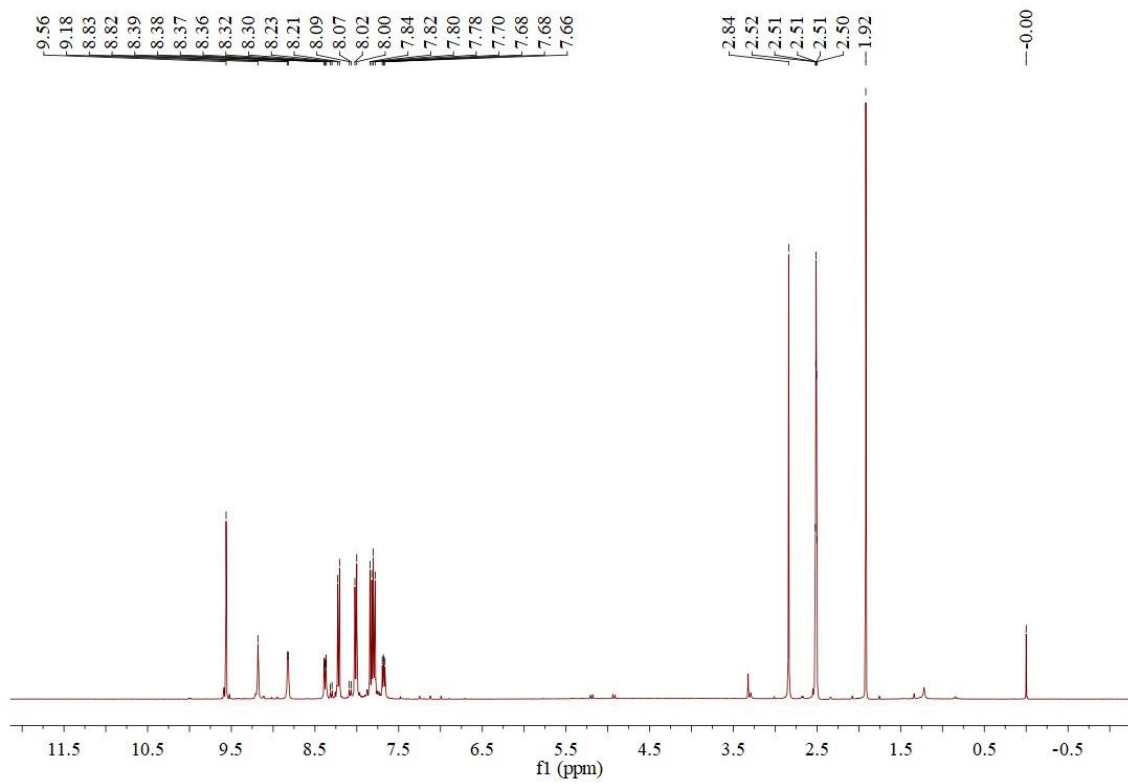
5e



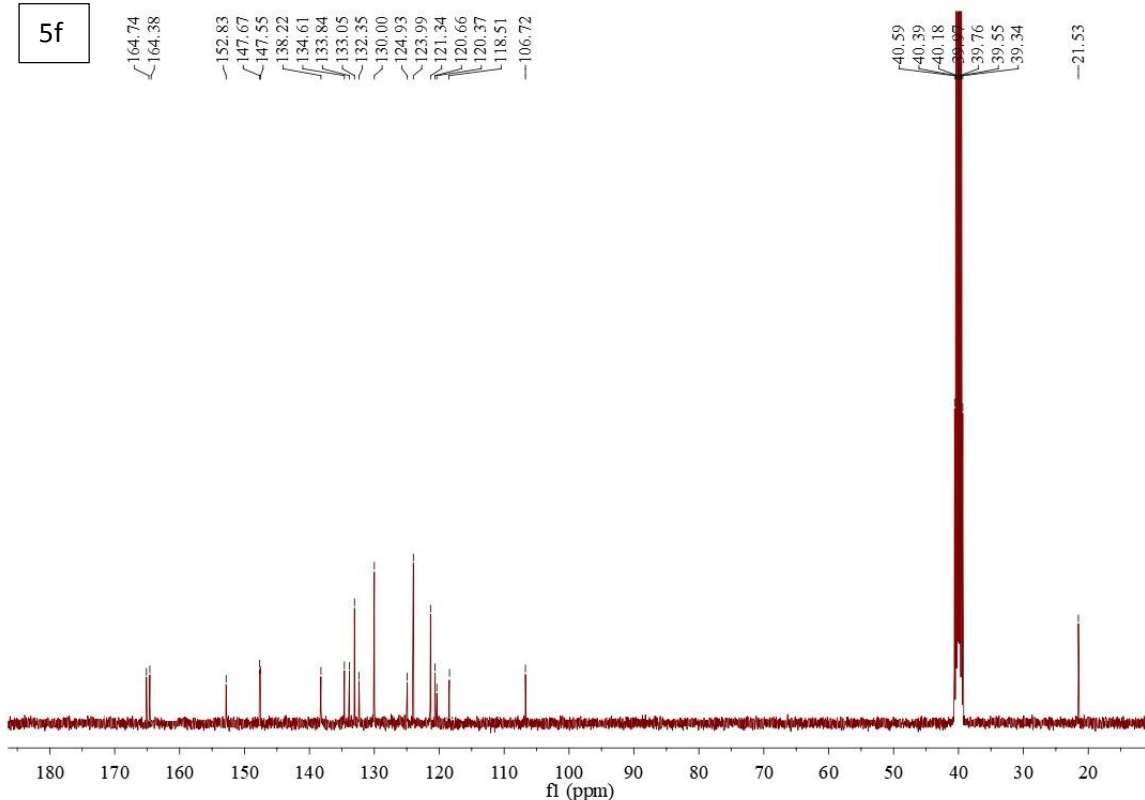
5e



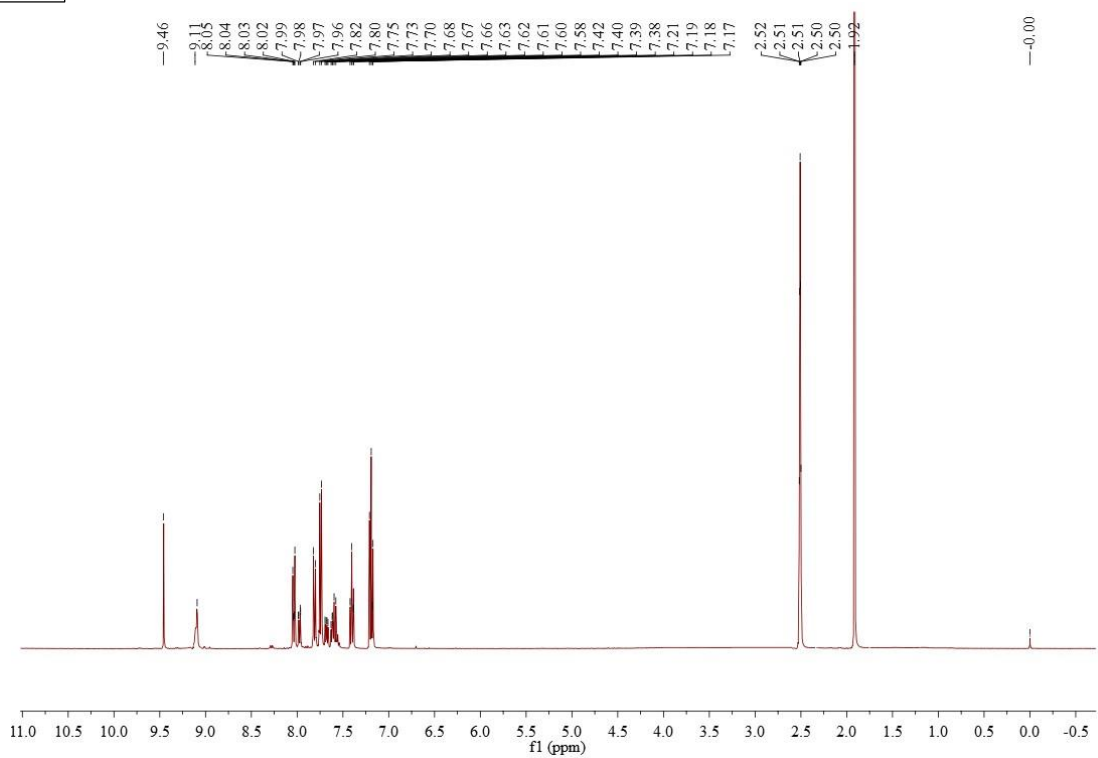
5f



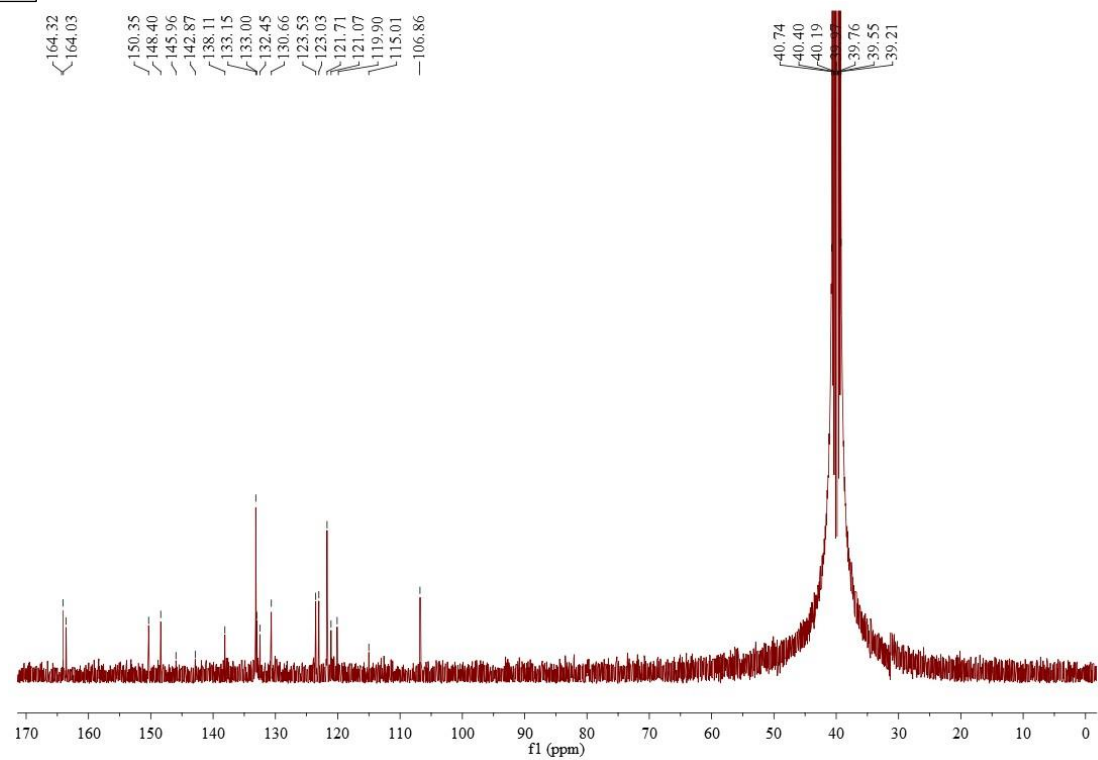
5f



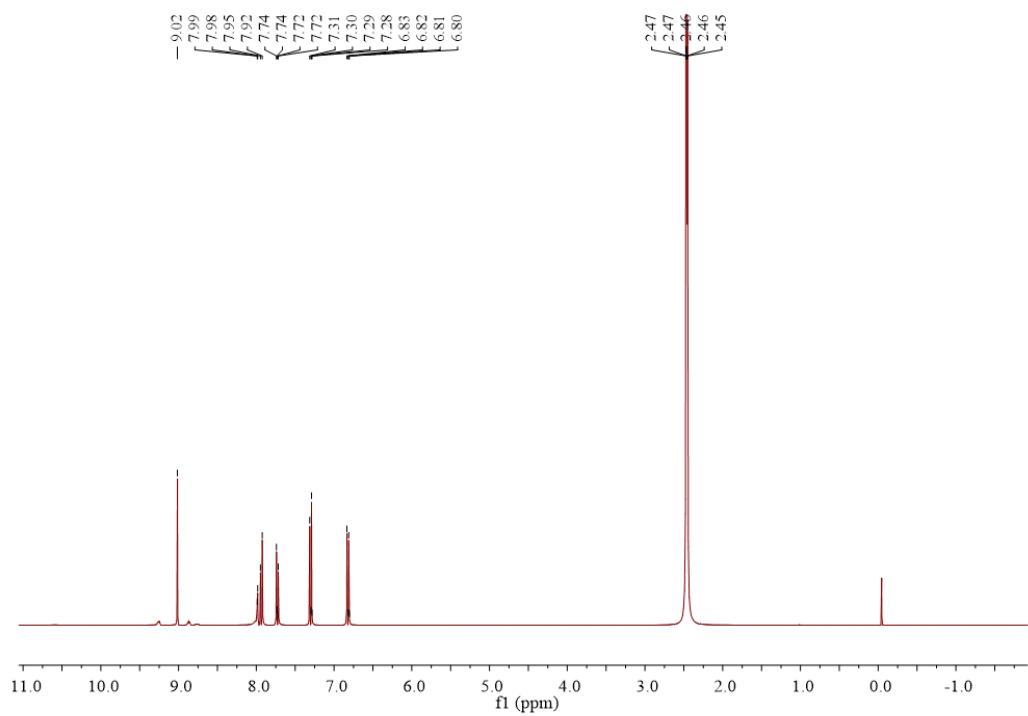
5g



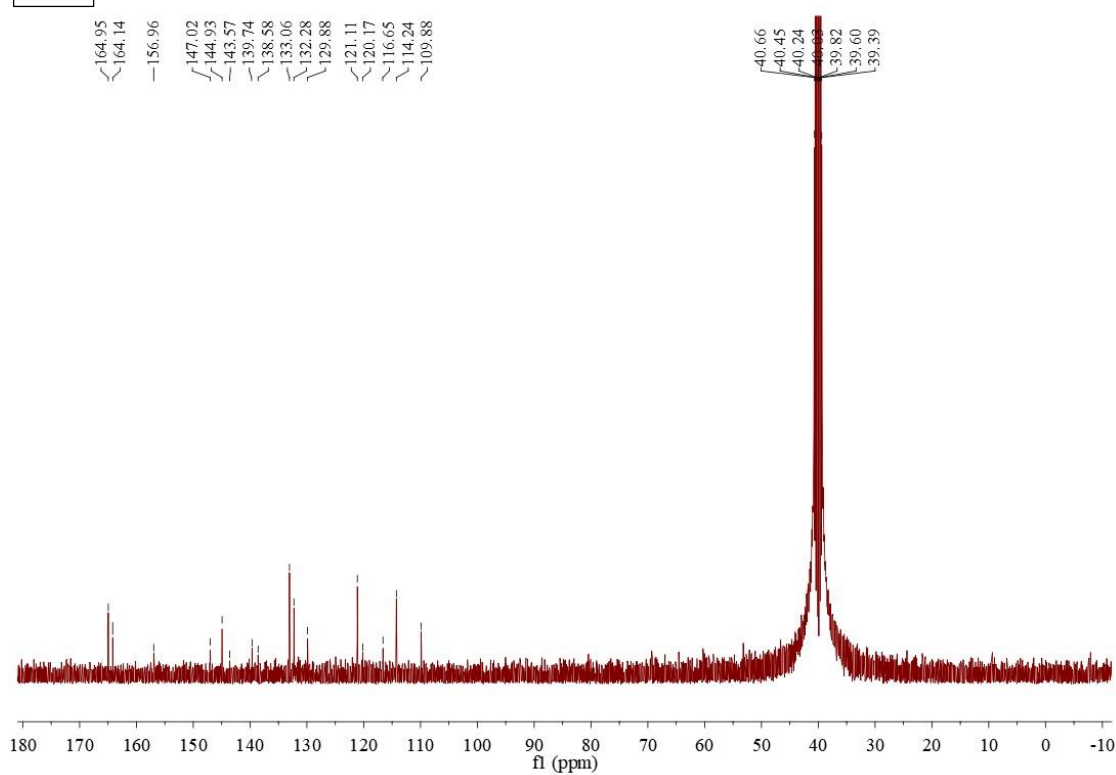
5g



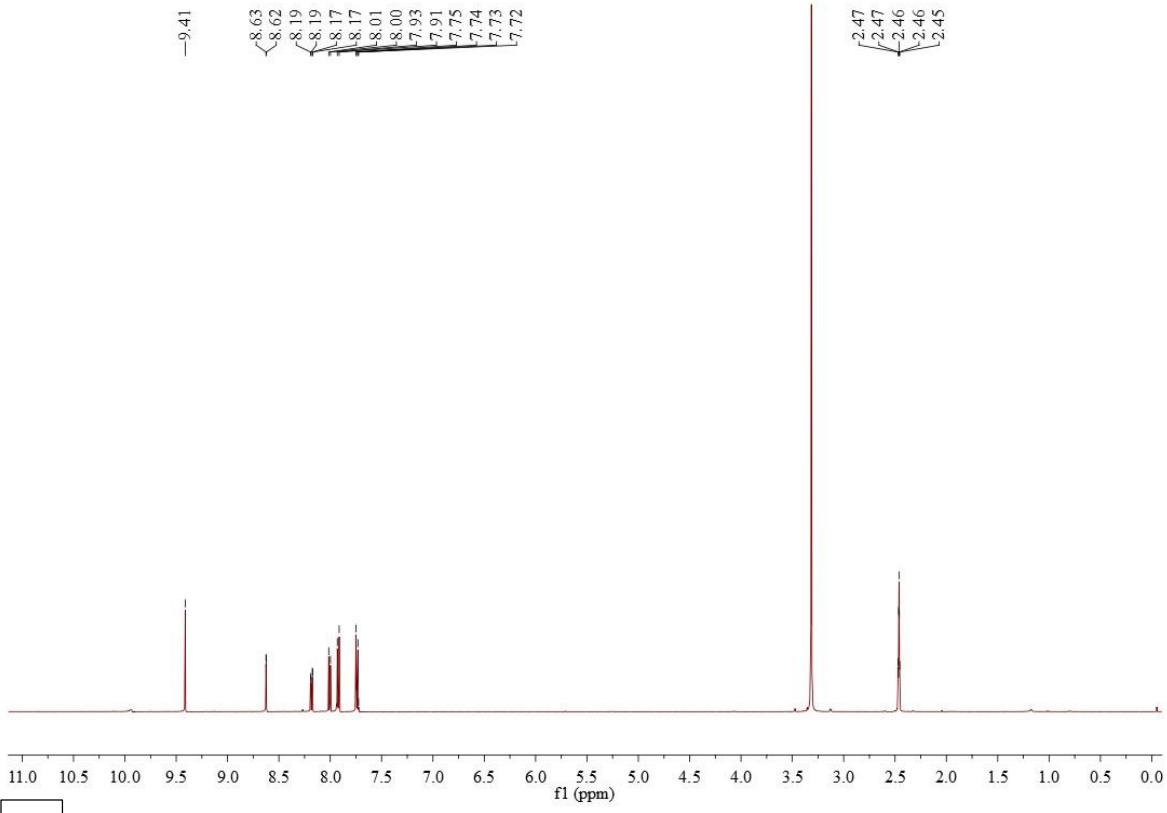
5h



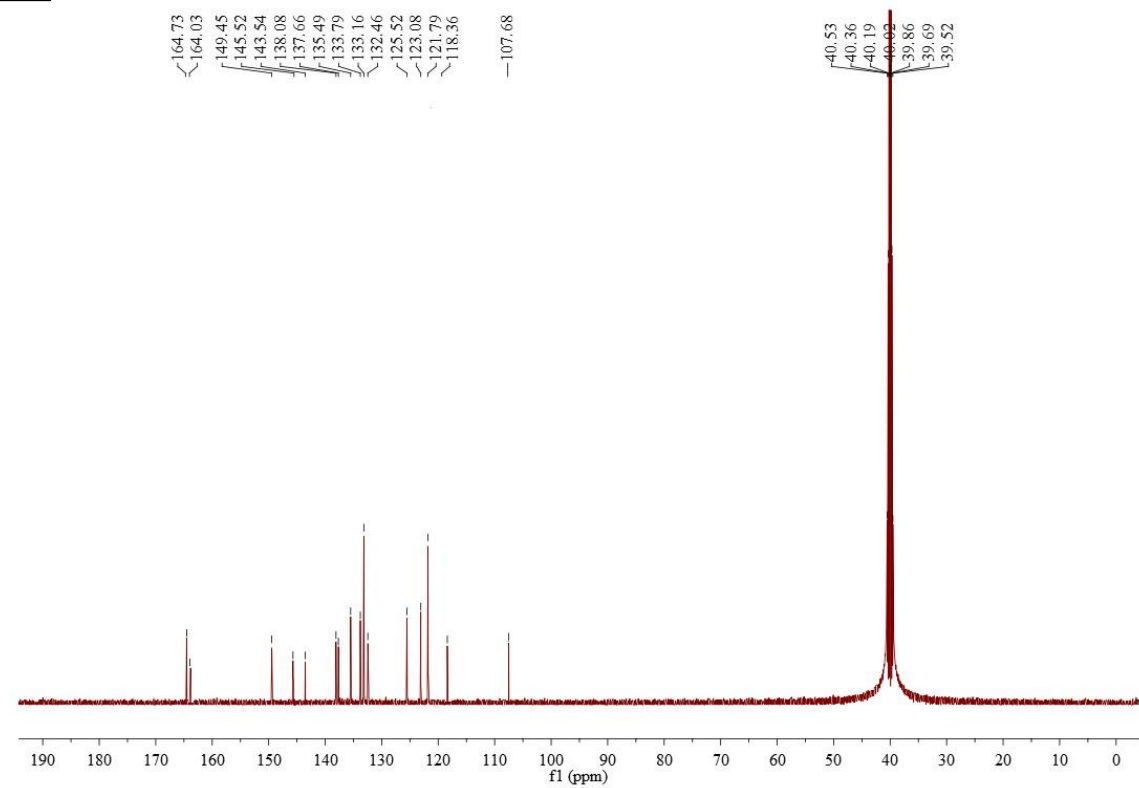
5h



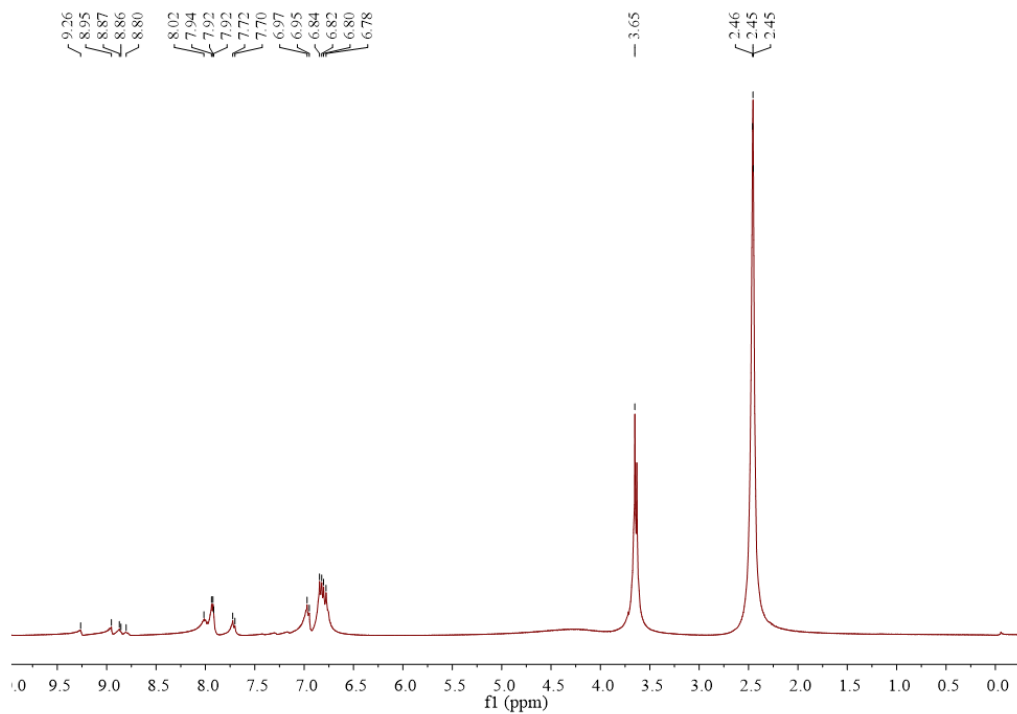
5i



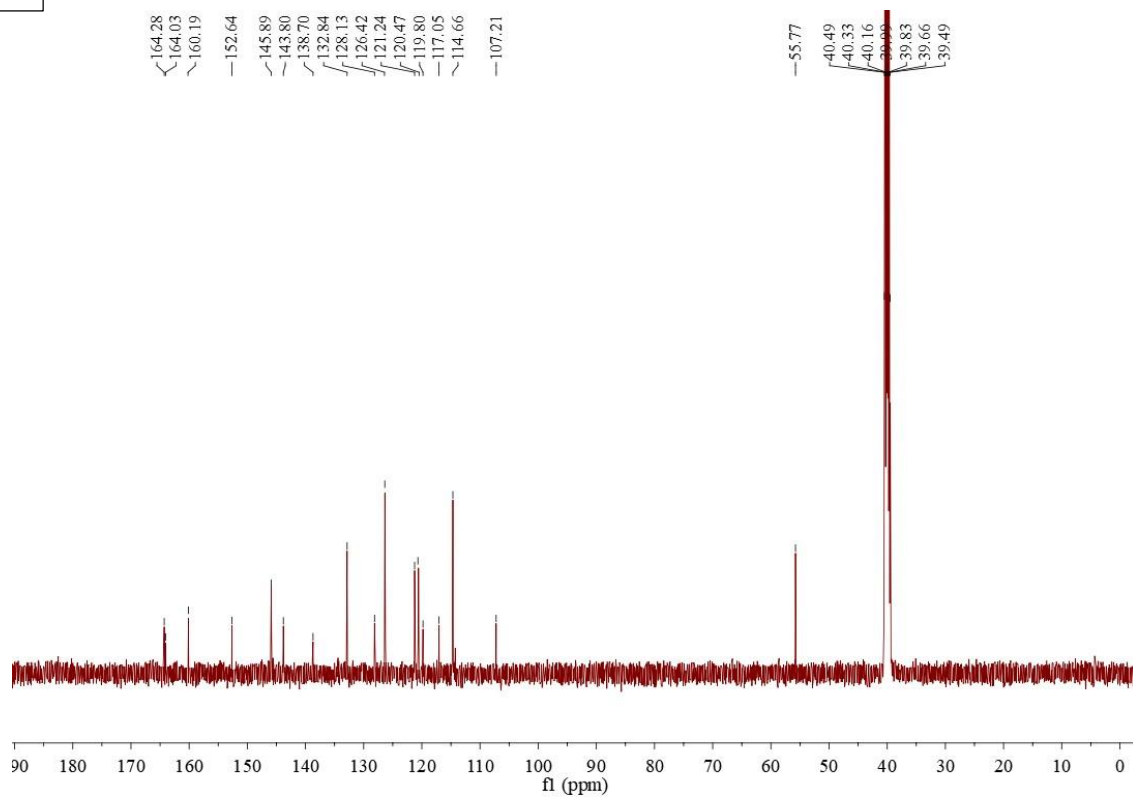
5i



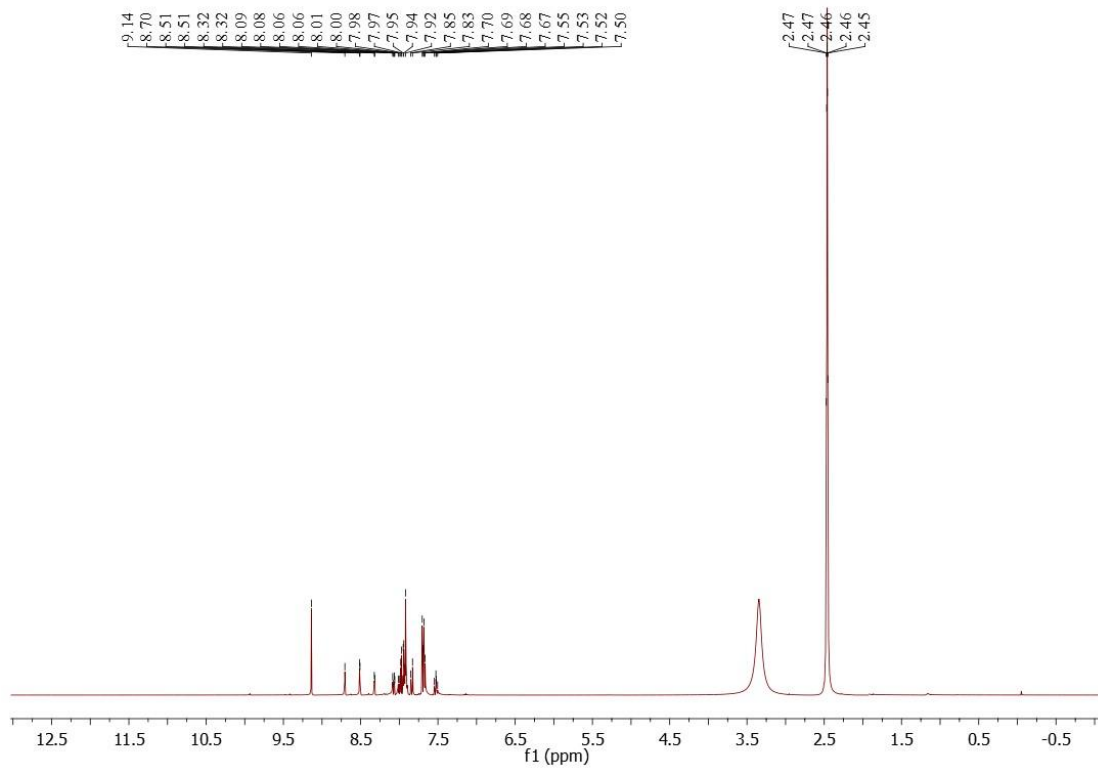
5j



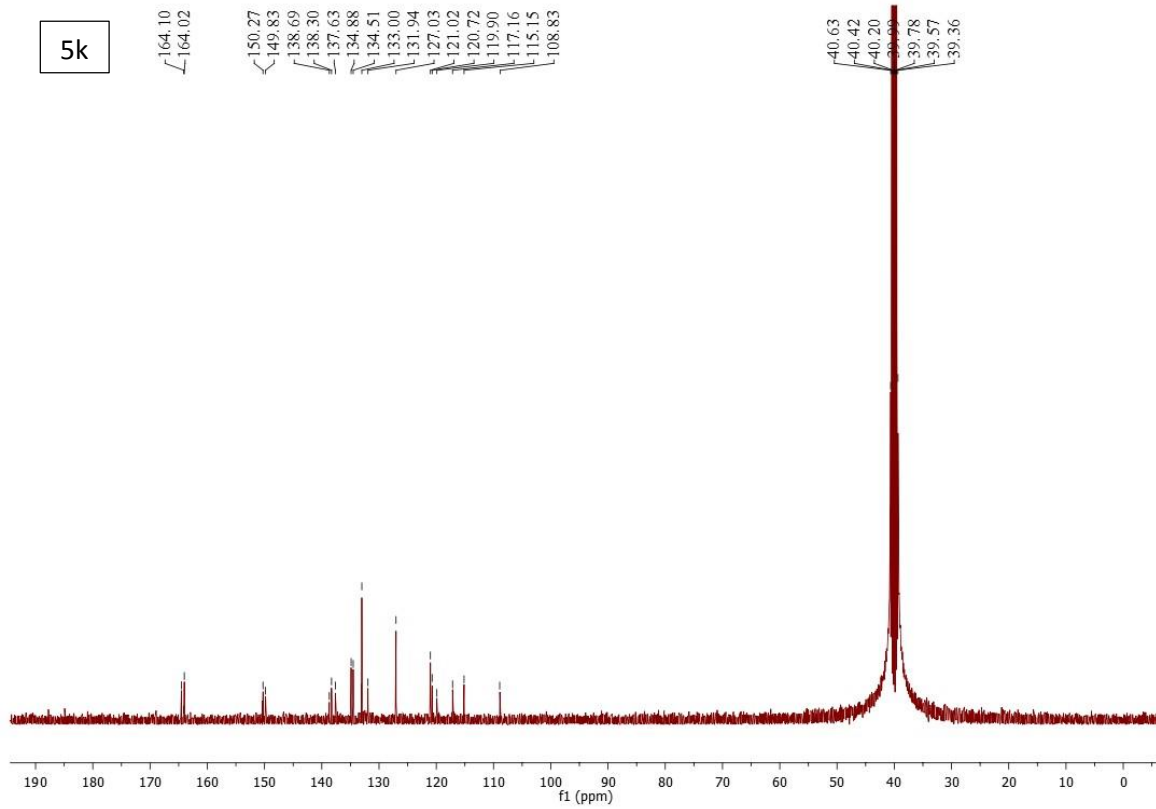
5j



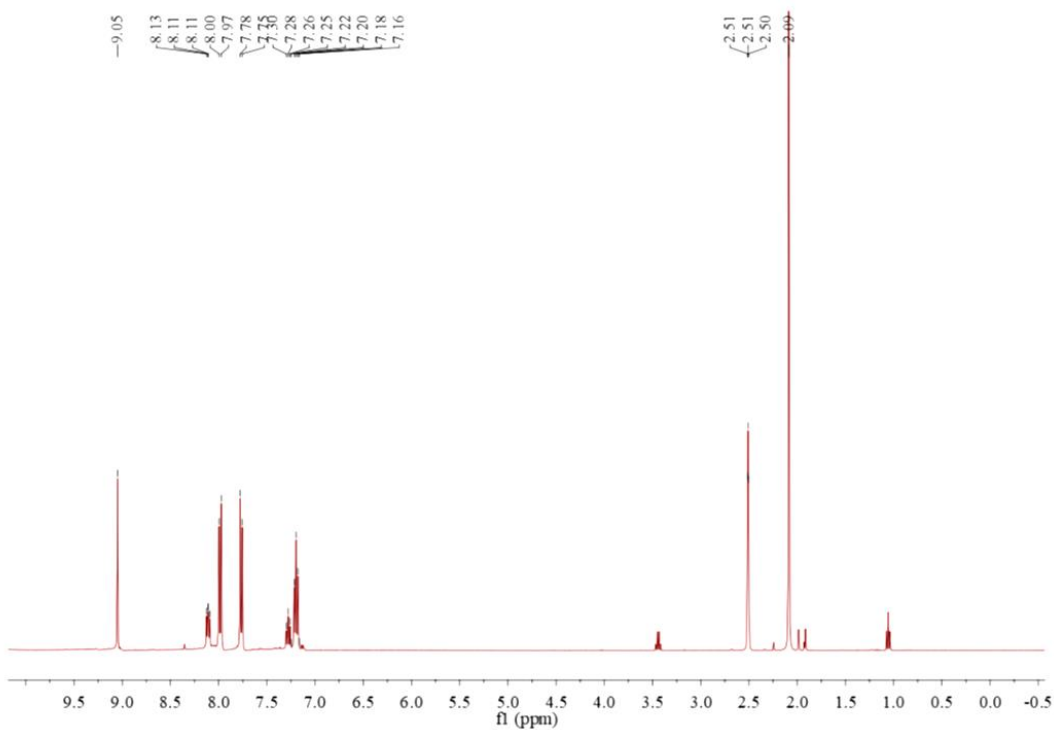
5k



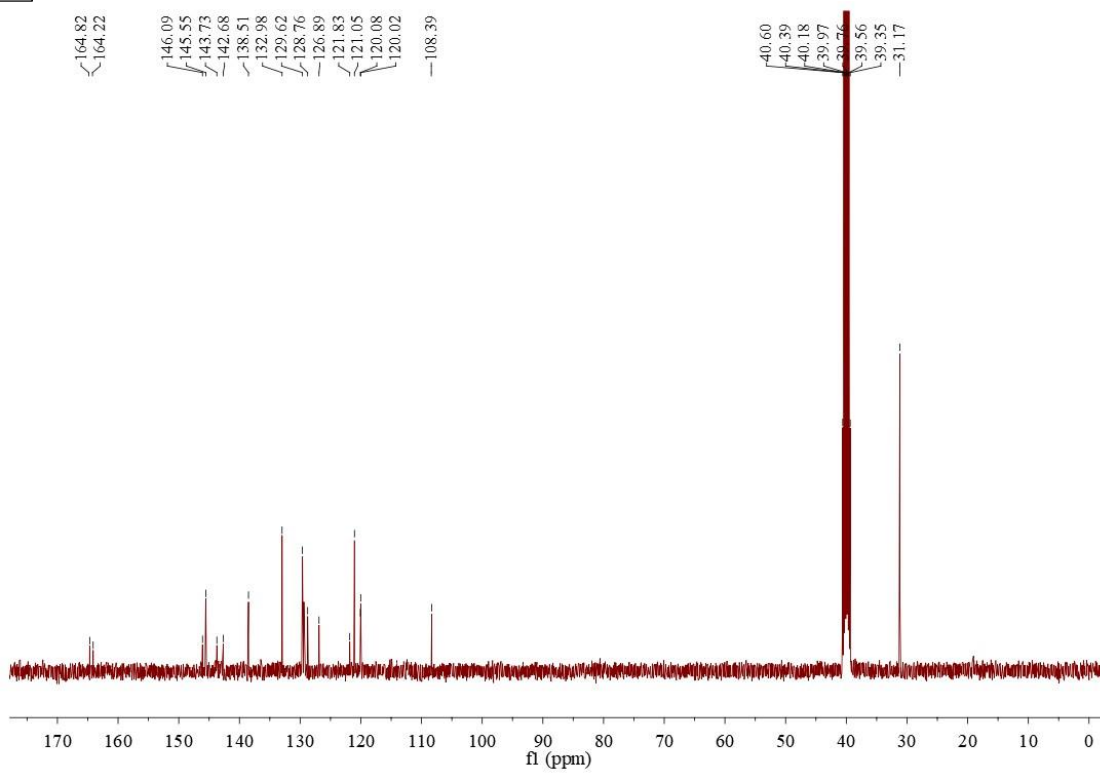
5k



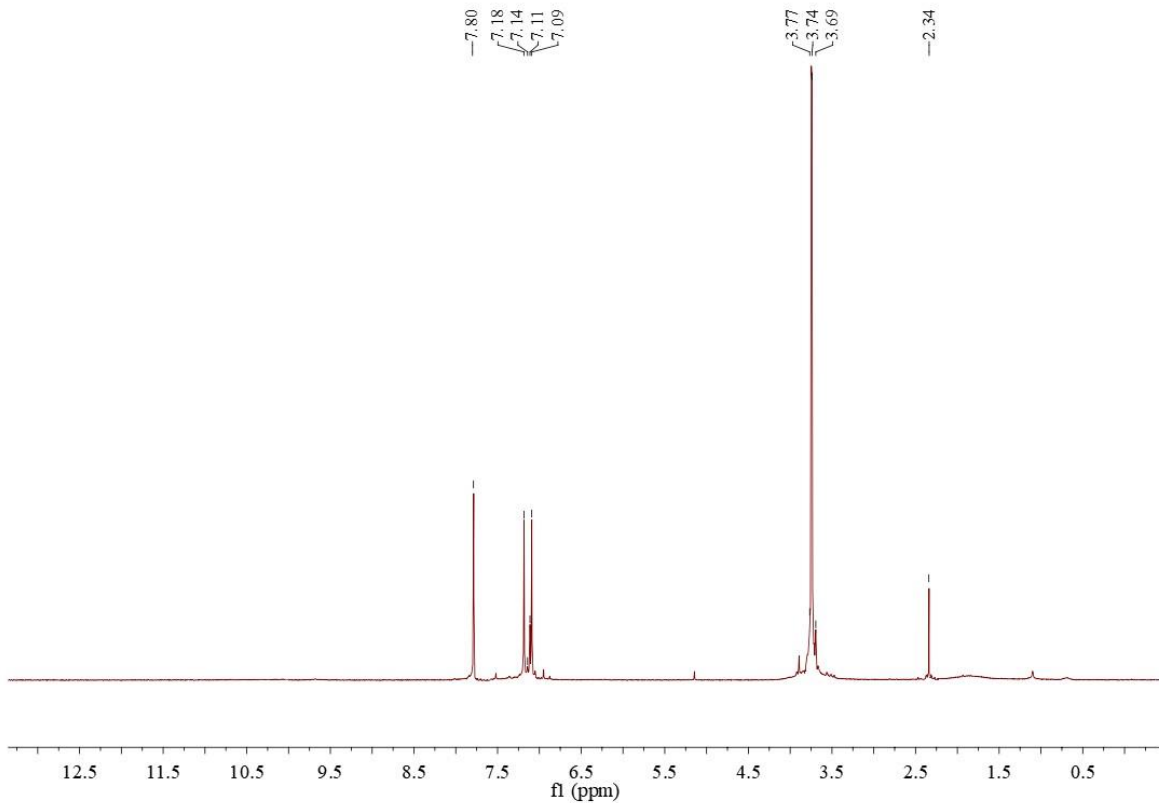
5I



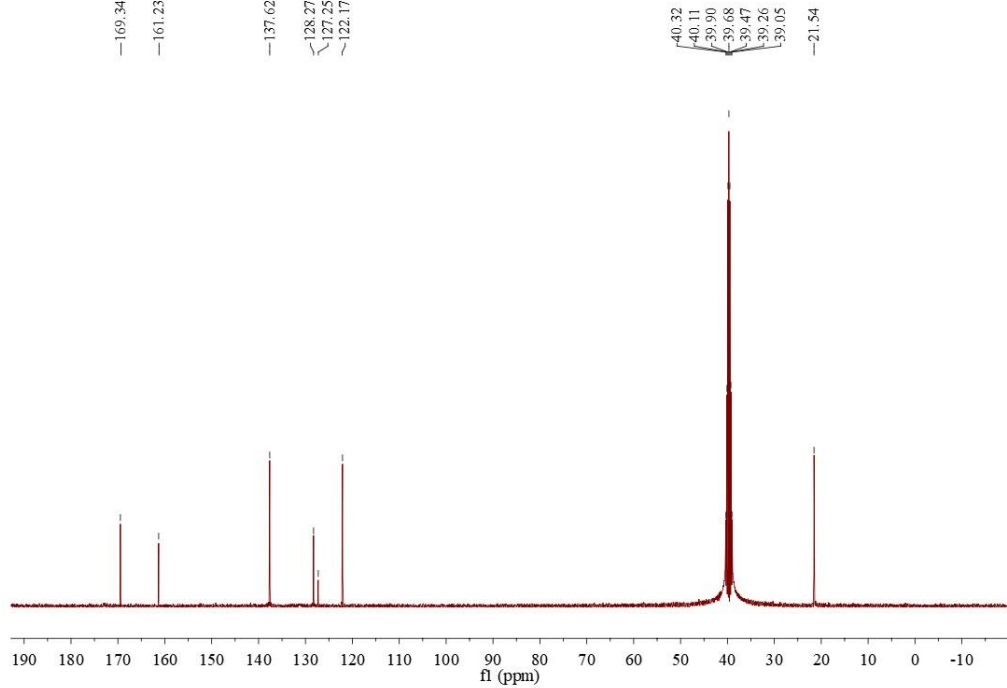
5I



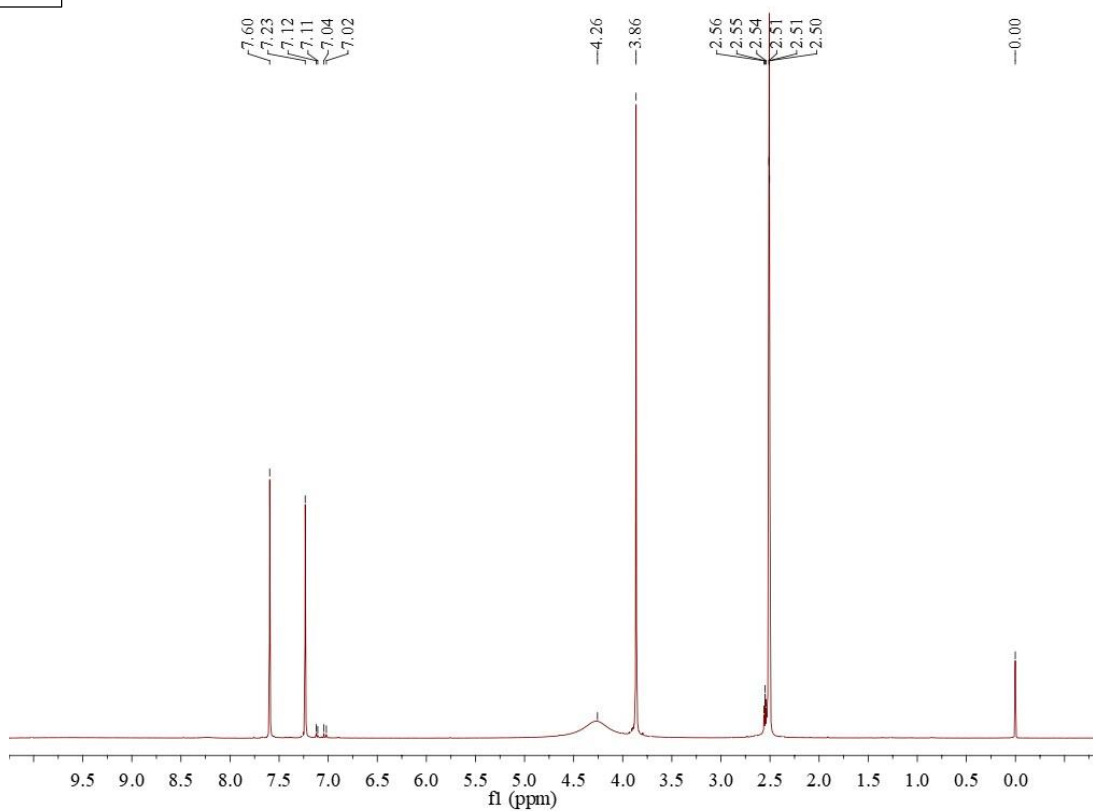
5m



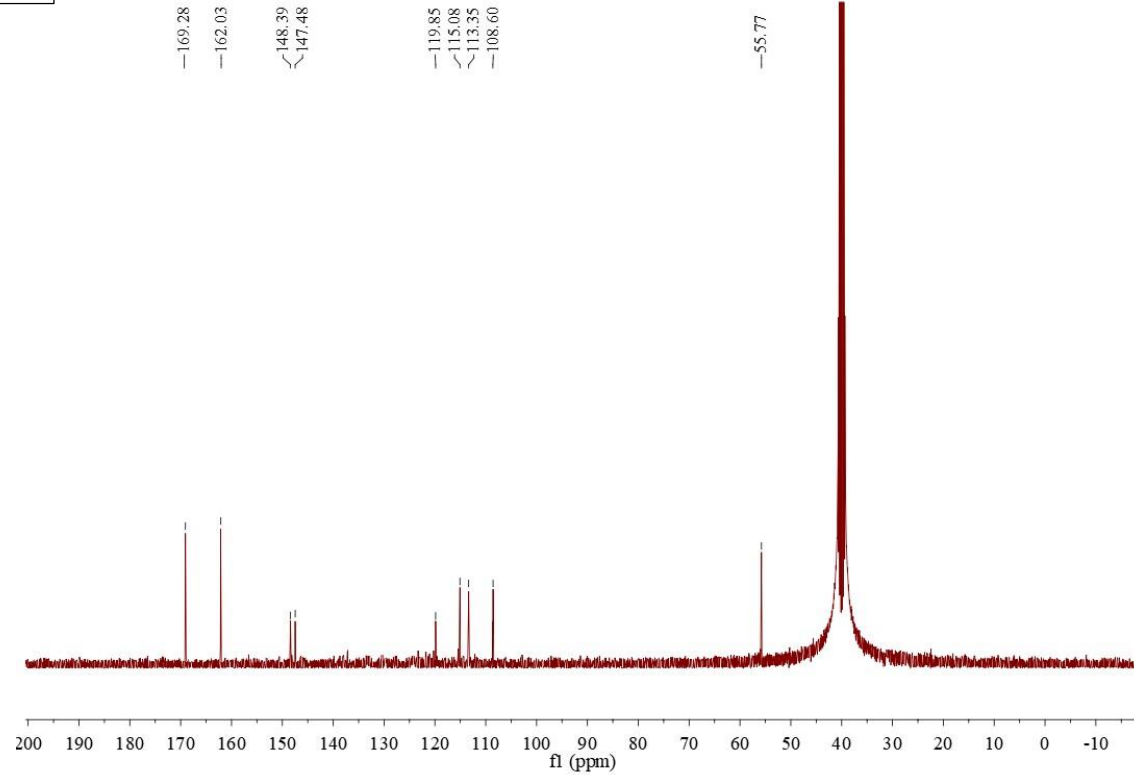
5m



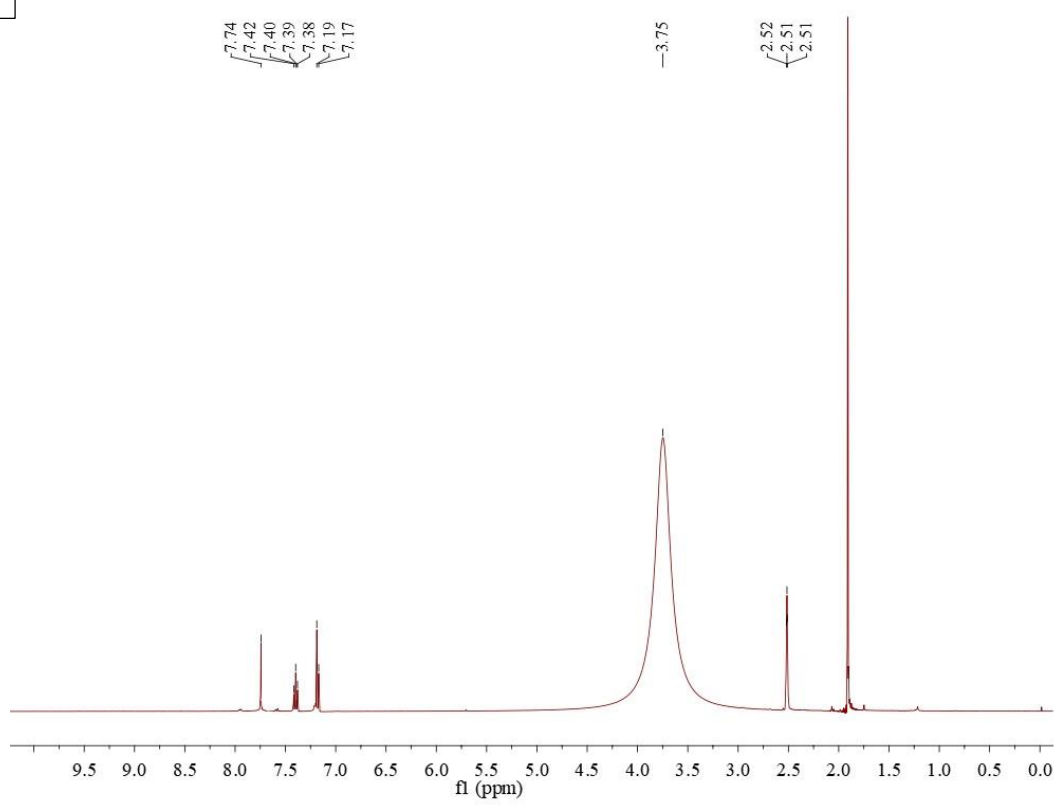
5n



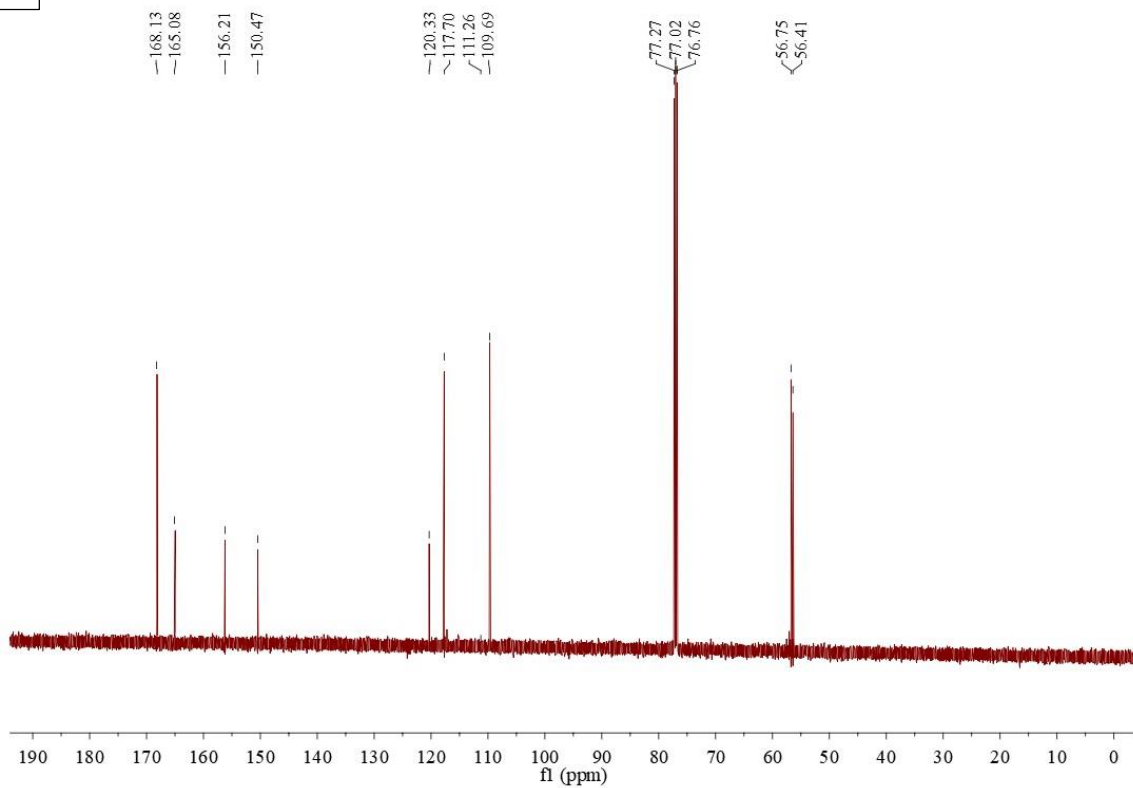
5n



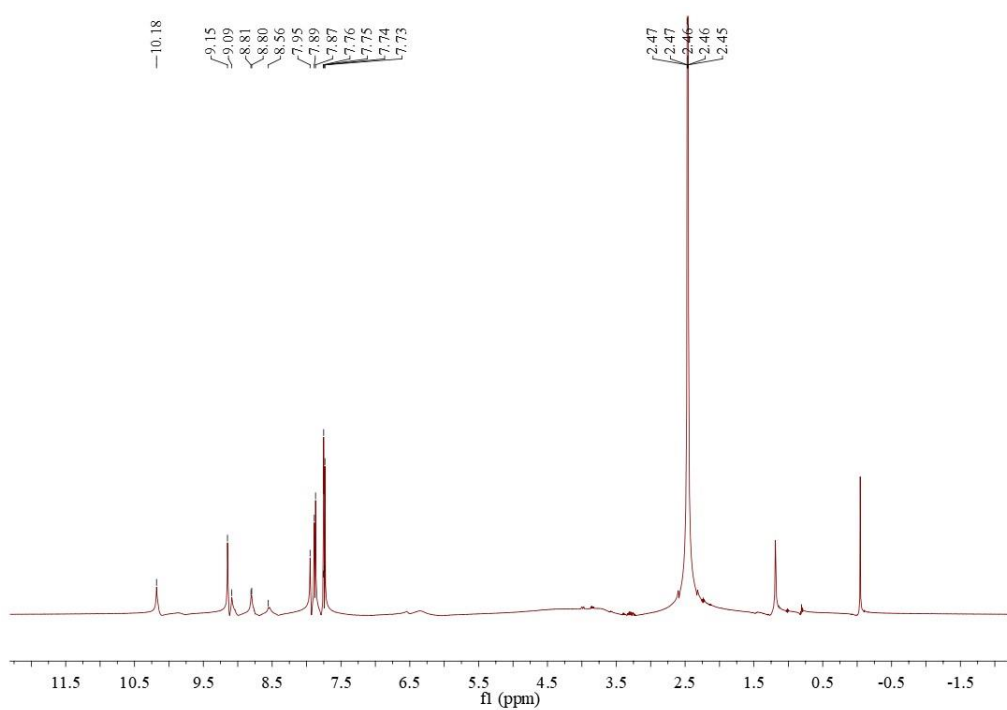
50



50



5p



5p

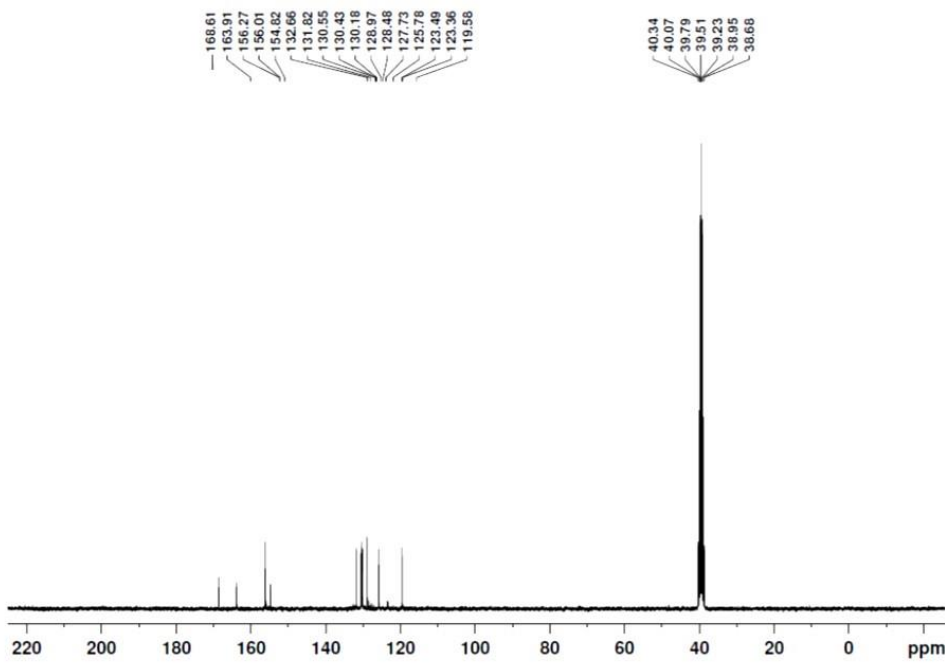
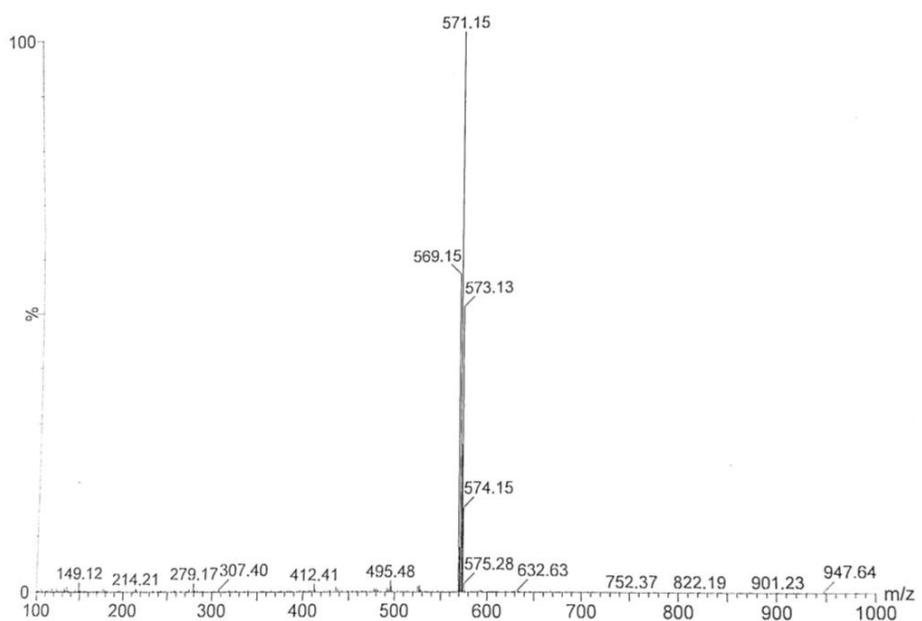
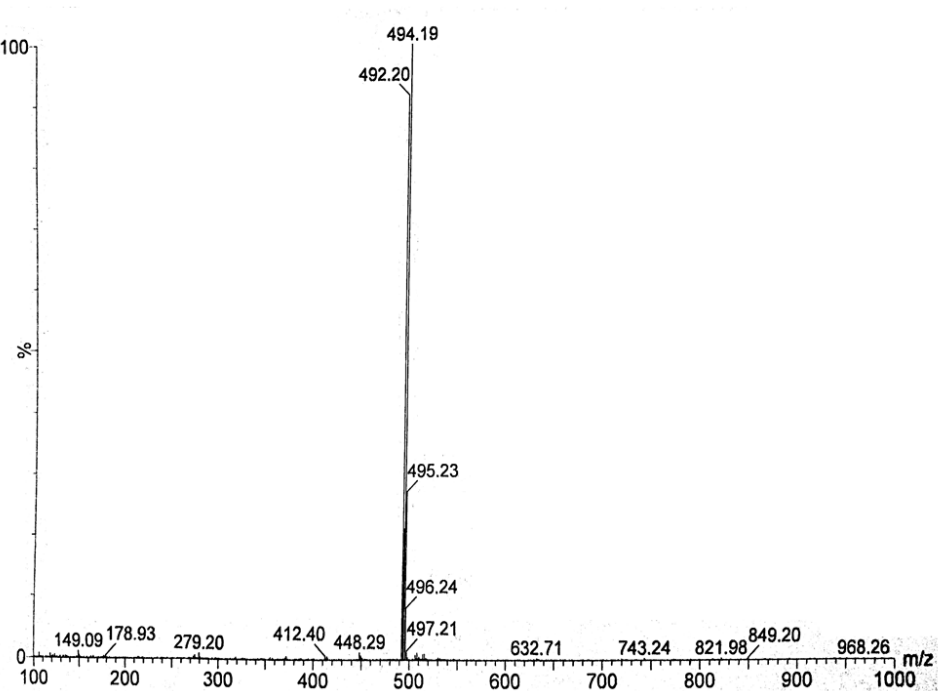


Fig. S2: ¹H and ¹³C NMR spectra of heterocyclic derivatives **4e-4l**, and **5a-5p**.

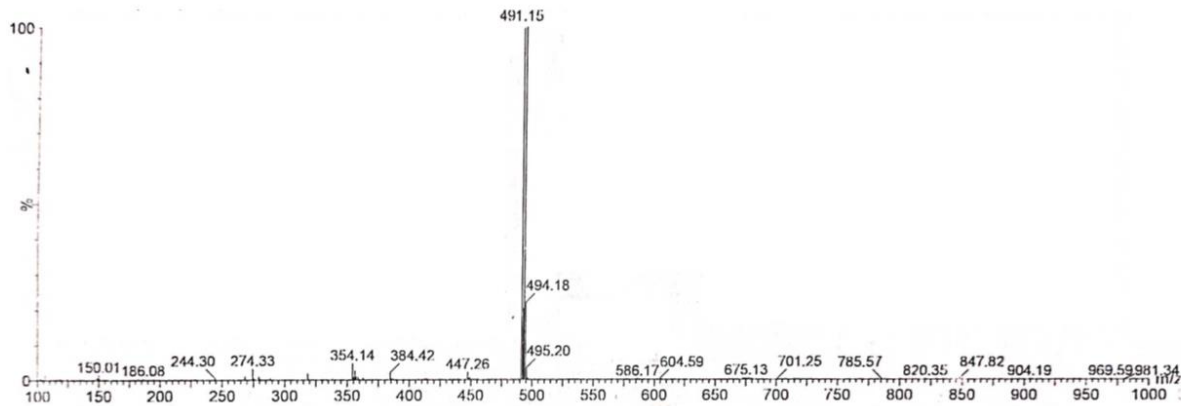
4e



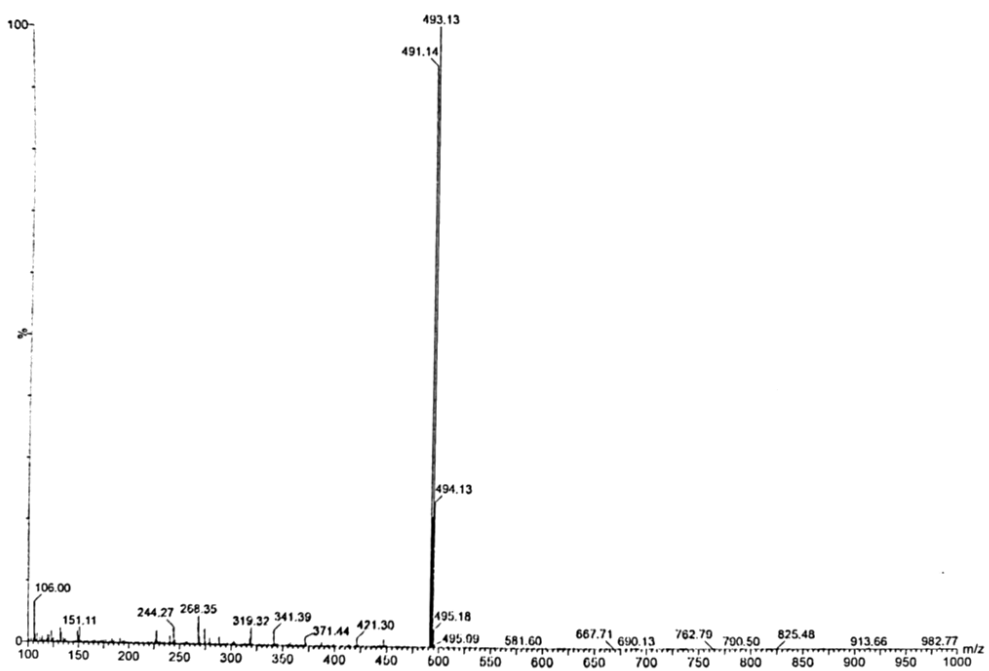
4f



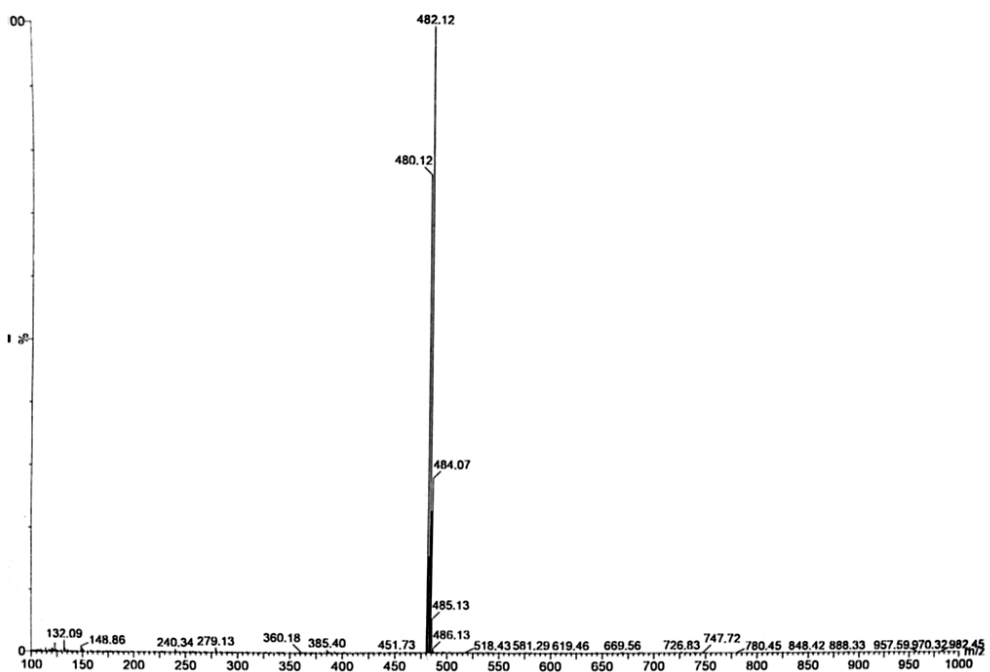
4g



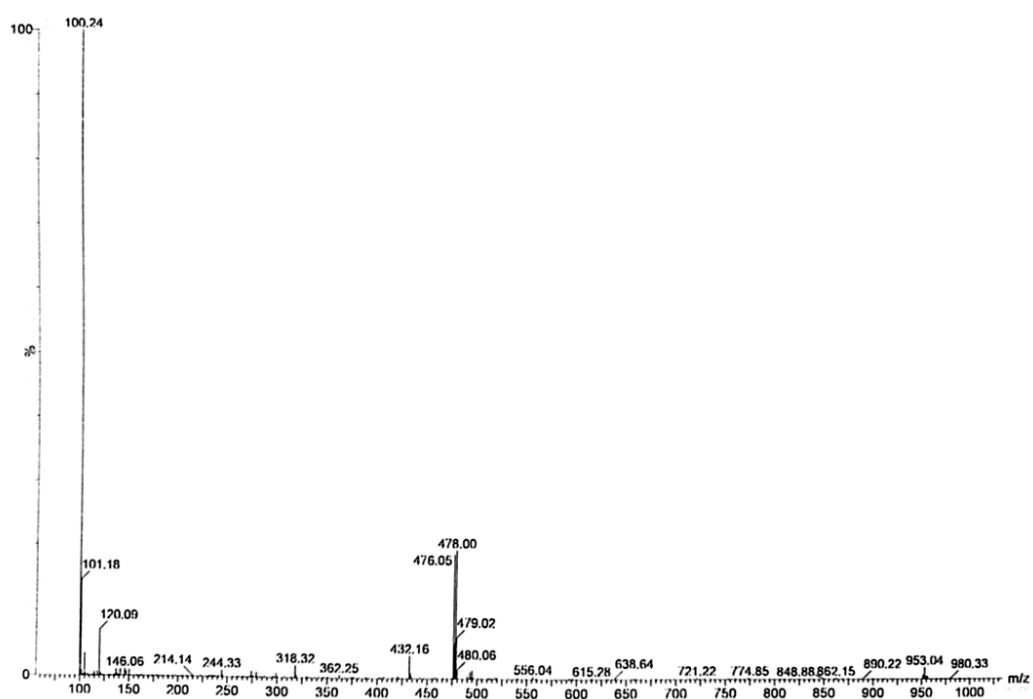
4h



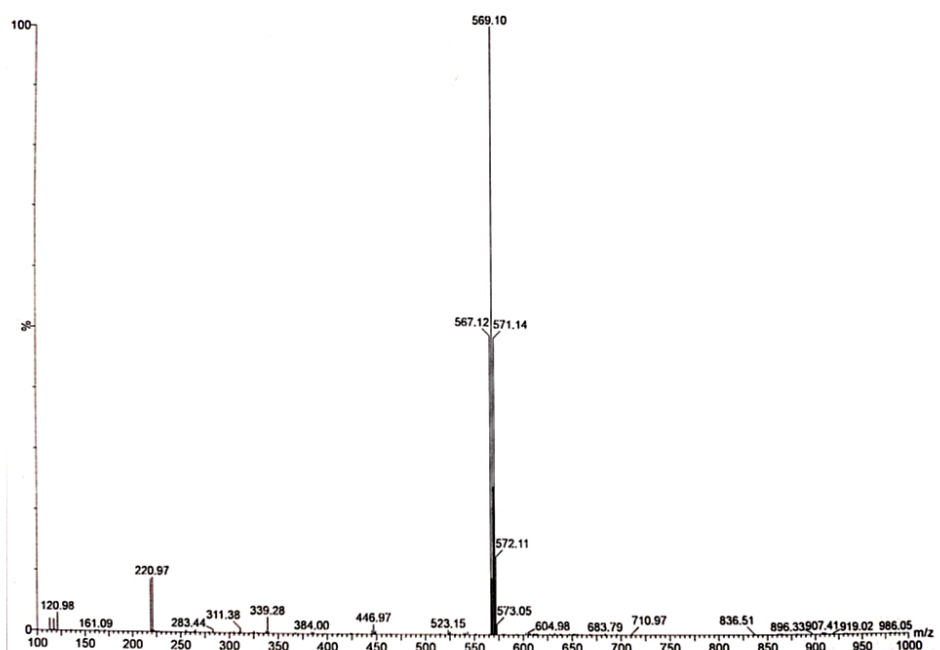
4i



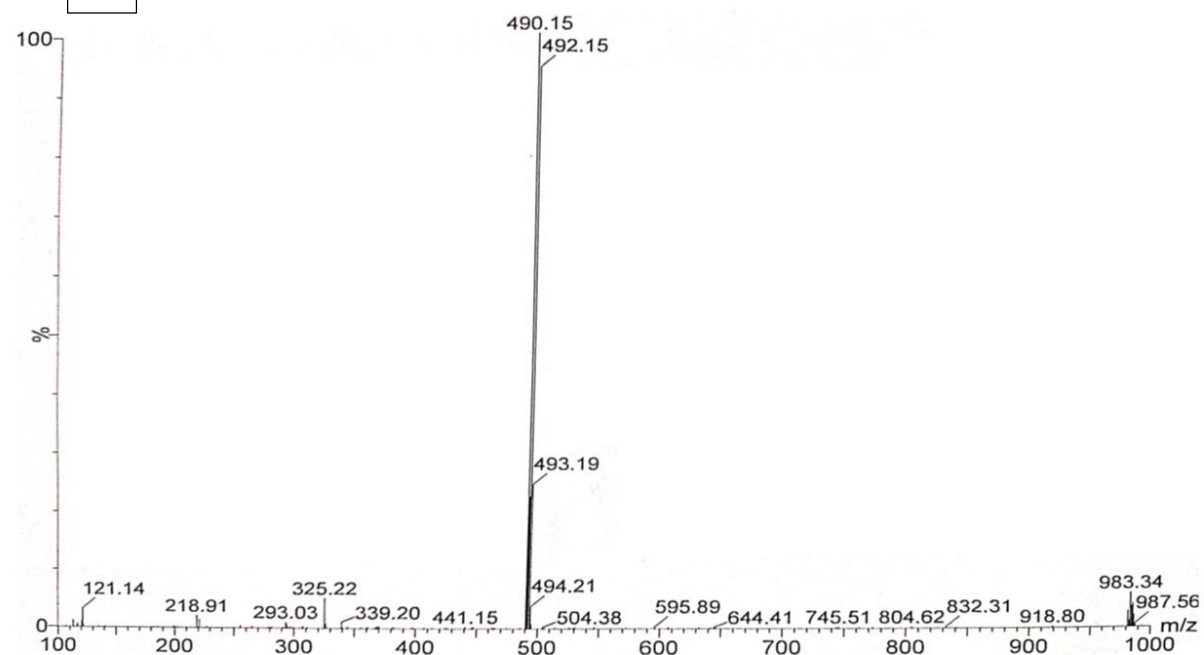
4j



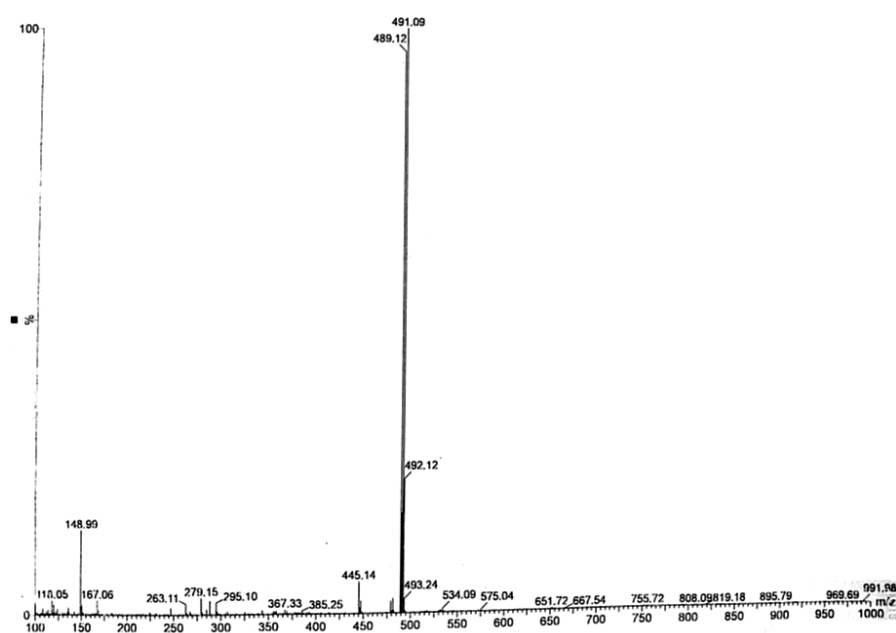
4k



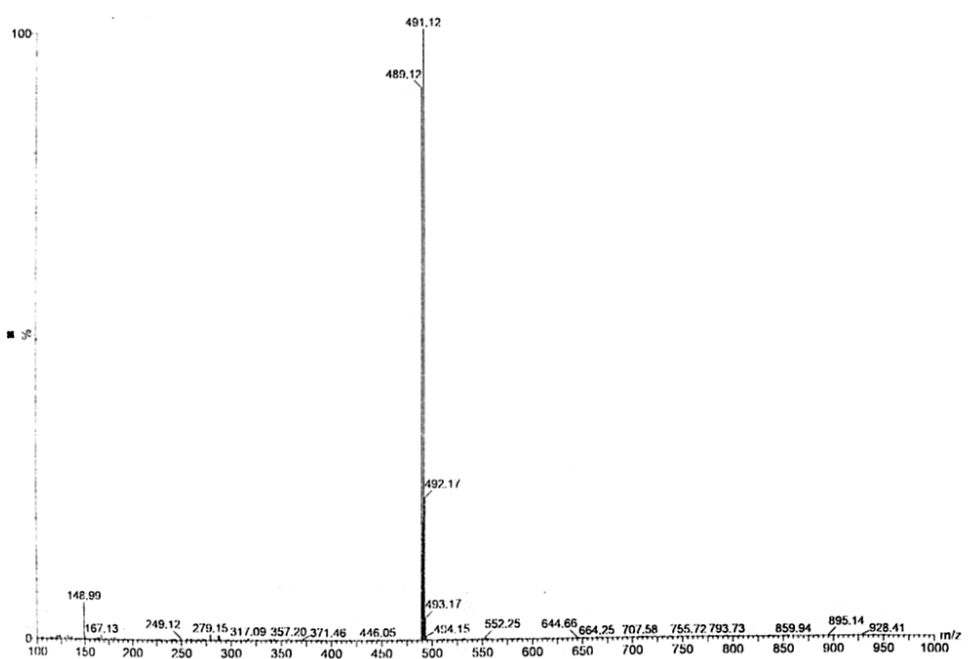
4l



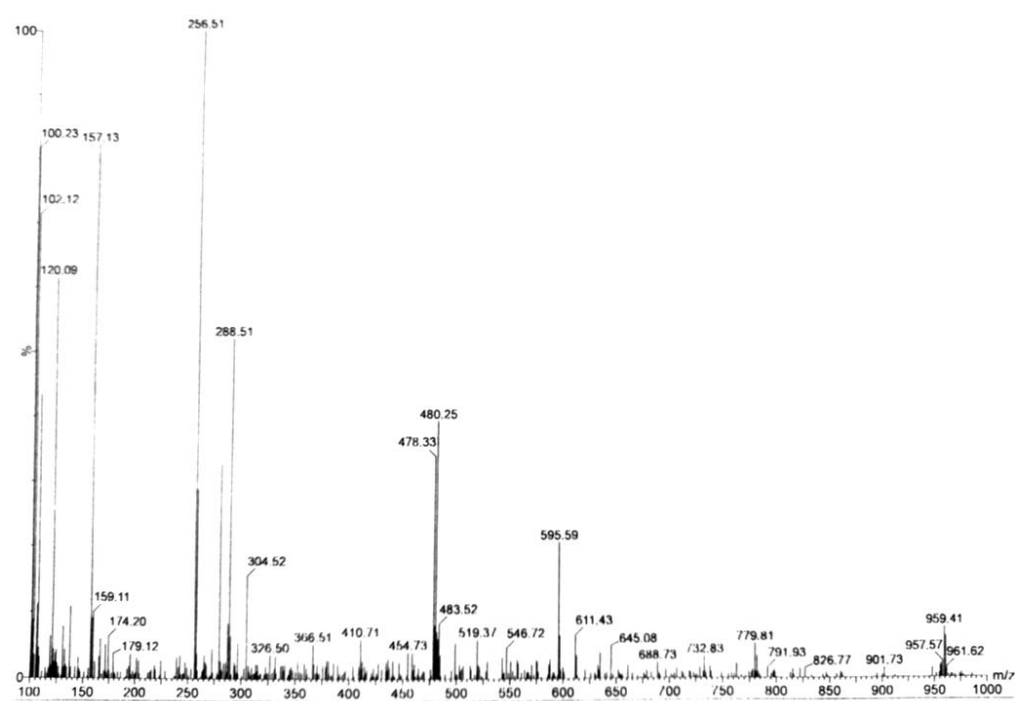
5a



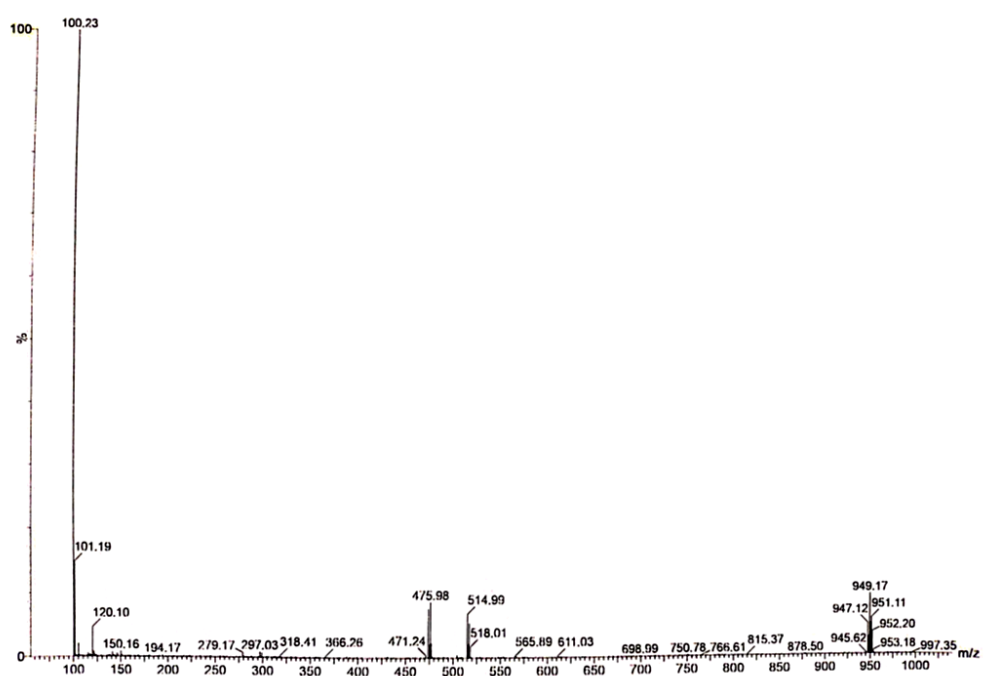
5b



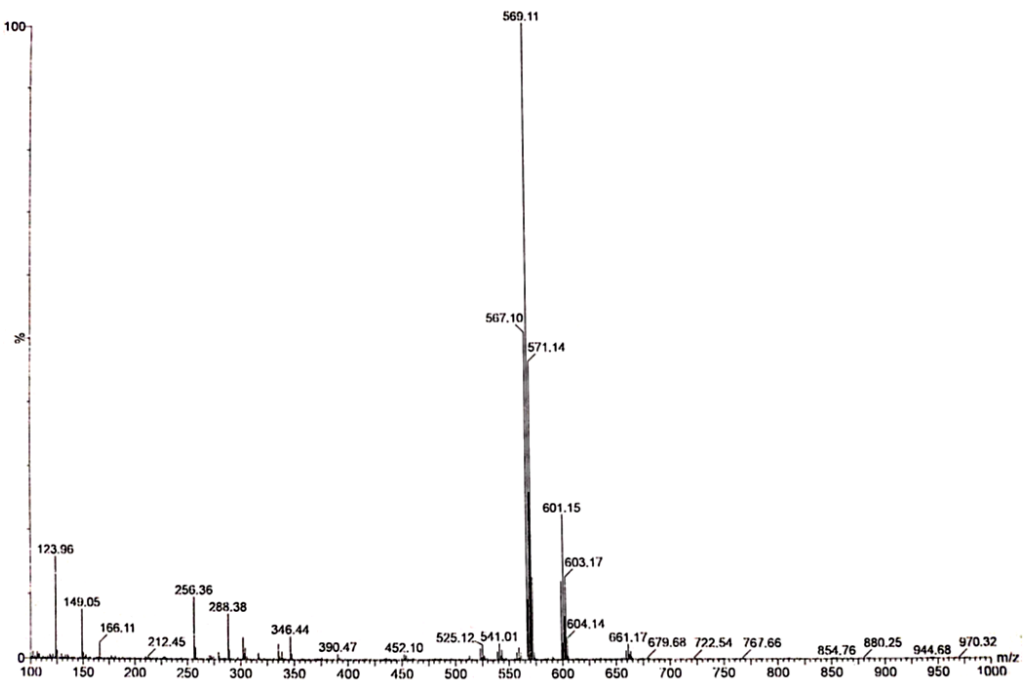
5c



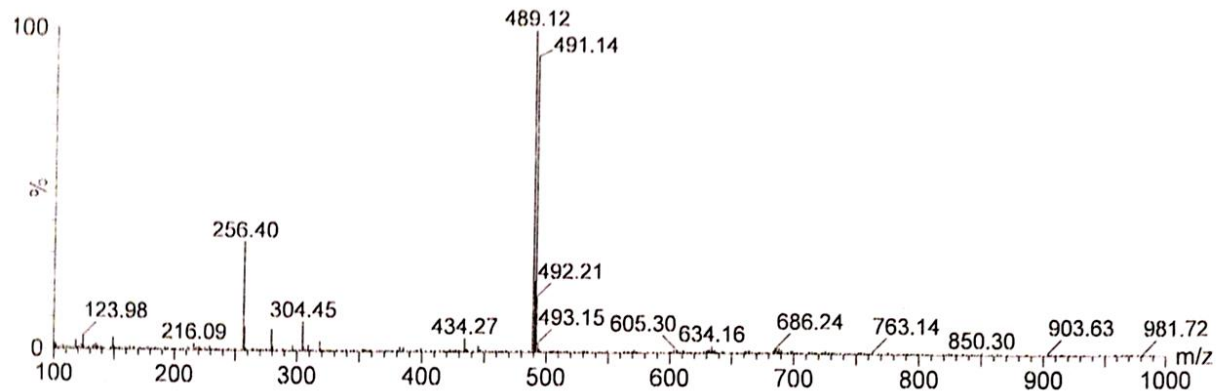
5d



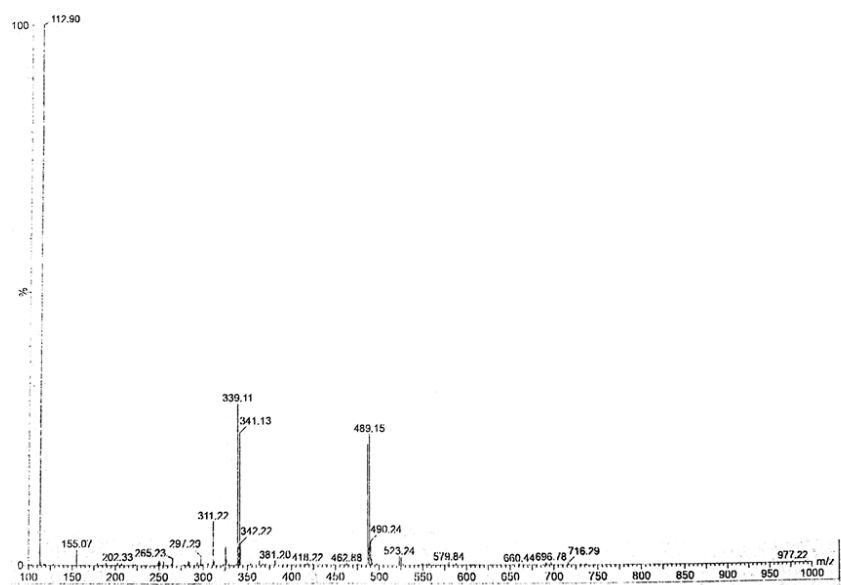
5e



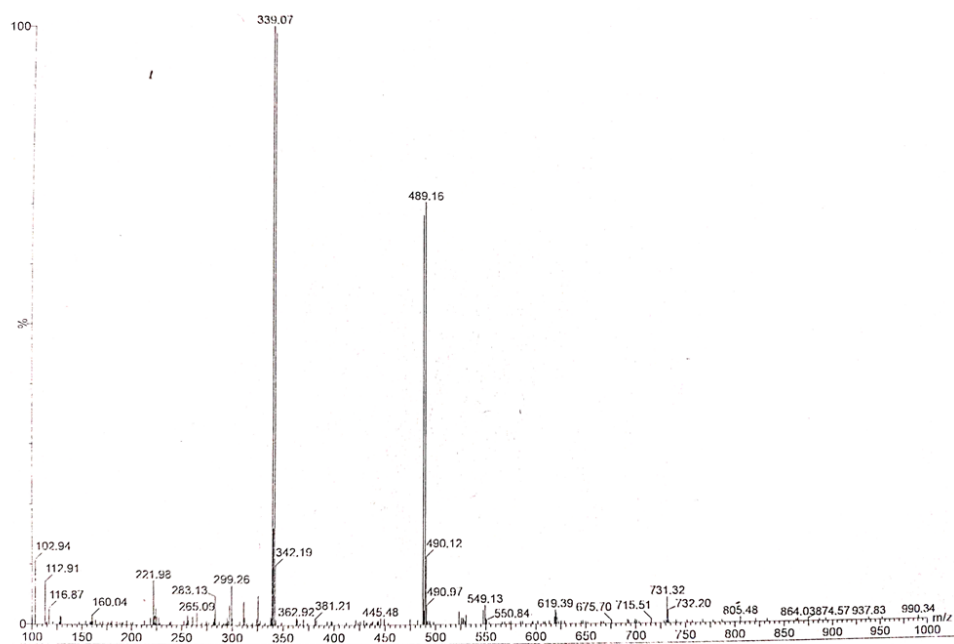
5f



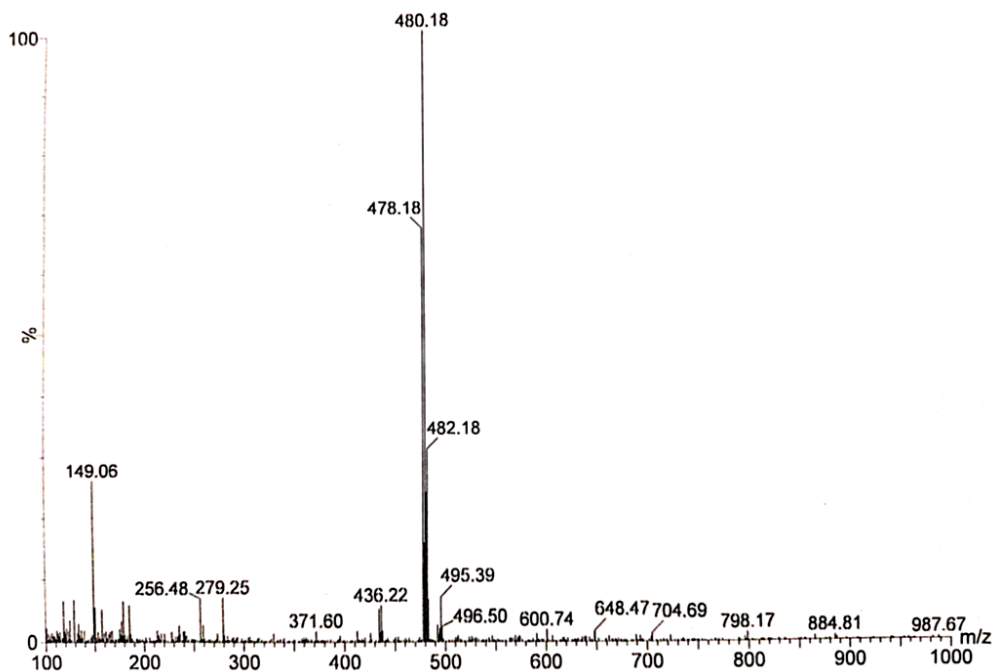
5g



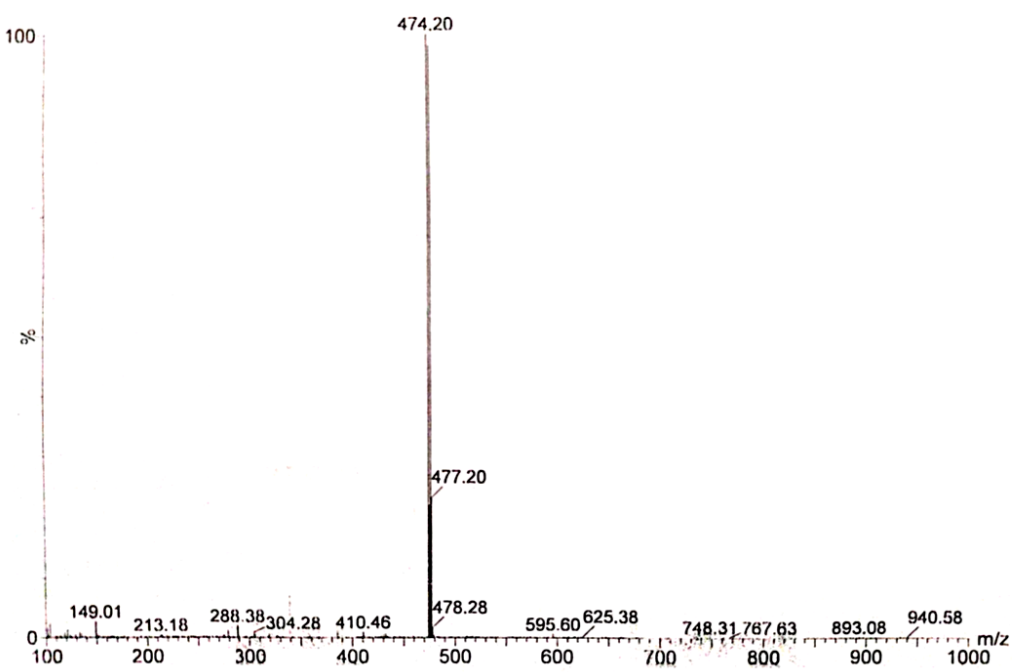
5h



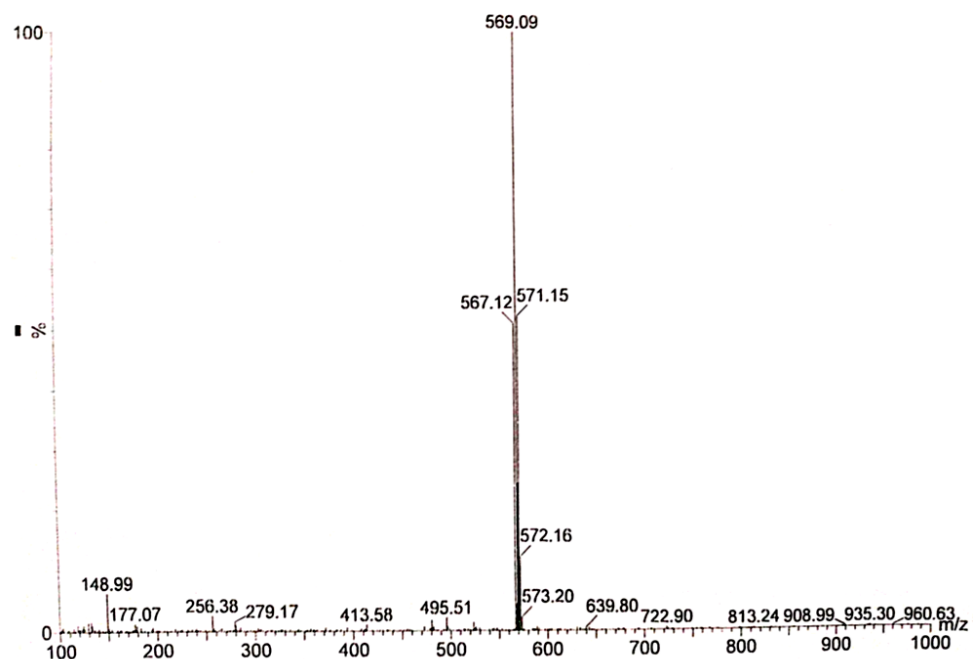
5i



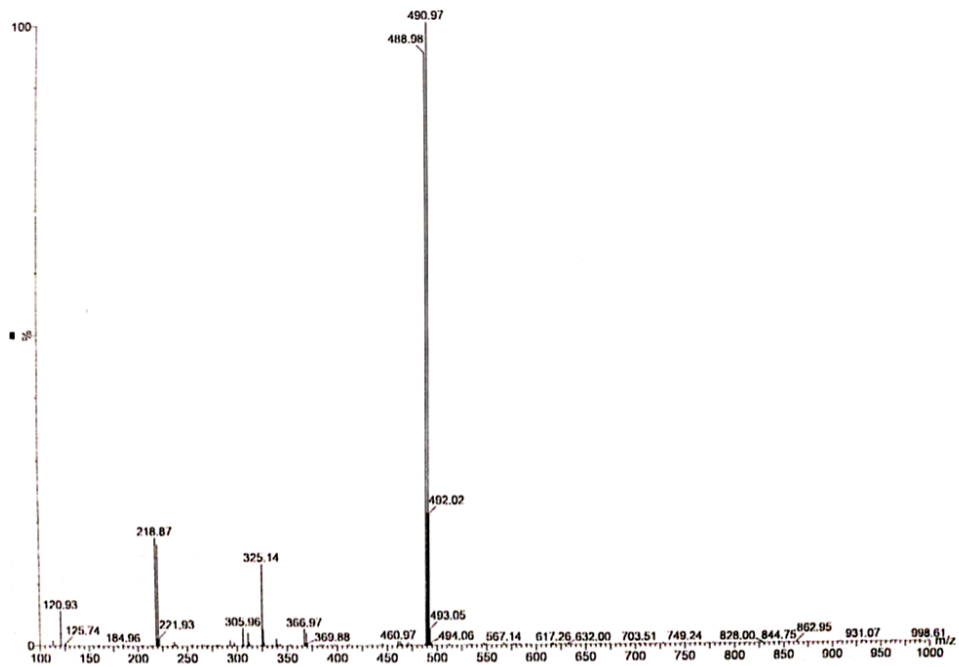
5j

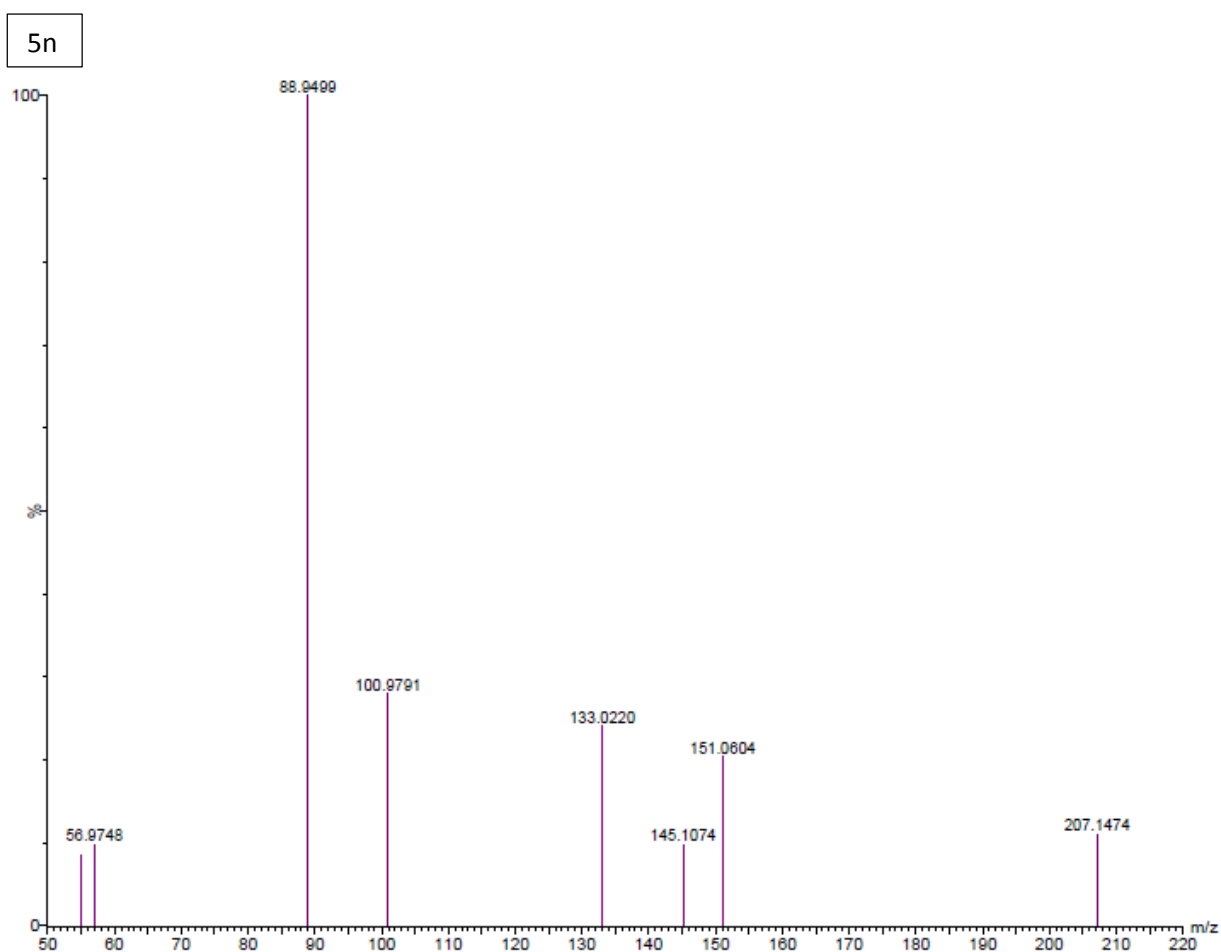
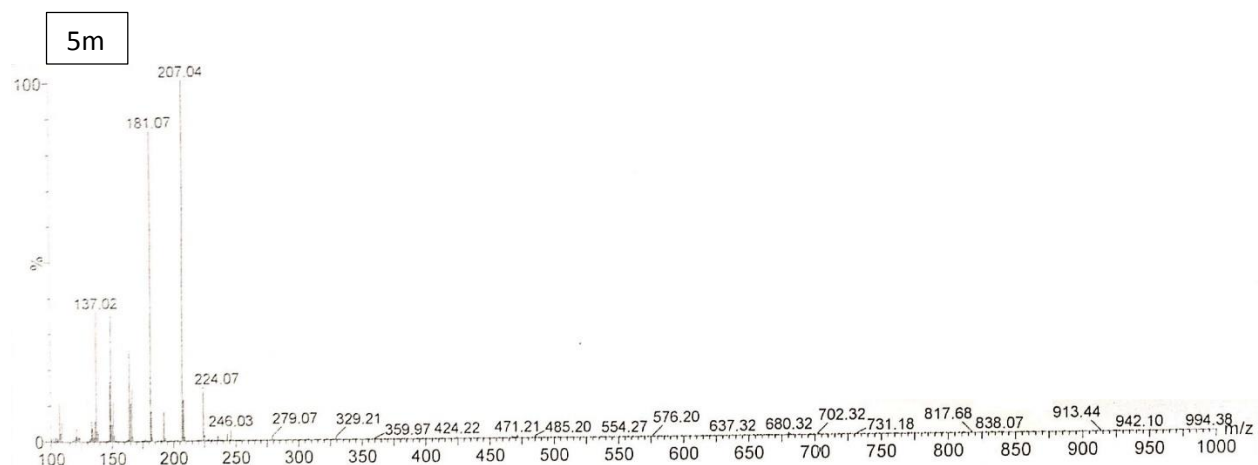


5k



5l





5p

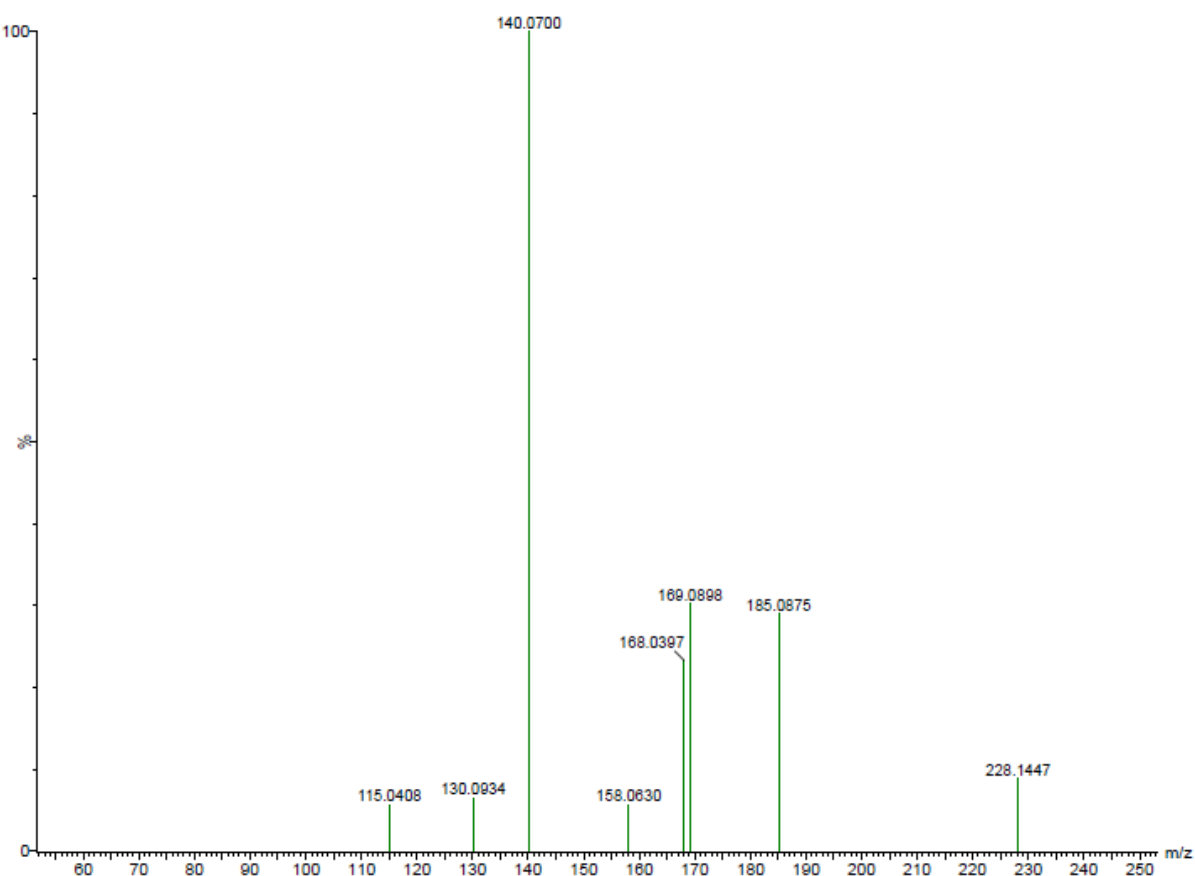


Fig. S3: Mass spectra of heterocyclic derivatives **4e-4l**, and **5a-5p**.

Declaration of interests

The authors declare that they have no known competing financial interests or personal relationships that could have appeared to influence the work reported in this paper.

The authors declare the following financial interests/personal relationships which may be considered as potential competing interests: